Contract Number 260165

E-Hub

Energy-Hub for residential and commercial districts and transport

SEVENTH FRAMEWORK PROGRAMME

Grant Agreement No: NMP2-SL-2010-260165

Call identifier: FP7-2010-NMP-ENV-ENERGY-ICT-EeB

Del 3.1 Report containing the proof-of-feasibility of integrated renewable energy generation concepts for the E-Hub on district level

Due date of deliverable: 31/12/2013

Actual submission date: 17/03/2014

Start date of project: 15/12/2010 Duration: 48 months

Organisation name of lead contractor for this deliverable: SOLINTEL

Author(s):

Jan Kuhlman, Björn Oldorf (HSW)

David Lanceta, Xiugang He, Arturo Marquina (SOLINTEL)

Kamil Otkałło (MOSTOSTAL)

François Badinier (ICAX)

Luis Juan, Juan Ramón de las Cuevas (ACCIONA)

Dissemination Level:

Public

Revision: final

date	status of document	by partner
January 17, 2014	draft distributed to partners for feedback	SOLINTEL
February 12, 2014	final draft sent to reviewer	SOLINTEL
February 21, 2014	document reviewed	ECN
March 13, 2014	final version submitted to coordinator	SOLINTEL
March 17, 2014	final version submitted to the Commission	TNO

Effort by partners for this deliverable:

Partner	Person months
ACCIONA	4
SOLINTEL	19
MOSTOSTAL	8
ICAX	10
HSW	19
TNO	2
PM total	62

Content

1 Executive Summary

The aim of the E-hub project is to develop energy systems that maximise the use of locally generated renewable energy on district level. This asks for components and technologies regarding energy generation, energy storage, efficient use of energy and techniques to balance different kinds of energy (electrical, thermal).

The objective of WP3 is to develop thermal energy technologies and components that are crucial to realize such an E-Hub system. Within WP3, the main aim of task 3.1 is to develop alternative concepts to harvest renewable energy, i.e. integrated concepts using thermo-active foundations and pavement foundations as solar collectors.

The main reason to develop these concepts is that in high building density areas often there is not enough suitable area available to apply sufficient amounts of PV (Photo Voltaic) panels or PVT (Photo Voltaic and Thermal) panels, generating renewable electricity and thermal energy in order to achieve low energy or even energy neutral districts. As a consequence, other sources of renewable energy need to be used as well, for example geothermal sources (foundations) or road surfaces.

The three main subtasks of task 3.1 were:

1.- Research on alternative materials for maximal efficiency of thermo-active foundations. Aim: Improving the thermal yield of **TAFs** (Thermo-active foundations) without compromising the structural functionality of the foundation.

2.- Research on alternative materials and layouts, to improve the heat transfer between pavement and piping network of the **TRSC** (Thermal Road Solar Collector). The objective is to determinate which factors and requirements are needed in order to obtain higher energy transfer rates. Aim: Improving thermal yield of the **TRSC** without compromising the structural integrity of the road.

3.- The integration of these two systems at district level. Regarding **TAFs**, the objective is to define an optimal district solution by connecting multiple thermo-active foundation systems through an underground piping network and integrate buildings that do not have their own geothermal energy system in an E-Hub network. Regarding the **TRSC**, the aim is the dimensioning and interconnection of the system at district level.

This deliverable provides a qualitative analysis of the different possible connections and yields calibrated mathematical models of both the **TAF** and the **TRSC**. These models were implemented into Matlab in task 3.3 and will be used in the simulation of scenarios of both systems at district level in task 4.5.

TAFs

A Thermo-active foundation (TAF) is a foundation pile or plate in which pipes or tubes are imbedded through which a fluid can be transported. The foundation can therefore act as a heat exchanger with the soil surrounding it, e.g. providing low temperature heat as the heat source for a heat pump or high temperature cold for cooling purposes.

The results of in-situ geothermal response test (**GRT**) measurements performed by partner HSW were used to calibrate EED and FEFLOW models (using commercial software). Once the software models were calibrated with experimental results, simplified mathematical models were developed and compared with the commercial models.

The following table describing the GRTs performed by HSW, gives an example of the typical variables involved in a geothermal response test,

location (in Germany)	Date	pile diameter [m]	pile length [m]	spacing of heat carrier pipes [m]	λ of pile concrete [W/m·K]	λ geology [W/m·K]	pile resistance R_P [m·K/W]
Oldenburg	12/2011	0.46	8.0	0.12	3.3	2.2	0.12
Kelheim	05/2012	0.9	15.0	0.7	2.0	1.6	0.07
Hamburg	05/2012	0.51	12.0	0.15	2.0	1.7	0.12
Nordenham	09/2012	0.5	18.0	0.22	1.7	1.4	0.09
Berlin	10/2012	0.46	9.0	0.12	1.7	1.2	0.25

Table 1. Tests which were used for E-Hub purposes.

The results of the test are used to calibrate unknown parameters such as the effective thermal conductivity of the underground (see next figure).

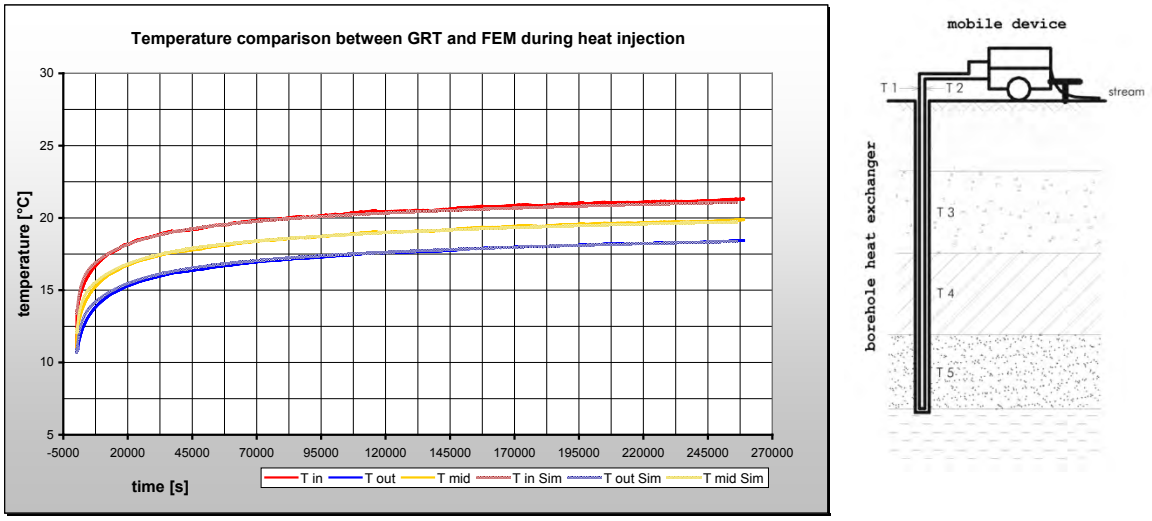

Fig. 1. Temperature comparison between the GRT and the FEM-model (FEFLOW) during heat injection. The solid lines are real GRT data; the dotted lines represent modelled temperatures (the model and experiment match very well).

Based on the calibrated high detail 3D-FEM (finite element method) model and also on the simplified analytical model, an optimization of heat exchanger materials and a thermally optimized concrete were investigated and evaluated in detail. An example of the highly detailed 3D-FEM model can be seen in the next figure.

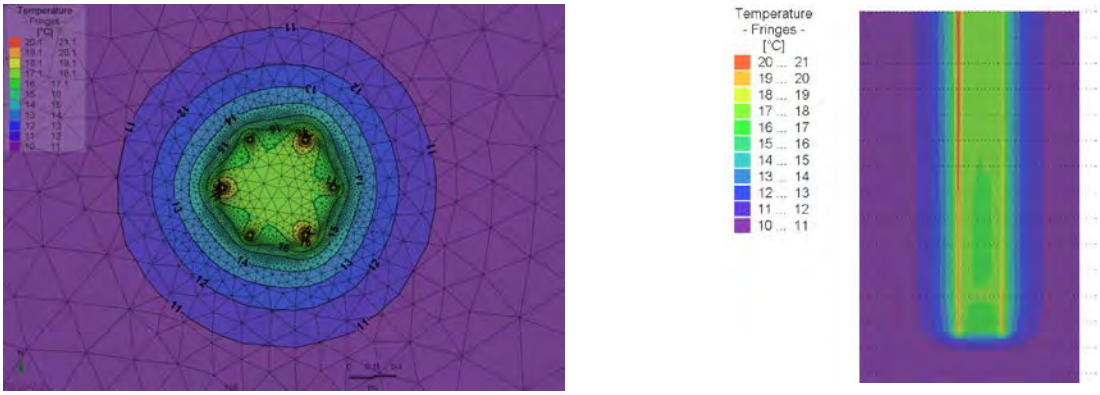

Fig. 2. Simulated temperatures after 3 days of heat injection (specific thermal load: 100 W/m), showing the gradual heating of the soil around the pile. Notice the finer mesh close to and inside the pile.

The most significant results obtained with the thermal simulation are the following:

- The use of thermally enhanced piping material has, according to the simulation runs, no measurable influence on the thermal performance of the energy pile,

- This effect remains unchanged even when thermally enhanced concrete is used,

- However, thermally enhanced concrete significantly increases the performance of energy piles in short term peak load operation, seemingly independent from the geology; the resulting effect can be as high as 25…40%. The effect is due to a much lower pile thermal resistance when using this improved concrete.

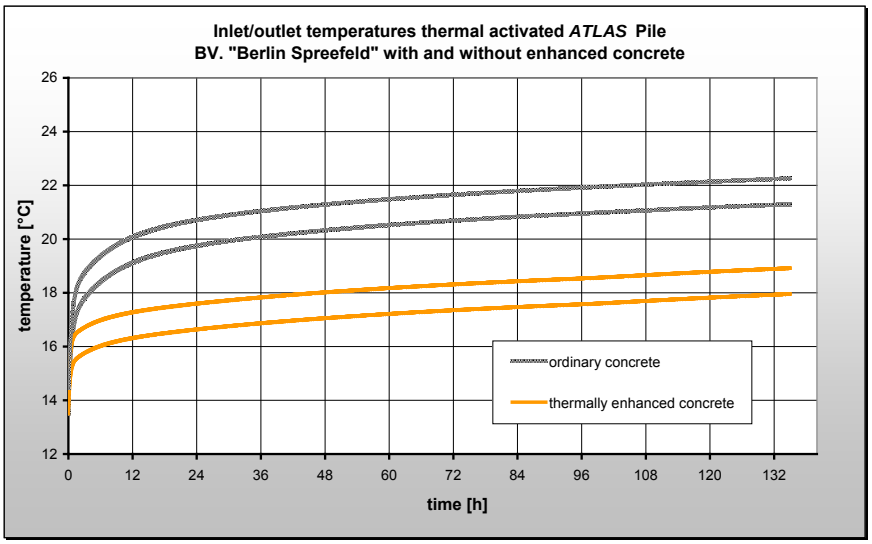

Fig. 3. Performance comparison, simulated with FEFLOW for an Atlas pile - simulated inlet/outlet temperatures for regular concrete are shown in grey and for thermally enhanced concrete in solid yellow. The two curves of each colour show inlet and outlet temperatures during heat injection.

The graph shows that when a fixed amount of heat is injected into the soil, the fluid temperatures are much lower when using the thermally enhanced concrete. This is due to the lower thermal resistance of the pile. This means that the heat that can be absorbed/released by a given pile, for a certain range of permitted fluid temperatures, is much larger. Conversely, when extracting heat, as in regular operation, lower heat resistances will result in higher heat transfer rates.

Regarding the integration/design of a district network to interconnect multiple thermo-active foundation systems, the two most efficient and practically proven possible ways of balancing thermal energy on a district level have been analysed. The first variant uses a single heat pump inside a centrally located building close to the TAF, from which “refined” thermal energy, i.e. at a medium temperature level (typically 45°C) is distributed towards the demanding buildings around it.

A second variant consists of two separate (but connected) networks over which the “unrefined raw energy”, i.e. at soil temperature level (typically 5-15ºC, depending on the location and season of the year) is gathered from the TAF’s and then distributed towards the heat pumps inside the heat demanding buildings. A first dimensioning has been done for the Amsterdam scenario of task 2.3. A quantitative analysis will be carried out by using the simulation platform developed in WP4.

Fig. 4. District lay-out (left) and piping network between buildings when using a central heat pump (right). The energy system includes an energy pile system underneath the office towers and a thermo-active plate foundation under the commercial building.

Besides the thermal analysis, a structural analysis has been performed to illustrate and quantify the loss of structural capacity expected in piles bearing internal pipes for thermal activation. Two representative pile layouts have been analysed from a structural point of view.

CASE A	CASE B
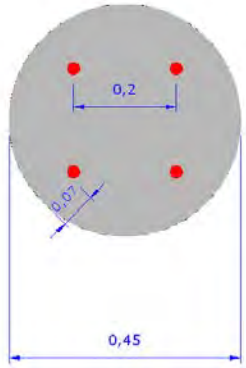	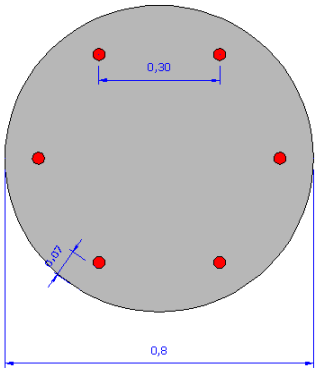

Fig. 5. Circular cross section of piles studied with the heat carrying pipes shown in red

The next table summarizes the results obtained:

	Case A	**Case B**
Compression loss	1.2%	0.9%
Tension loss	0%	0%
Shear loss	0.4%	0,2%
Flexure loss	0,4%	0,1%
Flexocompression loss	1,2%	0,8
Buckling loss	1,2%	0,9%

Table 2. Loss of structural capacity compared to regular foundation piles for the case studies.

From the results it can be concluded that the structural effect of thermal exchange piping on regular piles is comparatively small, almost irrelevant. Even more so since structural capacity is seldom reached in any case: more often than not, the limit is set by terrain resistance. That is to say the effect of the thermal pipes inserted in the piles is not enough to convert the verifications of the pile as structural element as dimensioning verifications, which means that the terrain continues being the weakest link of the structural "chain" of the foundations. The verifications regarding the terrain resistance are in both cases (thermal activated piles and regular piles) the most restrictive.

The study concludes that the use of thermally enhanced concrete leads to a performance improvement in peak load operation in the range of 25…40%. The study also defines feasible district strategies for TAF, in order to integrate the system in the E-Hub environment.

Thermal Road Solar Collector (TRSC)

A TRSC is a piece of asphalt with imbedded pipes or tubes through which a fluid can be transported. The pipes can therefore act as a solar heat collector, e.g. providing low temperature heat as the heat source for a heat pump or to be injected (stored) in the soil beneath it, using, for instance, TAF's.

Simulations to optimise thermal performance of the TRSC

The solar collection performance of the thermal road solar collector depends mostly on the position of the pipes carrying the heat transporting fluid, which are generally embedded in the top coat asphalt. Starting from a standard road composition, the thermal design of the solar collector has been developed, in particular with respect to the parameters:

- depth of pipes in the road used for heat collection
- diameter of pipes used
- lateral spacing of pipes used

As an illustration, Fig. 6 and Fig. 7 show simulations of the yield of road solar collectors as a function of these parameters.

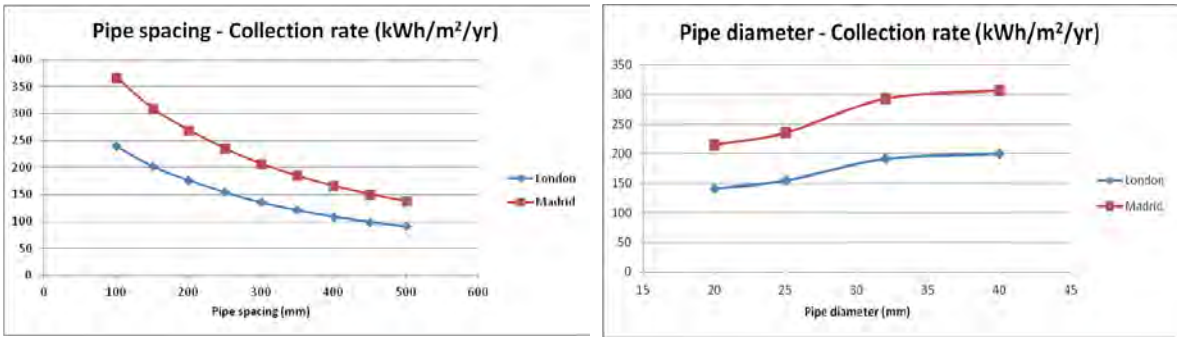

Fig. 6. Collection rate dependence on pipe spacing (left) and pipe diameter (right).

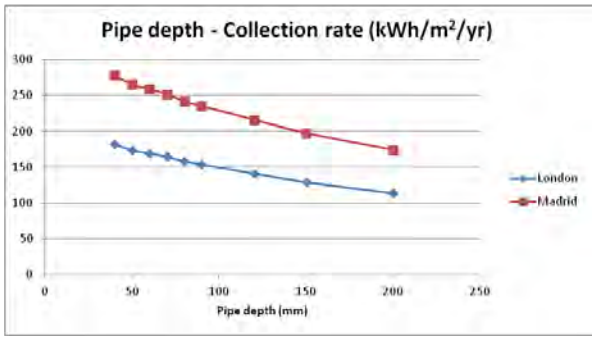

Fig. 7. Collection rate dependence on pipe depth.

The performance of alternative piping materials has been studied. A slight increase of heat transfer has been estimated when using more conductive pipes. However, in practical applications, parameters such as cost, structural issues and practicalities of installation will play a part in the selection of the material.

The influence of the thermal conductivity of the aggregate base layer (one of the road layers, which is located under the pipes) seems to be low. The study shows that there is almost no difference in the annual collection rate when the conductivity of the aggregate base layer is decreased. This shows that most of the heat absorbed at the top surface is transferred to the fluid, and therefore there is no need to improve the insulation characteristics of the aggregate base layer.

On the other hand, if a coating material with an emissivity value lower than 0.9 can be applied on the top of the road, it will significantly reduce heat losses due to IR emission from the surface to the surroundings and it will therefore improve the thermal yield of the TRSC.

Simulations to investigate structural performance of the TRSC

As the road has to fulfil structural requirements, not all the thermal designs are feasible. By means of calculation models, the road structural response to the traffic loads, in terms of stress, strain and displacement as a function of the TRSC parameters has been studied. The choice of the critical values for each case and its use in pavement deterioration models will allow an estimation of the global road durability. If the structural models showed that the TRSC designed did not fulfil the required durability, the structural data would feedback to the thermal design and so on, until an optimized design was obtained.

The main criterion to establish the most suitable depth/layout to locate the buried pipe system was the expected lifespan of the road which has to exceed twenty years. According to the results, a depth of 0.09 m (in the middle of the asphalt binding course) seems to be a suitable place for the system from a structural point of view. However, from a thermal point of view, the closer the pipes are placed to the surface, the better, as Fig. 7 shows.

With the goal of improving the structural behaviour of the road and being able to locate the buried pipe system closer to the surface of the road, an epoxy resin layer was placed on the top of the surface of the road. When this fine layer of resin (with aggregates) is applied, a redistribution of loads occurs. As can be seen in the section, this resin layer confers a significant improvement on the structural behaviour of the road, prolonging its lifespan.

According to the theoretical results, it was concluded that it was possible, by adding an epoxy resin layer, to locate the buried pipe system closer to the surface of the road. However, laboratory tests carried out (see below) show that the binding of the resin layer to the base layer is still a challenge. This effect needs to studied in more detail before recommending the application of a resin layer in practical applications.

Lab tests to study structural performance of the TRSC

In order to validate the structural simulations, detailed experiments were carried out in a laboratory by partner Mostostal. In the tests, small pieces of road were subjected to dynamic loads, representing the passing of vehicles (Fig. 8). The tests showed a small effect of the resin layer on the endurance and durability characteristics of the pavement. A clear positive effect of application of this layer was limitation of rut formation (rutting degrades the pavement), however, adhesion of such a layer to the base is too poor. The parameter lateral spacing was also checked in the structural tests.

Fig. 8. Sample R2/2 prepared for the test.

Taking into account all the results of the thermal optimisations and the results of the structural analyses, an optimum configuration for a TRSC could be proposed, as shown in Fig. 9.

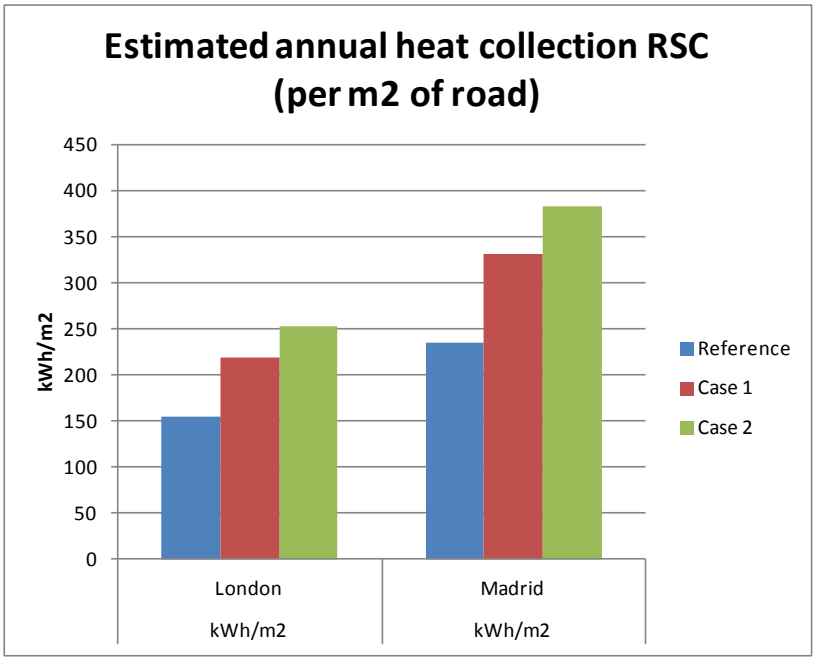

Fig. 9. Estimated TRSC thermal yield per m^2 of road for the optimized cases (reference: lat. spacing 250 mm, 25 mm diameter, pipes in binding asphalt course (pipe depth = 9 cm); case 1: lateral spacing 100 mm, 20 mm diameter, pipes in binding asphalt course (pipe depth = 9 cm); case 2: lateral spacing 100 mm, 20 mm diameter, pipes in wearing course (pipe depth = 5 cm).

The so called Case 1, improves the thermal yield compared to the reference case by 41%. This configuration has been tested in the laboratory from a structural point of view and it can be used in roads with medium traffic.

The Case 2 is a further step that places the pipes closer to the surface, by adding a resin on top of the road that increases the structural strength. It improves the thermal yield of the reference case by 63%. However, it has been observed in the laboratory test that adhesion of such a layer to the base is insufficient in the tests that have been carried out. Therefore this issue has to be solved before implementing this layout in a real road.

Conclusions

Both Thermo-active foundations and Road solar collectors can provide low temperature heat or high temperature cold that can be used in a district energy system aimed at maximising locally generated renewable energy. Several technical improvements were studied for these technologies such as the use of thermally enhanced concrete for the foundations and coating and resin layers for the road collector.

First proposals were made for an integrated renewable energy system that includes these technologies. A quantitative analysis of the extent to which these technologies can contribute to low energy or even energy neutral districts will be made using the simulation environment developed in work package 4 of this project.

2 Thermo-active foundations

2.1 General introduction of TAF

Geothermal heat pump systems have been identified as one of the best sustainable energy technologies for space heating and cooling in buildings. This type of system consists of a sealed loop of pipes buried in the ground, where water or antifreeze flows in order to absorb or dissipate heat into the ground. These loops are connected to a heat pump which "pumps" heat or cold to the building taking advantage of the mild temperature of the soil compared to the air temperature. The wide application of this technology has been hindered by its high initial cost and the land areas required to install the ground heat exchangers.

Vertical borehole heat exchangers are the most frequently used source system for geothermal heat pumps, because they offer a good performance and require a relatively small land area (compared, for example, with horizontal heat exchanger pipes in trenches).

The foundation piles of buildings can be used as geothermal heat exchangers ,"energy piles", as well. Possible pipe configurations inside energy piles are U-tubes or spiral coils, as shown in Fig. 10. In a similar way, other types of foundations, like base plates, can also be used as geothermal heat exchangers. All the different foundations utilized as heat exchangers are summed up as ”thermo-active foundations” (TAF).

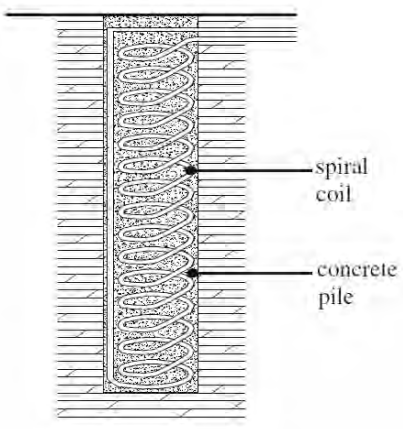

Fig. 10. Energy pile.

The objectives of the activities developed in this deliverable regarding TAFs are: finding alternative materials and layouts for enhancing the thermal yield (thermal optimization), carrying out structural research to calculate the weakening of the foundations and analysing the possibilities of integration of this system at district level.

2.2 Thermal Optimization of TAF

2.2.1 Introduction

As previously said in the general introduction, the use of geothermal source systems integrated in structural foundations (so called “thermo-active foundations” or TAF) at district level has the capability of being an efficient and cost effective solution for heating and cooling purposes as it is a robust and proven technology. TAFs are well liked by planners and building owners nowadays as they allow access to a renewable and “green” energy source.

Thermo active foundations will effectively reduce the need for traditional heating and cooling sources and thereby bring the idea of carbon-neutral buildings closer to reality. From both energy and an economic point of view the thermal use of the ground as a seasonal store for heating and cooling energy is the optimum operation mode for TAFs. The seasonal thermally balanced usage of the ground ensures a stable temperature regime and thus a good performance over long timescales.

To get an understanding of what determines the performance and economics of a TAF installation, past experiences have to be combined with recent scientific and practical information. First science-assisted, practical implementations of energy pile systems took place in the 1970s in Switzerland. Meanwhile, this innovative energy technology has been successfully implemented within many European countries and is regulated by national laws, guidelines and authorities, i.e. by the German Association of Engineers.

Typical foundations to be thermally activated are:

- foundation piles (“*energy piles*”)

- base plates

- bore pile or diaphragm walls

of which the most common are, by far, energy piles. Generally, each part of a building that is in contact with the earth or with water can be thermally activated to work as a heat exchanger.

Limiting factors for the performance of TAFs are 1º the underground with its thermo-physical properties and 2º the materials and constructive parameters of the geothermal source systems. With this in mind, a challenge for next generation TAFs is to find alternative materials and designs which are best suited for an optimal thermal performance.

The thermal simulation of highly thermal conductive materials like carbon fibre reinforced polymer composites or thermally enhanced concrete therefore is a major point in this E-Hub subtask. A second major point is to support the development of a simplified TAF simulation module for the software Matlab.

2.2.2 Description of typical thermo-active foundations (TAF)

Energy piles

Buildings which are founded in difficult geological conditions or have very high static loads, need to be founded with deep-seated foundations. Where such pile foundations are needed, an opportunity for a geothermal activation to energy piles is given (geo-thermally activated in-situ or pre-manufactured piles, see Fig. 11). A variety of designs such as bore piles, screw piles, displacement piles and precast concrete piles exist (e.g. Centrum piles, Fig. 12).

Nowadays most planners, which have to use foundation piles for larger buildings, at least consider a thermal activation to energy piles.

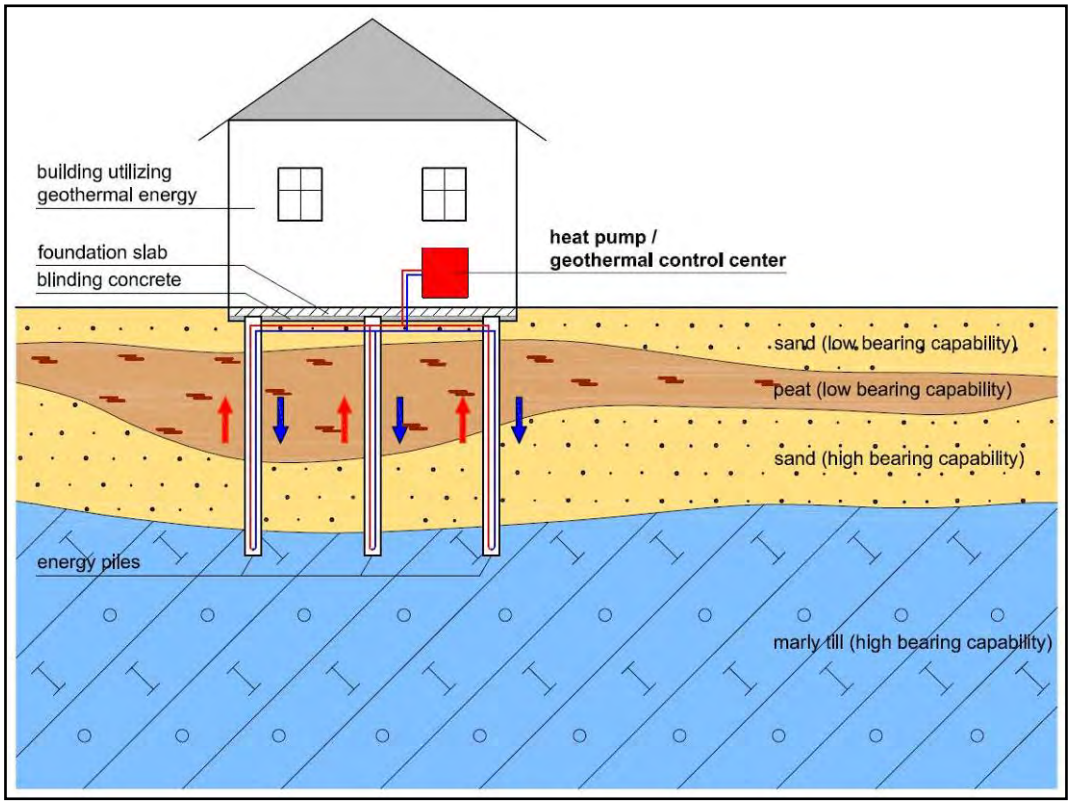

Fig. 11. Scheme of a building using energy piles for heating.

Reinforced concrete piles are state of the art for a long time now and have asserted themselves as the dominant system of deep foundation. They are characterised by a comparatively large static loading capacity and by a long service life in comparison with other foundation pile systems. Reinforced concrete piles can easily be thermally activated by the integration of heat exchange pipes (example see Fig. 13)

Fig. 12. precast concrete piles (“Centrum piles”), energy pile field Rostock “SILO 4+5”.

An energy pile field can be used for heating (heat withdrawal from the ground) and cooling (heat injection in the ground).

Energy piles are mostly used in base load operation with peak powers being covered by other source systems. Nevertheless, detached houses with energy pile foundations are known to work monovalent increasingly often, due to improved insulation/higher building standards.

Important parameters to consider when planning the thermal activation of a foundation are the geology/hydrogeology, constructive parameters of the foundation (size, depth etc.) and the buildings thermal demands.

While thermal demands have to be agreed upon between the planners and the constructive parameters are given by the buildings static demands, the last unknown component is the thermal yield of the underground for geothermal heating and cooling. It can be derived by a measurement of the thermo-physical underground parameters via a Geothermal Response Test (*GRT*).

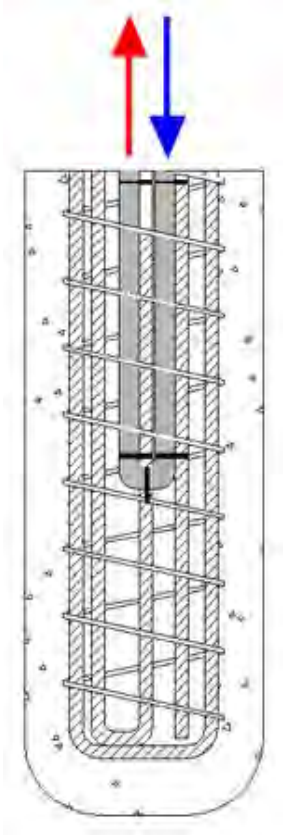

Fig. 13. thermally activated reinforced concrete piles.

Thermally activated base plates

Thermally activated base plates are much less common than energy piles. Their effectiveness strongly depends on the local hydrogeology, as flowing groundwater increases the thermal yield drastically. Dry sand generally can be regarded as the worst near-surface geology while wet sand gives the best performances.

The thermo physical exploration of the underground via specialised measurements (i.e. “thermal needle system”) is important for an assessment of its thermal performance. In addition, specialised simulations via thermo physics software (e.g. HEAT) are used to determine the long time performance for individual civil engineering projects. Two examples of heat simulations (cooling and heating mode) are shown in Fig. 14.

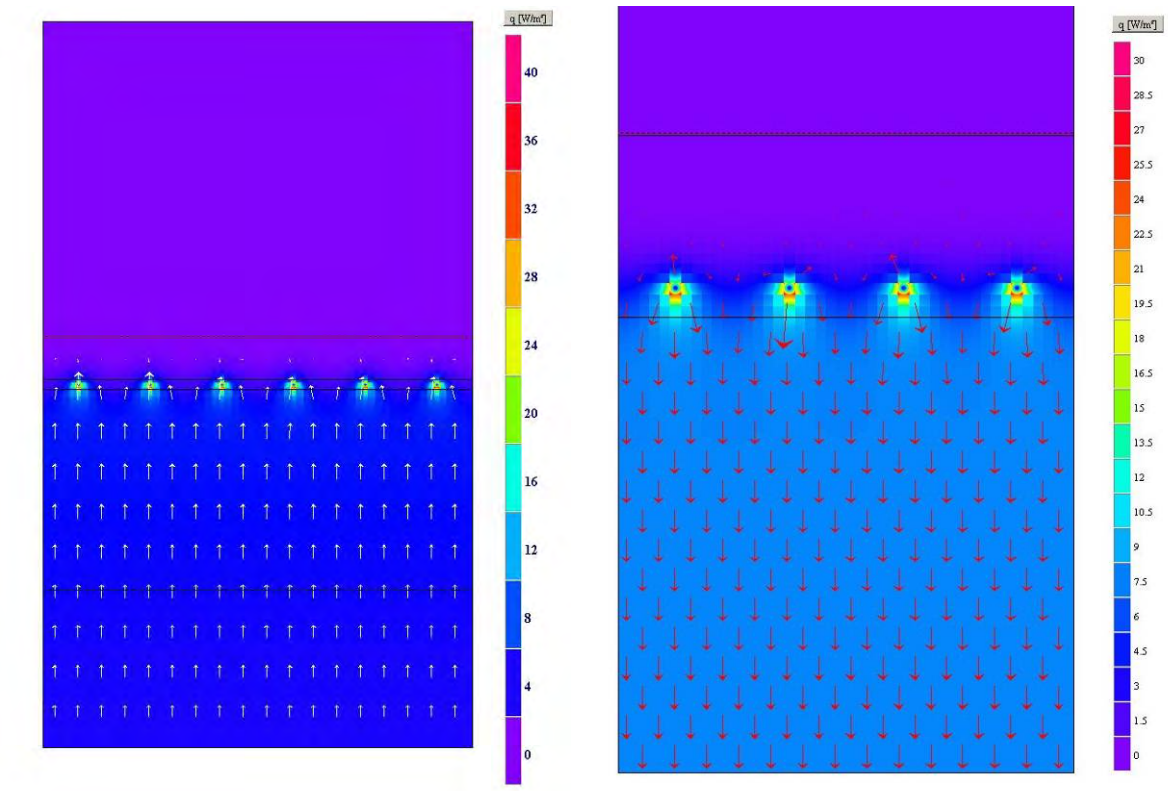

Fig. 14. Above, two pictures derived from individual thermo physical simulations of thermally activated base plates with the software HEAT are shown. On the left side the heat flow in heating mode (towards the base plate) is shown and on the right side a cooling mode heat flow (away from the base plate) can be seen.

Thermally activated bore pile or slotted walls

The thermal activation of slotted walls is rare amongst geothermal source systems. Nevertheless, this technology holds an enormous potential when it comes to the thermal performance because of its naturally big surface connected to the underground. In Fig. 15, an example of a thermally activated bore wall is shown. It was built in Rostock, Germany, in mid 2011, and since then supplies a residential house with thermal energy.

Fig. 15. Construction of a thermally activated bore pile wall in Rostock, Germany. every second segment of the wall is thermally activated, as can be seen by the PE-pipes pointing out of the individual segments.

The results of a long-term simulation of the underground temperature development in a seasonal heating/cooling cycle are shown in the following Fig. 16 and Fig. 17, which depict summer winter cross section-views respectively. The simulation from which the pictures are derived was made with the specialised numerical software FEFLOW.

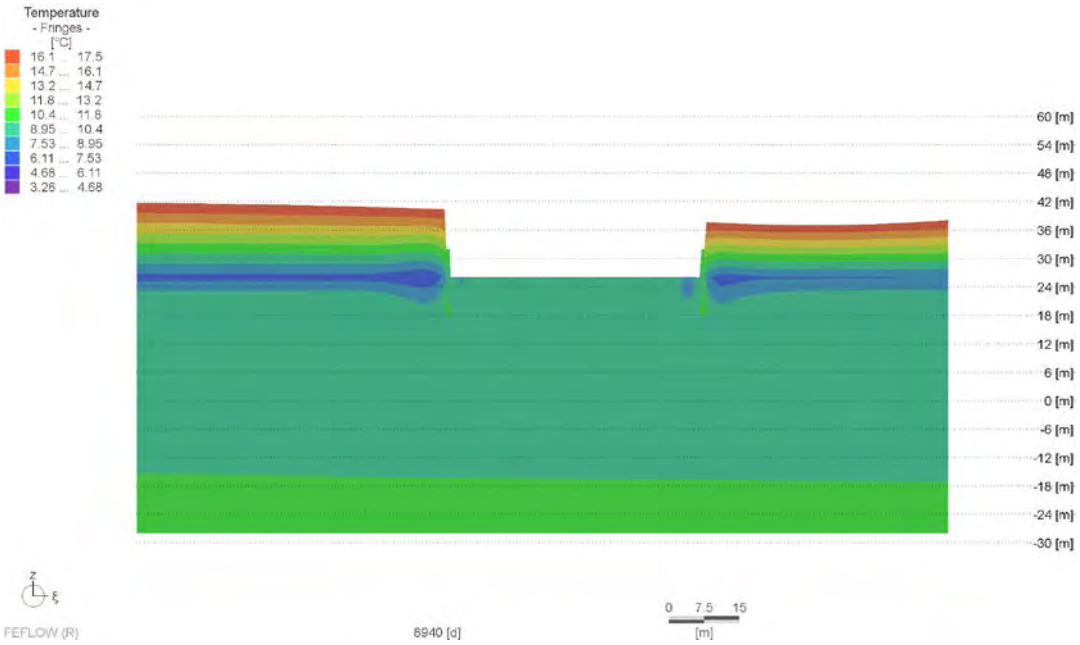

Fig. 16. Cross section through the building's fundaments (here: slotted wall) and the surrounding underground, summer, the effect of heat injection in the underground can be seen in the temperature distribution.

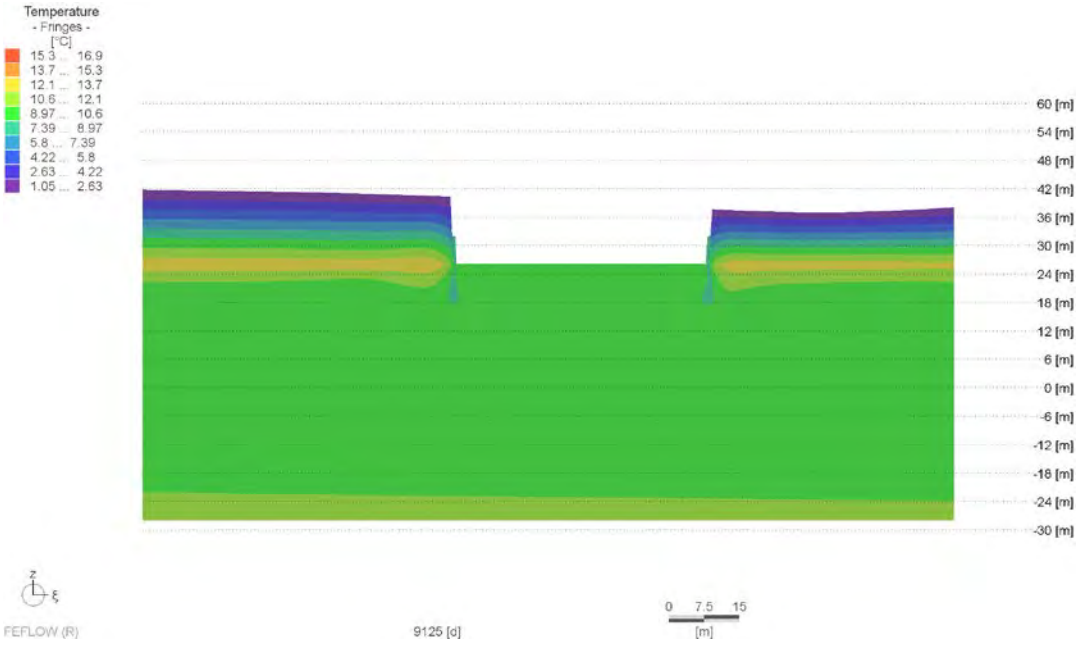

Fig. 17. Cross section through the building's fundaments (here: slotted wall) and the surrounding underground, winter, the effect of heat extraction from the underground can be seen in the temperature distribution.

2.2.3 Existing experiences and field tests with TAF

Principles of a Geothermal Response Test (GRT)

The Thermal Response Test (*TRT*), also referred to as Geothermal Response Test (*GRT*), is an accepted field method to determine the effective thermal conductivity of the underground (Fig. 18). When conducting a GRT, a defined power is injected in the underground. During the heating phase, all necessary parameters (e.g. inlet and outlet temperature, fluid volumetric stream and heating power) are monitored inside the device as well as inside the inlet/outlet pipes. For the evaluation of the test, the development of temperatures and the individual fixed parameters for each test are analysed calculative. As the main result a thermal conductivity of the underground is given out, which determines the yield for the planned thermal use.

When a GRT is conducted on the actual foundation, e.g. an energy pile, the quality of its thermal installation can as well be obtained from the GRT data. This allows for example conclusions regarding the thermal conductivity of the pile concrete or the internal spacing of heat exchanger pipes.

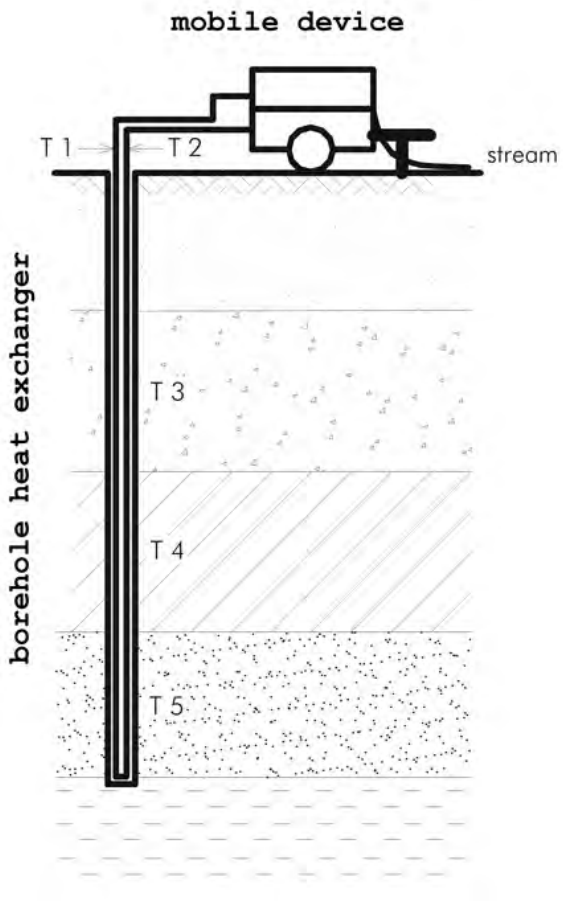

Fig. 18. Scheme of a GRT installation.

Task specific GRTs

For the purposes of the E-Hub project, several GRTs have been carried out and evaluated to compare the performance of different pile constructions in regard to their respective thermal pile resistance (see Table 3). This allows a first estimation of the decisive parameters for a good thermal performance of energy piles. The measured individual temperature behaviour of the tested piles is the determining factor when calibrating numerical or analytical thermal pile models.

Fig. 19 shows the setup of the GRT testing unit in Oldenburg. In addition to a standard GRT setup, temperature sensors were installed inside the energy pile as well as in a distance of 0.1 m respectively 0.6 m, thus allowing a measurement of the temperature development around the energy pile.

location (in Germany)	**date**	**pile diameter [m]**	**pile length [m]**	**spacing of heat carrier pipes [m]**	**λ of pile concrete [W/m·K]**	**λ geology [W/m·K]**	**pile resistance R_P [m·K/W]**
Oldenburg	12/2011	0.46	8.0	0.12	3.3	2.2	0.12
Kelheim	05/2012	0.9	15.0	0.7	2.0	1.6	0.07
Hamburg	05/2012	0.51	12.0	0.15	2.0	1.7	0.12
Nordenham	09/2012	0.5	18.0	0.22	1.7	1.4	0.09
Berlin	10/2012	0.46	9.0	0.12	1.7	1.2	0.25

Table 3. Geothermal Response Tests which were used for E-Hub purposes.

Fig. 19. Setup of the GRT and temperature measurement on the energy pile in Oldenburg. The metal box contains the GRT instrument; temperature sensors are located inside the pile as well as in two distances to it, visible here by the white PVC-pipes pointing out of the ground.

The thermal pile resistance is a sum parameter which describes the thermal quality of the energy pile installation. According to the data (Table 3) it seems to depend strongly on the thermal conductivity of the pile concrete as well as on the pile diameter and the spacing of the heat carrier pipes.

The temperature measurement data inside and outside of the energy pile in Oldenburg are shown in Fig. 20. Initial temperature is lower inside the energy pile probably due to the shallow installation depth of the sensor, which is located only 0.5 m underneath the pile head. As soon as the heat injection begins, a steep rise in the measured temperature is visible on the sensor inside the energy

pile. At a distance to the pile of 0.1 m the sensor shows a relatively fast response to the heat injection, while the most distant sensor merely documents a slight heating of the ground. Towards the end of the GRTs running time of 72 hours the two inner sensors are very even in the temperature they measure. The winter air temperature clearly cools the shallow sensor inside the pile.

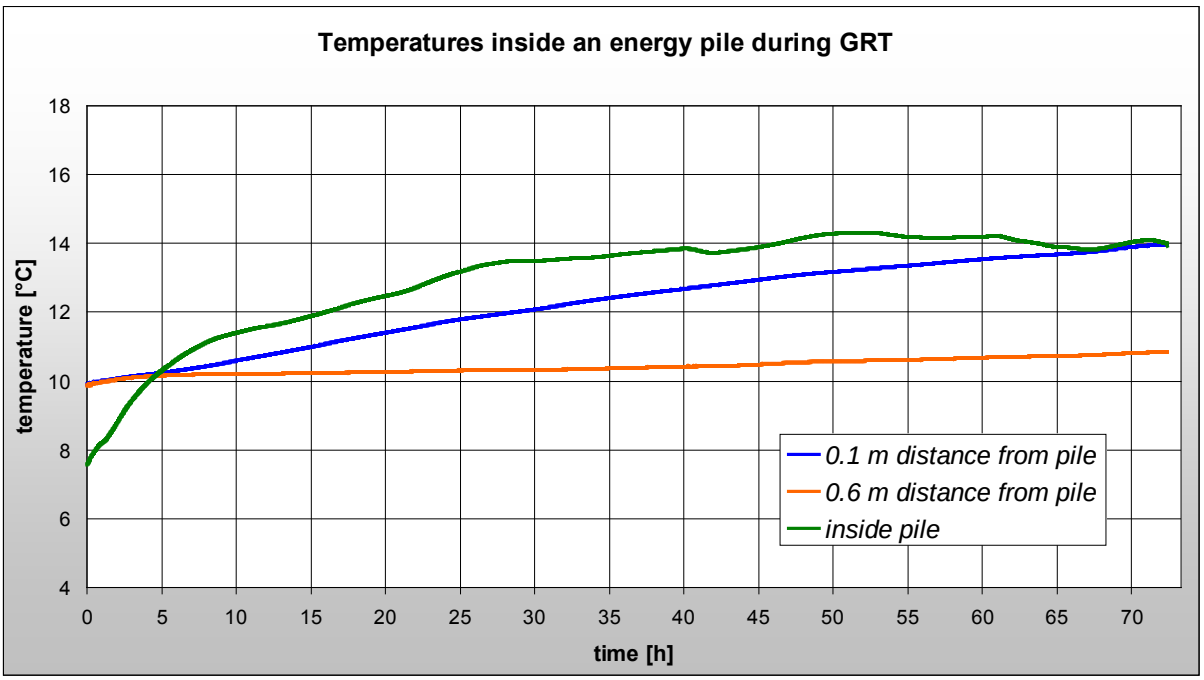

Fig. 20. Temperatures measured by Pt100 probes during a GRT inside and close to the pile.

2.2.4 Use of the GRT results to validate simulation models and give suggestions for a generalised energy pile model (Matlab)

In order to create an E-Hub simulation platform to balance the decentralized energy generation with these integrated renewable concepts and building/district energy demands, a common "language" has to be used. Commercial specific software output cannot be integrated easily into a global simulation environment. Because of that, simplified (but still accurate enough) models have to be created within a common framework. Matlab has been chosen as the language/software to integrate all the models and the control intelligence.

Matlab uses a different software approach than specialised geothermal software packages like EED or FEFLOW. Therefore it has to be compared to those for different load scenarios. Based on findings of that comparison, an iterative adaption of the Matlab model can be made, so that the Matlab model can process geological and thermal boundary conditions and thermal loads.

To achieve a plausible reconstruction of real conditions, the results of in-situ GRT measurements were used to validate EED- and FEFLOW-models (commercial software). Therefore it is, between others, necessary to obtain the individual constructive and material properties for the geothermal source system and to reconstruct that in the respective software. Fig. 21 and Fig. 22 show a comparison of resulting modelled temperatures with real data for one (exemplary) GRT.

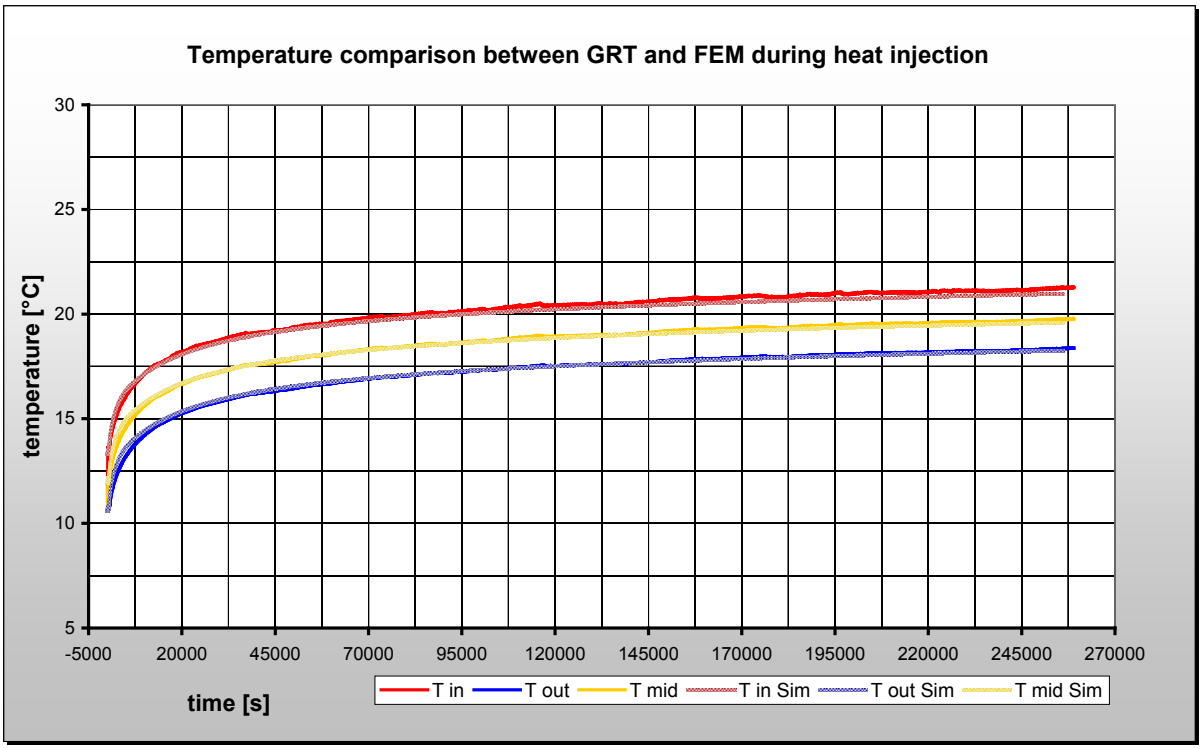

Fig. 21. Temperature comparison between the GRT and the FEM-model during heat injection. The solid lines are real GRT data; the dotted lines represent modelled temperatures.

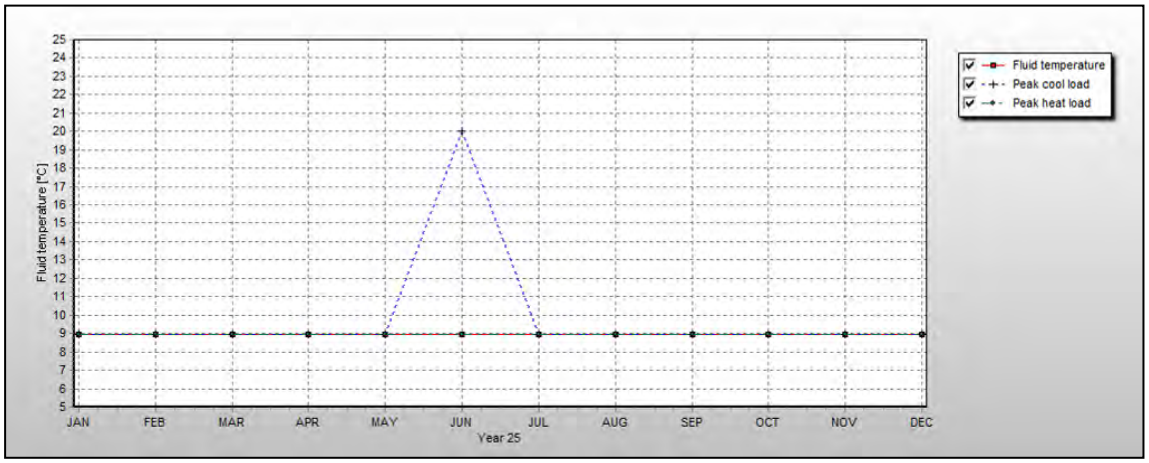

Fig. 22. Result of the EED-simulation of a GRT. Because of software limitations, only the medium peak fluid temperature for the GRT is given out in EED.

The two software outputs (EED and FEFLOW) have also been compared between each other to get the best possible results. EED allows a simplification in the approach to modelling both the constructive aspects of geothermal source systems and the thermal loads imprinted to those. As solutions are calculated analytical, results are obtained fast and reproducible. EED generally is in good agreement with much more complex calculations delivered by numerical thermo hydrodynamic models (e.g. FEFLOW, see Fig. 23, Fig. 24 and Fig. 25). Small temperature differences are system-immanent, as FEFLOW handles the input data “as is”, while EED uses an indirect approach containing certain safety assumptions.

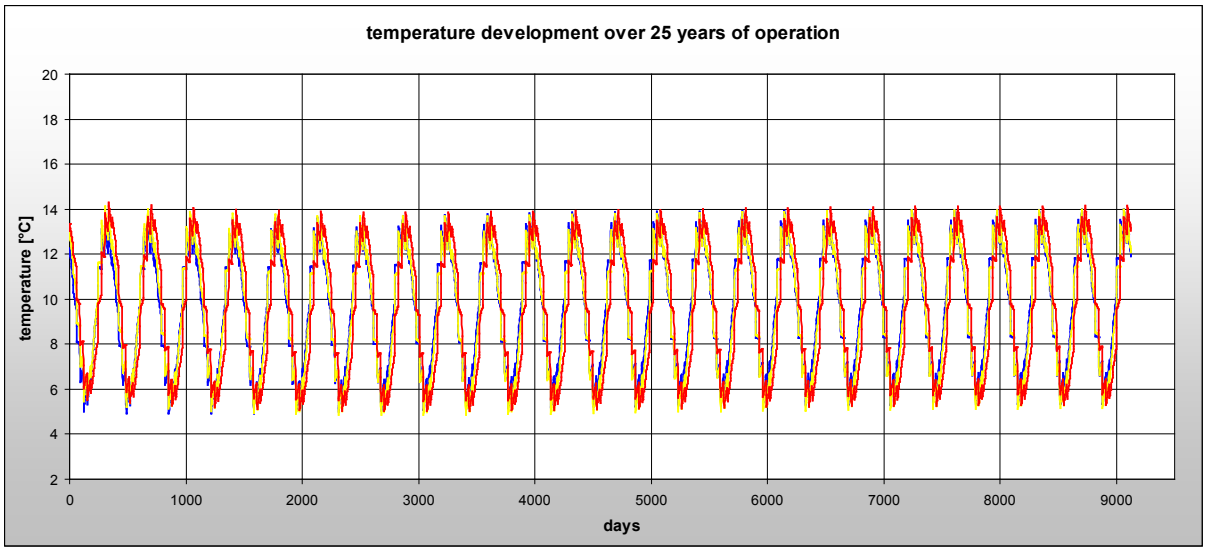

Fig. 23. FEFLOW - modelled mean fluid temperatures for a slotted wall over a period of 25 years (note: only base load, peak temperatures are not given).

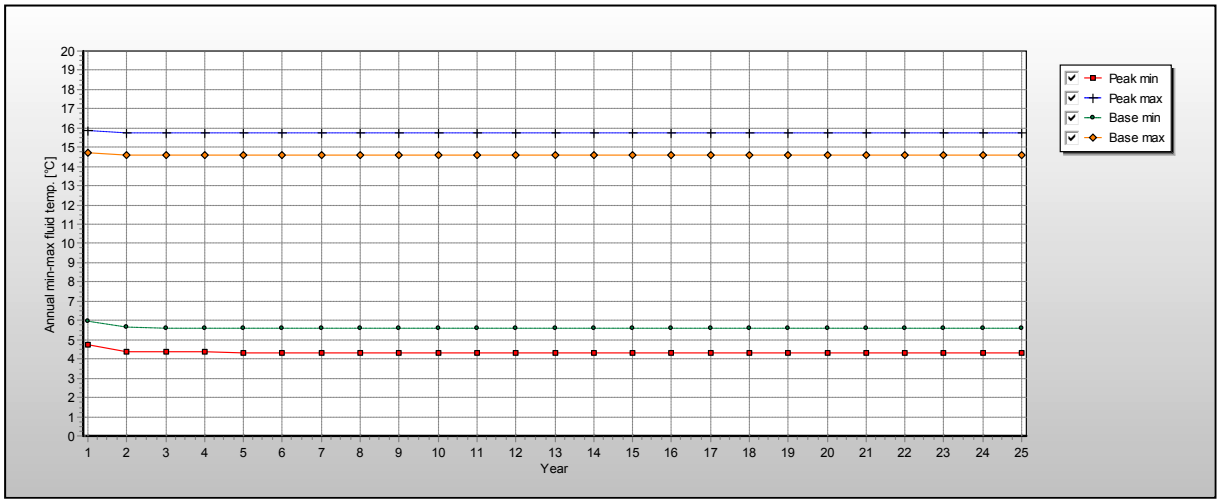

Fig. 24. EED - modelled mean fluid temperatures for the same slotted wall over 25 years (note: base load comparable, peak load is given as well).

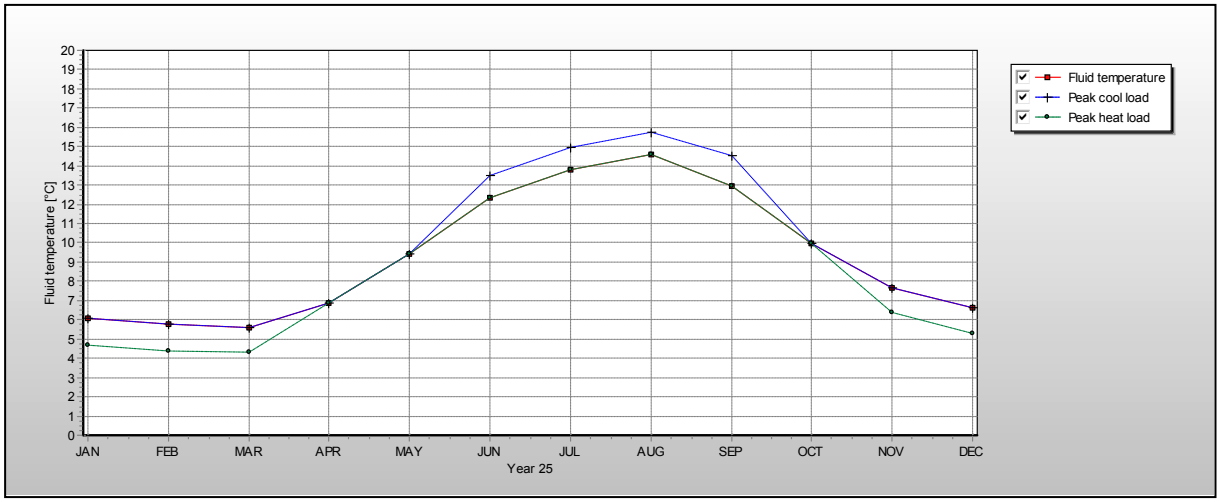

Fig. 25. EED - seasonal fluctuation of temperatures in the 25th year of operation for the slotted wall model.

The calibrated simplified EED-models are meant to contribute to the aggregated model because of the relative ease of comparison in the input data and the good software performance (calculation speed).

Simplified input parameters for the Matlab model have to be agreed upon. Those are the parameters an end-user has to put in to run the model. For easy accessibility the input options have to be chosen as short and simple as possible. The following inputs are proposed by HSW.:

- [region]

  maybe split each country in 3-4 climatic zones here

  (internally, an average underground temperature and a temperature load profile should be assigned)

- [geology]

  dry sand, wet sand, clay, bedrock etc.

  (internally, a thermal conductivity and heat capacity should be assigned)

- [average length of foundation piles]

- [average diameter of foundation piles]

- [number of foundation piles]

- [peak load and yearly work in heating and cooling mode]

All other parameters should be defined inside the model (i.e. operational temperature limits, load profile).

2.2.5 Investigation of optimized TAF design - Design studies with 3d-models

The experimentally calibrated commercial software models will not only be used for supporting the creation of TAF models in Matlab. They will be also used in order to evaluate new TAF designs that can perform better than standard layouts.

The most promising material parameters to be altered for the different model runs have, according to the state of the knowledge, been chosen to be piping material and construction concrete. The effect of these parameters was studied using highly detailed FEM-Software.

Material testing with a high discrete model (FEFLOW)

Some building projects have very specific demands considering boundary conditions, special materials or modes of operation. These projects often initiate technological development. The aim of this study is to take a closer look at some of the most promising innovations in the field of energy piles and evaluate their usefulness for practical application.

The FEM-Software FEFLOW allows detailed 3-dimensional modelling of the subsurface and numerical calculations of temperature developments over specified time spans.

The approach is described in the following. Originating from the detailed technical illustration of an energy pile, a detailed 3-dimensional model has been constructed. Fig. 26 and Fig. 27 show the horizontal discretisation of the respective model mesh. Vertical discretisation was achieved by the implementation of 28 horizontal slices with a mutual distance from 0.02 to 2.0 m between each other.

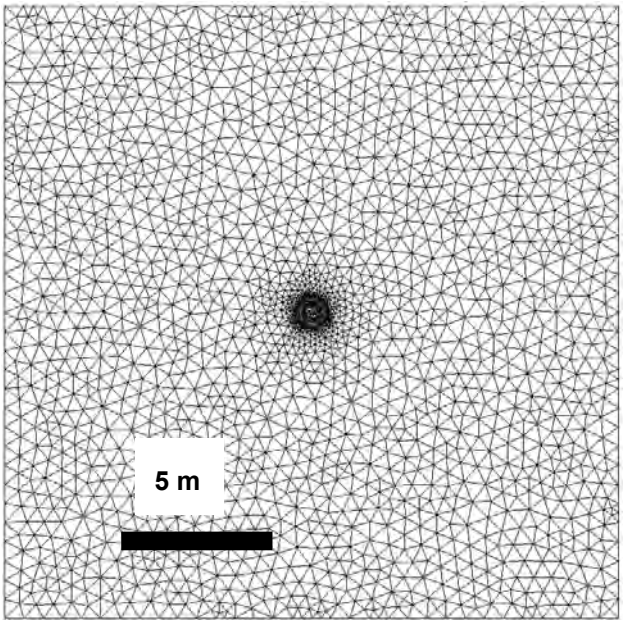

Fig. 26. Horizontal cross section of the model mesh for the energy pile model domain.

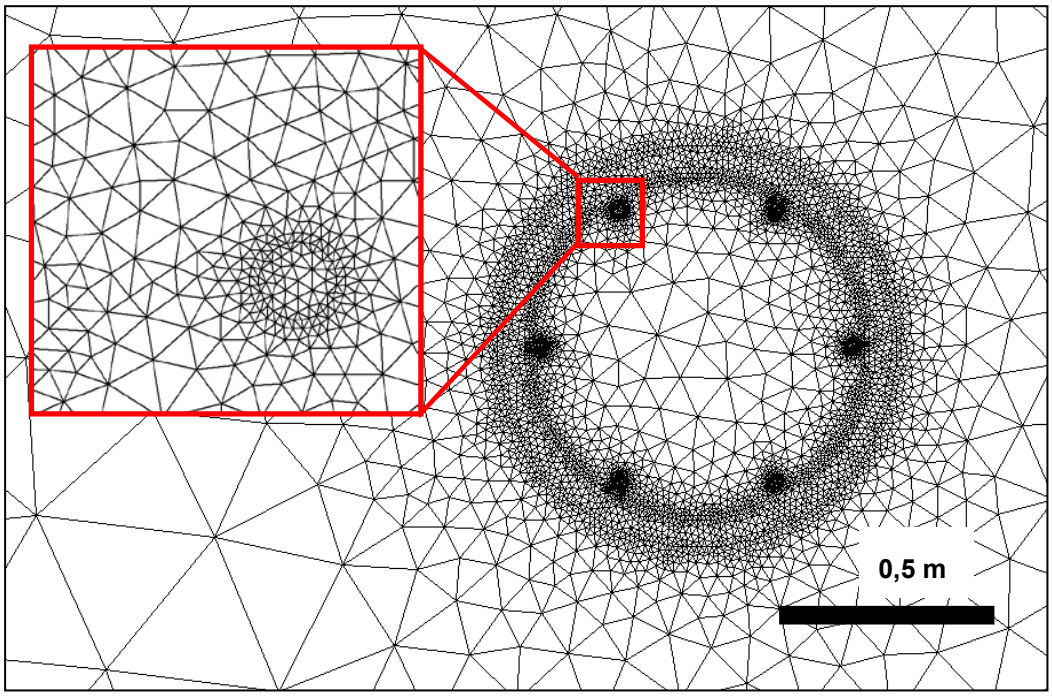

Fig. 27. Detailed discretisation of the model mesh for the energy pile model.

Each part of the pile, e.g. pile concrete, steel armament or pipe material, has been given its own properties and is interchangeable via the assignment of specific values for their mechanical and

thermal properties.

	horizontal hydraulic conductivity [m/s]	vertical hydraulic conductivity [m/s]	porosity [-]	heat capacity of fluid phase [MJ/m³ x K]	heat capacity of solid phase [MJ/m³ x K]	effective heat capacity [MJ/m³ x K]	heat conductivity of fluid phase [W/m x K]	heat conductivity of solid phase [W/m x K]	effective heat conductivity [W/m x K]
pipe inside	1.00E+00	1.00E+00	1.00	3.8	3.8	3.8	0.5	0.5	0.48
pipe wall	1.00E-15	5.00E-16	0.00	-	1.6	1.6	-	0.4	0.4
armament	1.00E-15	5.00E-16	0.00	-	3.1	3.1	-	60.0	60.0
pile body	1.00E-10	5.00E-11	0.10	4.2	1.0	1.3	0.6	1.6	1.50
geology - sand	1.00E-04	5.00E-05	0.40	4.2	1.5	2.6	0.6	3.3	2.22
geology - organic clay	1.00E-07	5.00E-08	0.60	4.2	1.5	3.1	0.6	2.5	1.36

Table 4 lists the underground and pile construction material properties. Note that two different parameter groups for the geology are given. They represent sandy underground as well as organic clay, which are typically very frequent close to the surface and/or represent relevant geologies for pile foundations.

	horizontal hydraulic conductivity [m/s]	vertical hydraulic conductivity [m/s]	porosity [-]	heat capacity of fluid phase [MJ/m³ x K]	heat capacity of solid phase [MJ/m³ x K]	effective heat capacity [MJ/m³ x K]	heat conductivity of fluid phase [W/m x K]	heat conductivity of solid phase [W/m x K]	effective heat conductivity [W/m x K]
pipe inside	1.00E+00	1.00E+00	1.00	3.8	3.8	3.8	0.5	0.5	0.48
pipe wall	1.00E-15	5.00E-16	0.00	-	1.6	1.6	-	0.4	0.4
armament	1.00E-15	5.00E-16	0.00	-	3.1	3.1	-	60.0	60.0
pile body	1.00E-10	5.00E-11	0.10	4.2	1.0	1.3	0.6	1.6	1.50
geology - sand	1.00E-04	5.00E-05	0.40	4.2	1.5	2.6	0.6	3.3	2.22
geology - organic clay	1.00E-07	5.00E-08	0.60	4.2	1.5	3.1	0.6	2.5	1.36

Table 4. Material properties used in the detailed energy pile model.

In the numerical model, material-related studies (in contrast to configuration-related studies) of the thermal energy pile performance can be conducted. Its single parts all influence the pile's ability to transfer thermal energy from the circulating heat carrier fluid over the heat-carrier pipes and the pile concrete towards the surrounding soil. A detailed cross-section of the energy pile construction which shows the different materials (here: thermal capacity of solid phase) is shown in Fig. 28.

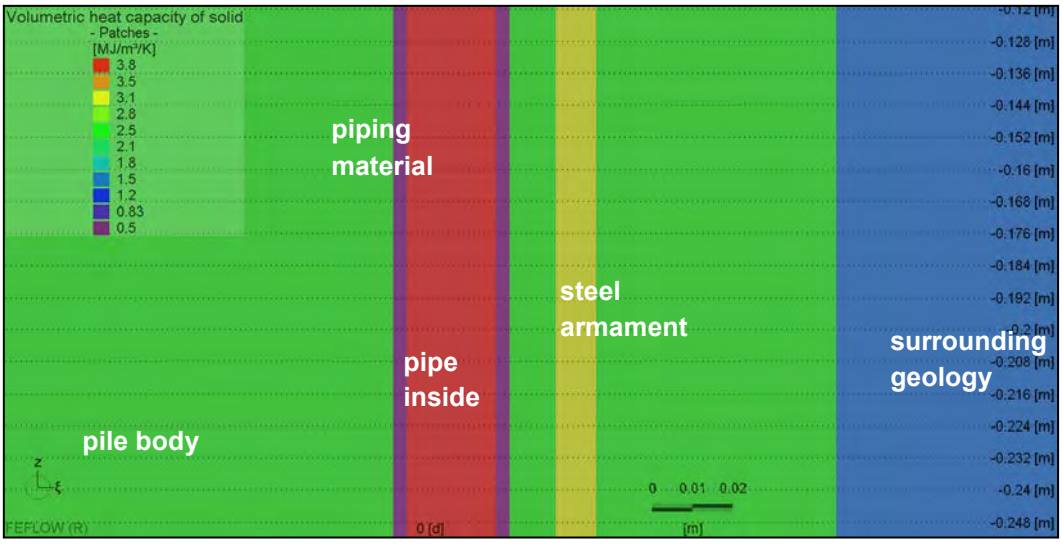

Fig. 28. Detail of the pile construction (cross-section) - the heat capacity of the solid material phase shows differences between the geology (blue), the pile concrete (green), steel armament (yellow), the heat pipe's wall (pink) and its interior (red).

For reference, ordinary energy piles consist of regular construction concrete and polyethylene pipes (PE100, PE-RC, PE-Xa), typically with a diameter from 25 to 32 mm. Energy piles are usually between 5 and 50 m long and between 0.2 and 2.0 m wide, depending strongly on the local geology and the static requirements of the building they support.

E-Hub partner SOLINTEL, who already has extensive experience with the investigation of thermally optimized materials for heat exchangers, suggested carbon fibre pipes to be tested as a substitution for ordinary PE-pipes. The analysis of steel pipes as heat exchanger materials leads back to German investigations, in which similar pipes have proven to be highly effective under certain conditions (GRT results on a steel BHE, HSW, 2009).

The second main parameter to be changed for the simulation runs is thermally enhanced concrete. Therein, the normal construction concrete is partly substituted by materials with a high thermal conductivity and thermal capacity. Quartzite and graphite are typical ingredients to fulfil this role. Thermally enhanced concrete already is in daily use in borehole heat exchangers because of its proven effectiveness especially under peak load conditions (high thermal loads in a relatively short time). Although not yet proven in practise, the theoretical improvements in thermal performance are significant.

In Table 5 the detailed material parameters are listed and Table 6 shows the setup (main interchangeable parameters) for the different test runs.

	horizontal hydraulic conductivity [m/s]	vertical hydraulic conductivity [m/s]	porosity [-]	heat capacity of fluid phase [MJ/m³ x K]	heat capacity of solid phase [MJ/m³ x K]	effective heat capacity [MJ/m³ x K]	heat conductivity of fluid phase [W/m x K]	heat conductivity of solid phase [W/m x K]	effective heat conductivity [W/m x K]
ordinary concrete	1.00E-10	5.00E-11	0.10	4.2	1.0	1.3	0.6	1.6	1.50
thermally enhanced concrete	1.00E-10	5.00E-11	0.10	4.2	2.5	2.7	0.6	3.5	3.21
ordinary PE pipe	1.00E-15	5.00E-16	0.00	-	1.6	1.6	-	0.4	0.42
carbon fibre pipe	1.00E-15	5.00E-16	0.00	-	1.3	1.3	-	1.5	1.50
steel pipe	1.00E-15	5.00E-16	0.00	-	1.6	1.6	-	60.0	60.00

Table 5. Detailed material parameters.

model run [#]	geology	piping	concrete
1	sand	polyethylene	regular
2	sand	carbon fibre	regular
3	sand	steel	regular
4	sand	polyethylene	thermally enhanced
5	sand	carbon fibre	thermally enhanced
6	sand	steel	thermally enhanced
7	organic clay	polyethylene	regular
8	organic clay	polyethylene	thermally enhanced

Table 6. Main interchangeable parameters for the model runs.

All simulation runs were conducted over a period of 3 days with a specific thermal load of 100 W/m. The temperatures were monitored at “temperature observation points” which have been placed inside the model. Fig. 29 and Fig. 30 show the temperatures inside the energy pile at the end of the simulation time.

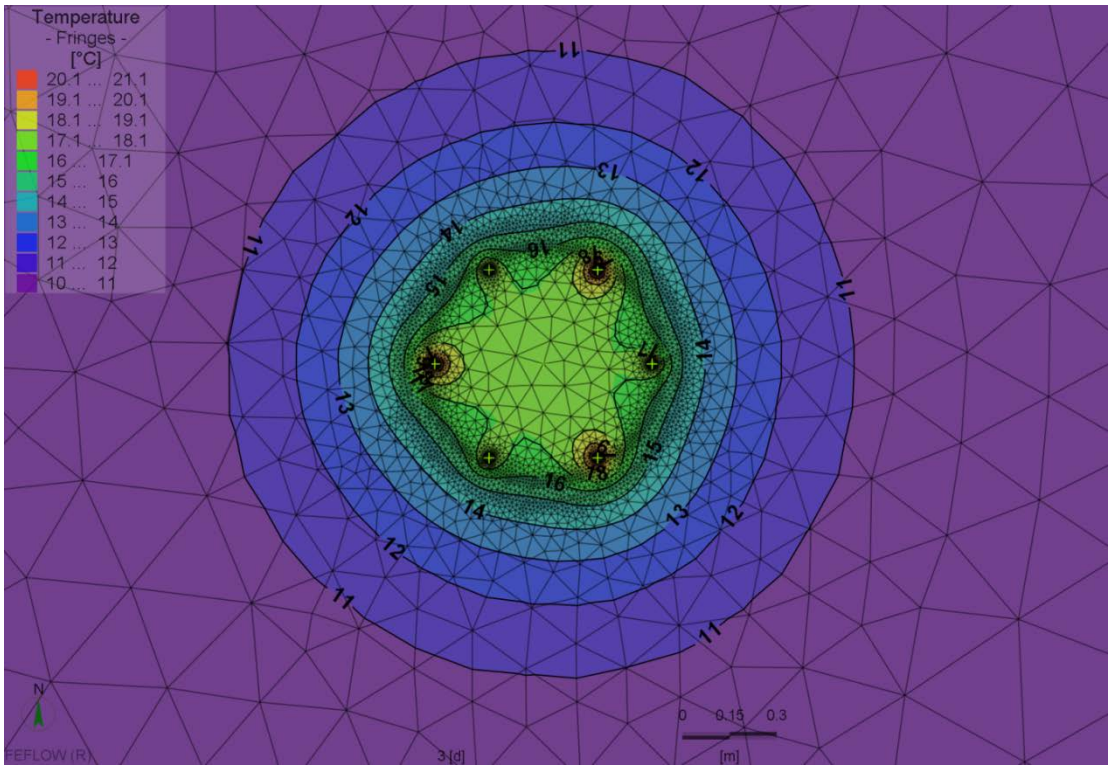

Fig. 29. Simulated temperatures after 3 days of heat injection (specific thermal load: 100 W/m).

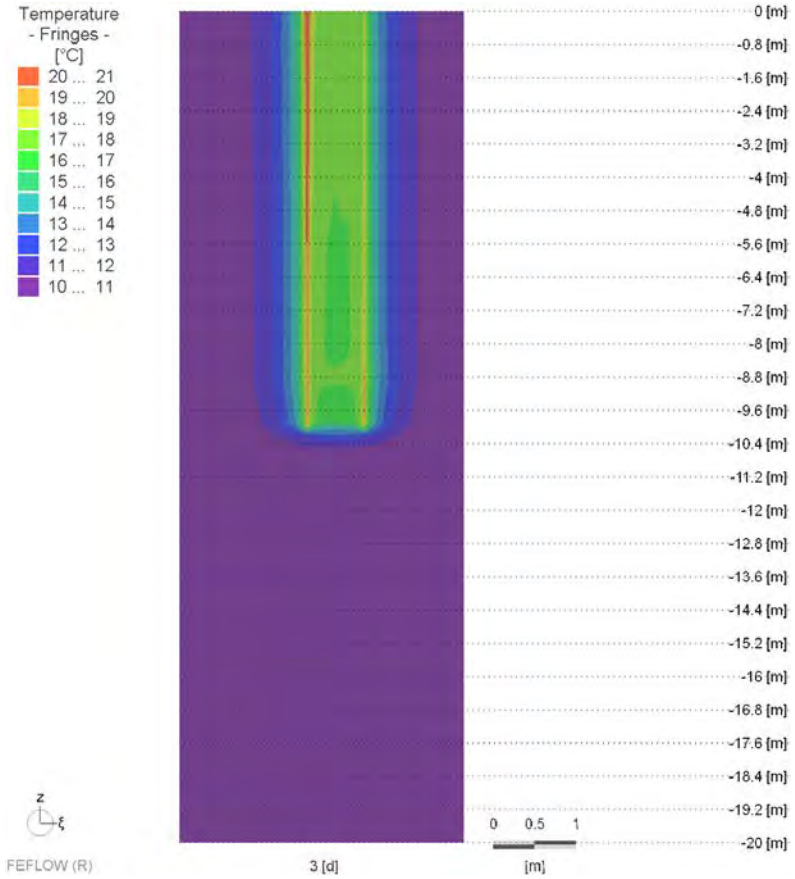

Fig. 30. Vertical Cross section of the energy pile after 3 days of heating (specific thermal load: 100 W/m).

Fig. 31 shows the temperature development inside the inlet and outlet heat exchanger pipe during simulation, for the model runs 1 & 4. The complete comparison of all the model runs can be found in Annex A.

All model runs show that the piping material has literally no influence on the performance of the energy pile system. Probably due to the very small diameter of the heat exchanger pipe wall in comparison to the complete energy pile the supposedly lower thermal resistance of carbon fibre and steel pipes in comparison to PE-material have only a negligible effect.

Thermally enhanced concrete, as used in simulation runs 4, 5, 6 and 8, however does influence the energy piles peak load performance significantly, as can be seen in Fig. 31. That seems highly plausible, as the concrete volumetrically represents the biggest portion of the complex system "energy pile".

Again, also when thermally enhanced concrete is used, the piping material seems to have no effect whatsoever, according to the numerical simulations.

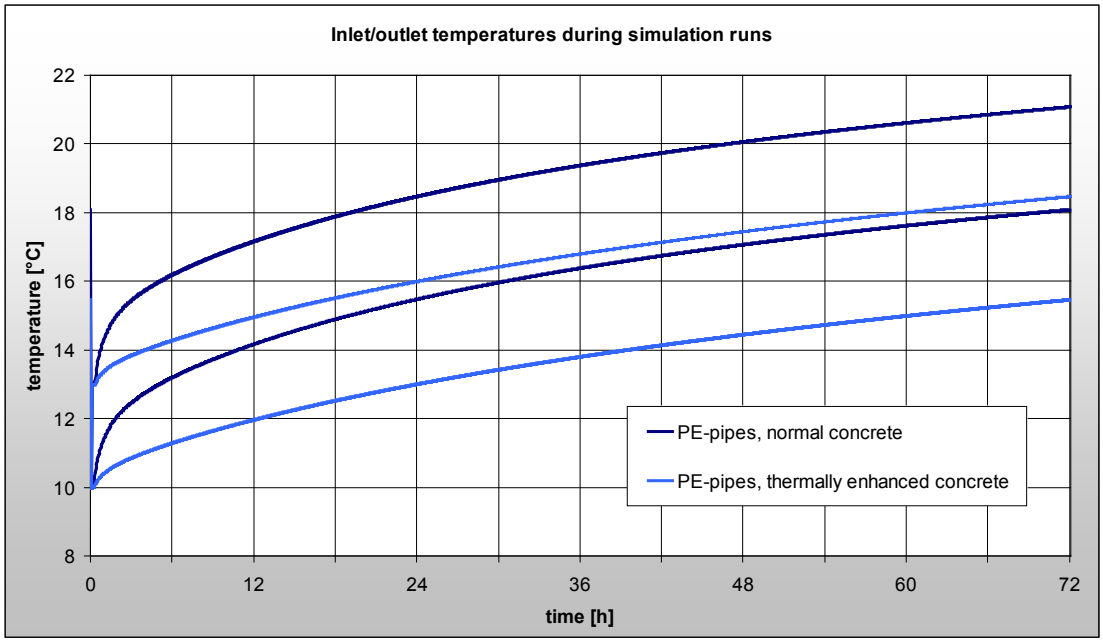

Fig. 31. The diagram above show the inlet and outlet temperatures of the heat exchanger pipes which were monitored during the simulation via observation points (model run #1 and #4).

The maximum mean temperatures inside the heat carrier pipes reach 19.6 °C (sandy underground) respectively 20.7 °C (organic clay underground) when normal concrete is used. With the use of thermally enhanced concrete the mean fluid temperatures peak at 17.0 °C (sand) respectively 17.8 °C (clay).

Testing energy piles with the BHE (Borehole Heat Exchanger) boundary condition (inside FEFLOW)

The fully discretized model that has been used until now by the FEM software is very time consuming, as the exact geometry of the piles and the embedded pipes has to be implemented. In this section, the use of the so-called BHE (borehole heat exchanger) boundary condition is going to be analysed. If the results are acceptable, this BHE condition will be used to speed up the creation of detailed models to calibrate the Matlab model and also to test new TAF designs that can perform better.

FEFLOW uses this boundary condition to define temperatures and hydraulics inside a model. The “BHE boundary condition”, as mentioned above, takes a bit of a special position as it implements a “sub-model” into the 3d model. Inside the BHE boundary condition it is possible to implement:

- Constructive parameters (borehole diameter, spacing of heat exchanger pipes…),

- Hydraulic parameters (type of heat carrier fluid, volumetric flow…) and

- Thermal parameters (initial temperature, thermal conductivity of grout, power difference…).

As this boundary condition is not specifically designed for energy piles, there exist limitations. So for example it was found that the maximum diameter for the BHE is limited to about 0.7 m, otherwise the numerical solution is erroneous.

One of the positive aspects of the BHE boundary condition is that it has a built-in temperature-logging function which allows a continuous monitoring. By this, the effects of material change etc. can be seen directly. Furthermore, parameters can be exchanged relatively simple via a special menu (Fig. 32).

Especially for the 3d-modelling of energy pile fields the use of BHE boundary conditions provides a massive advantage when model construction is regarded.

For comparative purposes an “Atlas”-pile (constructor: Franki piles) was rebuilt as a BHE boundary condition. Atlas-piles are a fairly common kind of foundation pile and have been used for the building projects in Oldenburg and Berlin.

Afterwards, the thermal load which was used for the Response Test was theoretically injected into the energy pile. Fig. 33 shows the temperature development during the GRT duration compared to the modelled temperatures over the same time. In this step, a calibration of the model has led to comparable and very satisfying results.

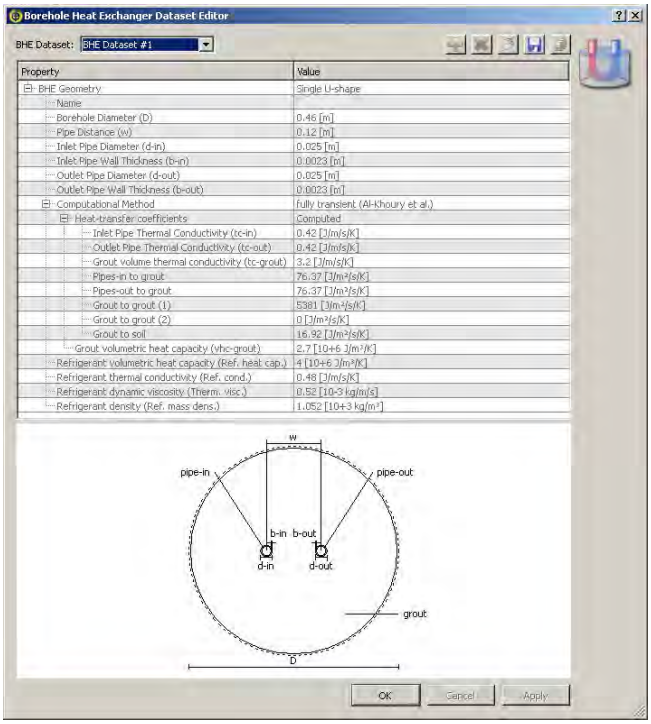

Fig. 32. BHE Dataset Editor for the FEFLOW used for energy pile simulation.

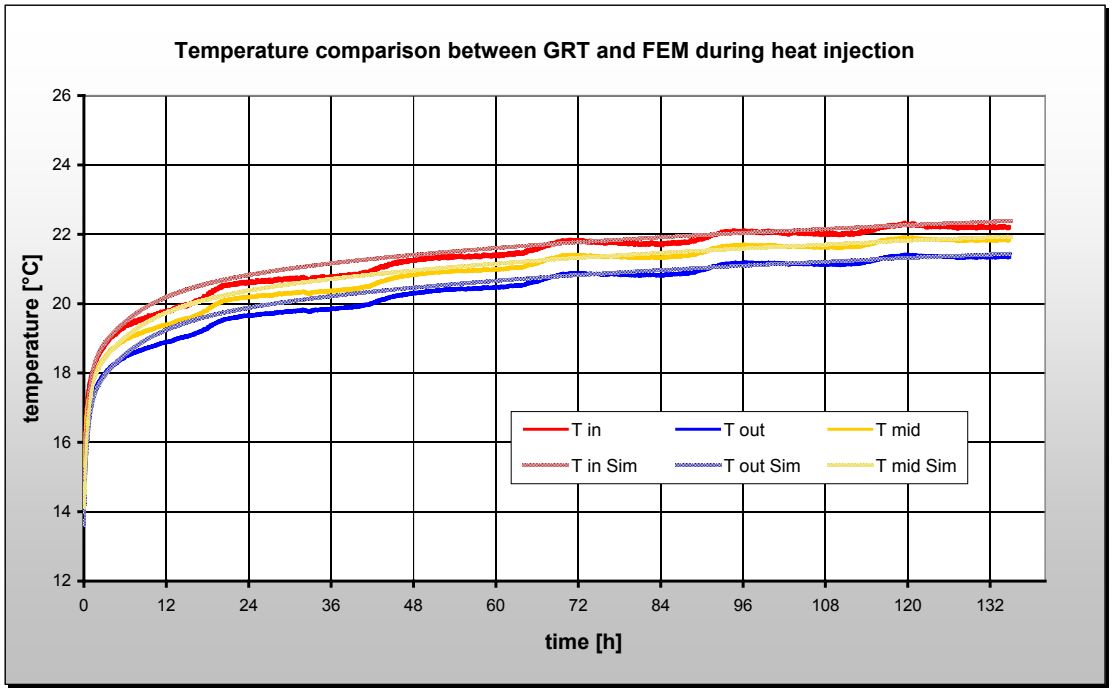

Fig. 33. Comparison of GRT data (solid lines) and the temperatures simulated by FEFLOW for an Atlas-pile via the BHE boundary condition (dotted lines).

The final temperatures after 5 days of simulated GRT duration are shown in Fig. 34 compared to Fig. 29, which shows the spatial temperature distribution for the high discrete model, the differences are clearly visible. The temperature here radiates from the centre of the pile in contrast to the highly discrete model, where the heat exchanger pipes are visible and act as such.

Despite of this simplified look, also the BHE model succeeds at predicting temperatures in good agreement with real GRT data. On bigger scales, the small temperature effects inside single piles become less relevant, thus further promoting the use of BHE boundary conditions for energy pile fields.

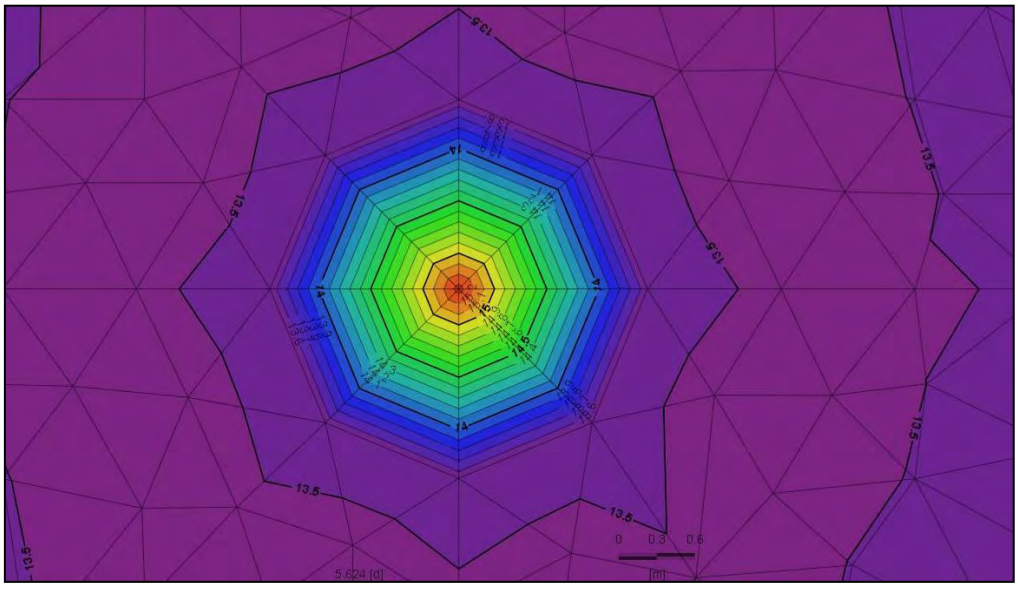

Fig. 34. FEFLOW - simulated temperatures after a heat injection of 5 days, which resembles the real GRT.

To test the BHE boundary condition for energy piles, also in this model the pile concrete has been switched to thermally enhanced concrete. Fig. 35 depicts the results of this test.

The maximum mean fluid temperature inside the heat carrier pipes reaches 21.8°C when normal concrete is used. With the use of thermally enhanced concrete the mean fluid temperature peaks at 18.5°C.

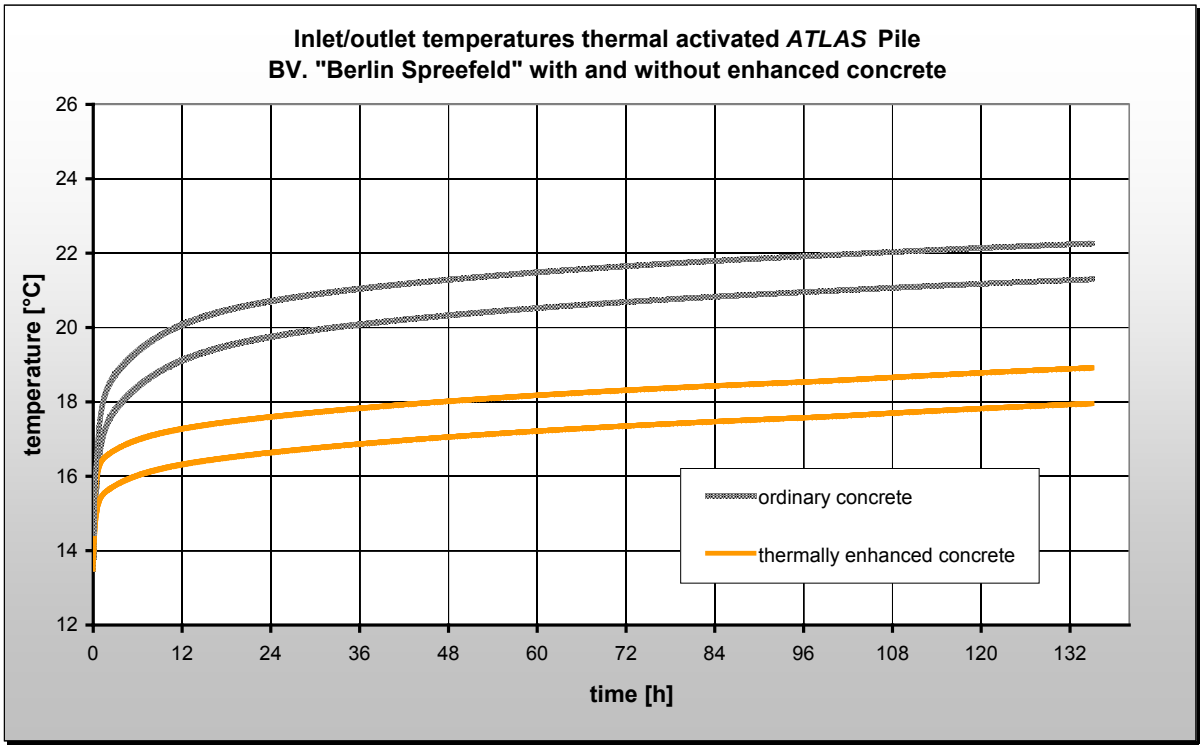

Fig. 35. Performance comparison, simulated with FEFLOW for an Atlas pile - simulated inlet/outlet temperatures for regular concrete are shown dotted and for thermally enhanced concrete in solid yellow.

Cost-benefit analysis for optimized TAF design

The numerical simulations were conducted for peak load conditions, where thermally enhanced components have proven to possess an increased effectiveness.

Main advantages over regular energy piles are therefore for peak load applications. For example it could be possible to use more powerful heat pumps and therefore cover bigger thermal loads. A second power source could become obsolete or be dimensioned smaller for some projects.

To give a quantitative estimation of the thermal improvement by using thermally enhanced concrete in the detailed model, the following formula was used:

$1-(T_{tec}-T_{ini})/(T_{nc}-T_{ini}) = 0.27$ (value obtained with FEFLOW + high detailed model) (1)

$1-(T_{tec}-T_{ini})/(T_{nc}-T_{ini}) = 0.40$ (value obtained with FEFLOW + BHE boundary condition) (2)

with T_{ini} = initial temperature, T_{tec} = temperature resulting from the use of thermally enhanced concrete and T_{nc} = temperature resulting from the use of ordinary concrete.

It can be concluded that the usage of thermally enhanced concrete leads to a performance improvement in peak load operation in the range of 25…40%.

Reliable economic decisions can only be made for individual projects. Despite of this, an estimation of the costs and benefits for the use of thermally enhanced concrete is given.

So called “steel fibre concrete”, available on the market for constructive purposes, comes closest to the thermally enhanced concrete used in the FEFLOW models. It is priced about 20 €/m³ higher than ordinary construction concrete for foundations (approx. 130 €/m³ vs. 150 €/m³). For the following it is assumed that this price difference is realistic for thermally enhanced concrete.

The following Table 7 gives a comparison of the estimated additional costs and resulting benefits for the use of thermally enhanced concrete in energy piles. The numbers clearly indicate that, if it is possible to make use of the potential performance gain, the additional costs for the use of thermally enhanced concrete can pay off directly.

	performance (higher = better)	**estimated costs (lower = better)**	**performance/cost (higher = better)**
ordinary concrete	100 %	**100 %** (130 €/m³)	100 %
thermally enhanced concrete	**127 - 140 %**	115 % (150 €/m³)	**110 - 122 %**

Table 7. Estimation of costs and benefits.

The additional specific costs (€/m) depend strongly on the constructive parameters of the energy piles, respectively the energy pile field. They range from about 2.5 €/m pile length for a pile diameter of 0.4 m to about 16.0 €/m pile length for a pile diameter of 1.0 m.

The realisation of the pay-off-effect however requires target-oriented planning from the beginning of the project to its construction.

2.2.6 Summary of results and conclusion

To sum up the results of the material testing via numerical simulations, the following conclusions can be drawn for the thermal activation of energy piles:

- Thermal effects of different piping material and pile concrete have been analysed individually as well as coupled for two different representative undergrounds and with two different methodological approaches (highly detailed, BHE boundary condition),

- The use of thermally enhanced piping material has, according to the simulation runs, no measurable influence on the thermal performance of the energy pile,

- This effect remains unchanged even when thermally enhanced concrete is used,

- Thermally enhanced concrete significantly increases the performance of energy piles in peak load operation, seemingly independent from the geology; the resulting effect can be as high as 25…40 %. While reliable economic decisions can only be made for individual projects, it can generally be said that additional costs for the use of thermally enhanced concrete can pay off directly.

There has been a significant increase in the realisation of building projects utilising thermo-active construction parts in recent years. Valuable experience has been obtained in the construction of thermo-active foundations and in related individual technical solutions.

Thus it is safe to say that energy piles and other thermo-active components with ground-contact will continue to gain importance for upcoming building projects. For future energy networks between

buildings the possibility of seasonal thermal energy storage, as it can be delivered by TAFs, will become increasingly important. Discussions about connecting TAFs with thermally activated infrastructure areas, such as streets and sidewalks, but also with buildings facades appear realistic.

Still, there is a significant open potential in the technical development of TAFs, for example by combining different systems (e.g. with air heat absorbers or solar thermal systems).

2.3 District network to interconnect thermo-active foundations

2.3.1 Introduction and task specific approach

The key idea for the E-Hub project is the distribution of the available energy between the network participants. The respective energy demands and supplies are internally balanced and then allocated via the monitoring and control system.

According to the E-Hub idea, in this deliverable the goal is the definition of a hydraulic low-temperature piping network, in which a market-oriented distribution of thermal energy demand and supply is possible. Therefore all potential sources of low-level thermal energy as well as all buildings have to be interconnected via the network.

For geothermal energy, provided e.g. by thermo-active foundations (TAF), such a demand and supply oriented distribution has to account for a) the type of energy - low temperature thermal energy, b) the transport medium (brine, water), c) geographical distances between supply and demand and d) the state of the art.

The basic considerations for the design of a network able to interconnect thermo-active foundations can be found in Annex B.

2.3.2 Design of a low temperature thermal energy distribution network

Foregoing considerations

A holistic approach must consider the low temperature level of geothermal source systems from the beginning of planning efforts. Therefore, a shared distribution network with other higher level temperature sources is highly unlikely to be feasible. Geothermal source systems generally require a good connection to the heating system, because already small temperature losses during transport will lead to a reduced efficiency of the heating/cooling system.

There are certain limits to the maximum temperature changes which are acceptable for the underground. These limits are e.g. given by the system itself (operation boundary of heat pumps), by static demands (usually temperatures under 0°C are not allowed for TAF) or by authorities (max. deviations from undisturbed temperature levels, proportion of heat injection and extraction).

Generally, several participants can share a geothermal source system and fluctuating demands can be balanced between each respective building. If it is not possible (in existing buildings) or otherwise undesirable to install geothermal source systems for a respective building, despite of this geothermal source systems can be used via so called “low temperature district heating network” to deliver thermal energy.

The same technological foundation allows a synergetic dual usage of geothermal source systems. Building concepts mainly requiring heating (residential buildings) and building concepts requiring large amounts of cooling (commercial and office buildings) can complement one another and use a geothermal source system efficiently as a coupled heat and cold storage. Seasonal or alternating use of geothermal energy sources for heating and cooling purposes both lead to a sustainable stable temperature regime in the underground and thereby to a maximum yield of energy (for further information on seasonal heat storage see deliverable 2.3).

Furthermore, TAF can be utilized to preheat or pre-chill the inflow of other heating or cooling systems. In converse argument it is as well possible to increase backflow temperature for TAF via second heat sources to increase the TAFs thermal load and avoid temperatures below the systems specifications.

Specific premises

The following premises are true for “low temperature district heating networks”, as they could potentially be realized together with the E-Hub regulation system:

- Temperature losses during thermal energy transport have to be minimized. Hence, the thermal energy should preferably be transported in a “low grade” as extracted from the underground. Transporting higher temperatures (“high grade”, raised by heat pumps) will potentially result in higher temperature losses during transport.

- Piping length has to be kept as short as possible to avoid losses of thermal energy during transport.

- A hydraulic design of the pipes must adhere to different load and demand scenarios.

- The control and regulation installations should be designed considering an implementation inside the E-Hub system. That means that all data has to be accessible for E-Hub and be provided in a usable format.

Choice of model district

Model district 4 (D2.3), located in Amsterdam, was chosen to build an exemplary low temperature district heating network. It contains five buildings with a ground area of 6,500 m² in a total area of 16,500 m². The five buildings are composed of two multi-level residential houses, a large retail centre and two office towers.

Fig. 36 shows the district as it will be used for further considerations. Important criteria for the choice of the model district are the (relatively young) age of the buildings and their usage. Following factors are crucial:

- In younger buildings, heating systems are often designed to operate with relatively low fluid temperatures, which is essential for an economical heat pump operation.

- Economically and technically, thermo-active foundations are only suited for newly constructed buildings.

- Thermal insulation norms are better in younger buildings which leads to a more advantageous proportion of the size of the thermal source system in relation to the buildings thermal energy demand.

- A widespread distribution of usage (living, retail stores, and offices) is further beneficial for the use of thermo-active foundations. This is because a good mixture of heating and cooling demand possibly leads to a balanced thermal yield of the underground.

So in summary, a district with good prerequisites for the use of TAF has been chosen. This way, a widely connected and efficiently used network can be achieved. The principles which are used for designing the specific network for district 4 are generally assignable to the other model districts as well.

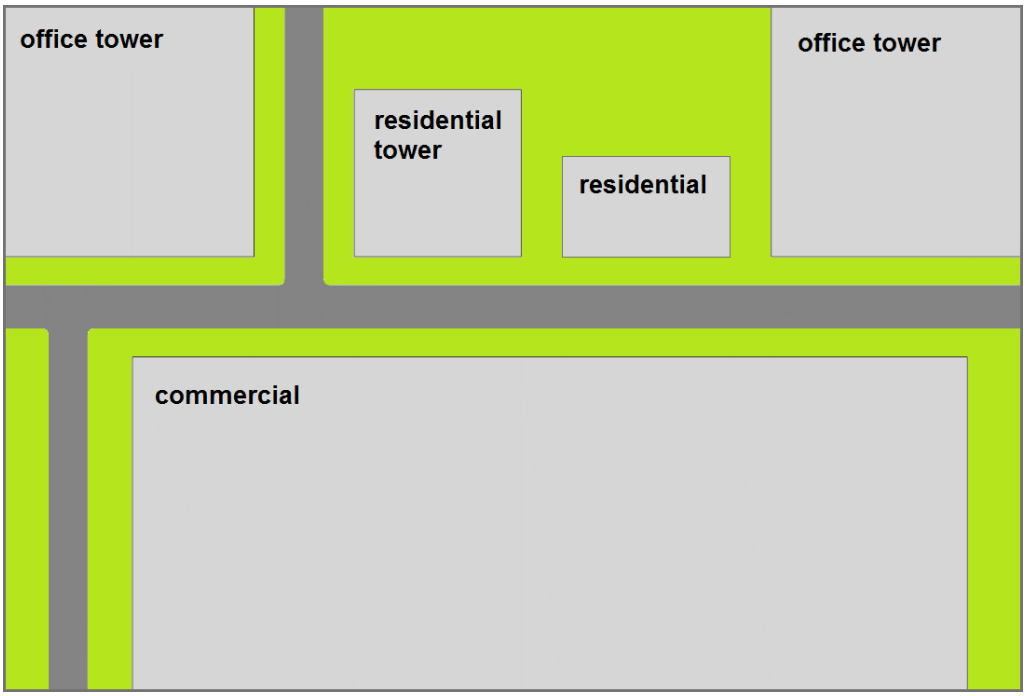

Fig. 36. district model schematic for district 4 as seen from above.

Thermo-active foundations as thermal source systems

The buildings inside the model districts and the respective site geology have been evaluated with respect to their potential for thermo-active foundations. Table 8 shows the input data for an estimation of the constructive parameters of energy piles, respectively the available area for thermally activated base plates. Note that this table has been reworked comparing to the version used in deliverable 2.3 to fit in a thermally active base plate for the retail building.

District 4, Amsterdam		near-surface geology: peat, clay, sandy glacial sediments at 10, 20, 35 m depth to water table: 0-5 m						
building	**building [#]**	**area [m²]**	**height [m]**	**pile distance [m]**	**pile depth [m]**	**pile diameter [m]**	**total piles [#]**	**activated foundations [m²]**
1 residential	1	240	18	4	15	0,8	24	0
2 residential tower	1	400	25	5	30	1.5	25	0
3 retail flat long	1	4000	10	-	-	-	0	3600
4+5 office tower	2	900	48	5	45	1.5	98	0

Table 8. Input parameters and resulting constructive parameters for TAF.

The thermal activation of the foundation piles with a diameter of 0.8 m should be realized in a 3 u-pipes setup and in a 5 u-pipes setup for the piles with a diameter of 1.5 m. The u-pipes are directly connected to the horizontal connection pipes. Depth of thermal activation is about 1-2 m less than the total pile length for constructive purposes and to avoid damage to the heat exchanger tubes while pouring of concrete.

90% of the base plate area of building no. 3 is considered usable for a thermal activation with heat exchanger pipes due to elevator shafts, sanitary and other installations that penetrate the base plate. All heat exchanger pipes are considered to consist of PE 100-RC material and have an outer diameter of 25 mm.

Further source systems to be implemented into the network

Often it is meaningful to use more than one thermal source system in bigger building projects. But it is not always meaningful to interconnect these systems via the same distribution network. Because geothermal source systems, which include TAF, have relatively special prerequisites, in the following a short overview of possible system combinations in a combined distribution network is being given.

On the one hand, low temperature thermal source systems (BHE, road collector etc.) and storage systems (Aquifer Thermal Energy Storage, Borehole Thermal Energy Storage) can possibly be connected with benefit. On the other hand, sources which can input excess heat into the network or into a thermal storage are useful (solar thermal).

Generally it is not meaningful to combine geothermal source systems with either high temperature source systems (gas- or oil boiler) or further base load systems usually operating with higher temperature levels (co-generator, district heating). There are, of course, exceptions to these general rules taking into account special demands of building-owners, which have to be discussed on each project.

Building circle pipe dimensioning and pressure drops

Generally speaking, geothermal source systems are designed cascading. Starting with single pipe circuits inside the energy piles respectively in the TAF, the hydraulic flow increases, together with the pipe cross section. So the biggest pipe diameter, where the whole volumetric stream of the heat pump occurs, is the collecting pipe right before the heat central respectively the main collector and distributor pipe.

For the dimensioning of these pipes, pressure drops inside the hydraulic distribution have to be calculated. Those occur in every hydraulic system and basically depend on the pipe diameter, volumetric flow, flow resistance inside the pipe (including narrow parts, curves and turns) and total flow length. Hydraulic parameters of the heat carrier fluid and topography influence pressure drops as well. For the energy pile source underneath the office towers and for the thermally activated base plate beneath the commercial building a detailed calculation of pressure drops has been undertaken:

Energy pile system underneath the office towers:

max. volumetric stream: 40 m³/h

max. length of collector/distributor pipes: 50 m (Ø 125 x 11.4 mm)

collector/distributor: pressure drop flat 0.1 bar

max. length horizontal connection: 100 m (Ø 50 x 4.6 mm)

individual energy pile circuits: 20 (2 m³/h per circuit)

length of single U-pipe per pile: 90 m (Ø 32 x 2.9 mm)

heat carrier fluid:

- concentration of antifreeze: 25 % (freezing point ~ - 14 °C)
- density: 1,052 kg/m³
- temperature of interest: 0 °C
- viscosity at 0 °C: ca. 0.052 kg/m·s

total pressure drop: 0.37 bar

Thermo-active foundation underneath the retail building:

max. volumetric stream: 20 m³/h

max. length of collector/distributor pipes: 100 m (Ø 50 x 4.6 mm)

collector/distributor: pressure drop flat 0.1 bar

max. length horizontal connection: 40 m (Ø 25 x 2.3 mm)

individual pipe circuits: 99 (0.2 m³/h per circuit)

length of single pipe circuit: 200 m (Ø 25 x 2.3 mm)

heat carrier fluid:

- concentration of antifreeze: 25 % (freezing point ~ - 14 °C)
- density: 1,052 kg/m³
- temperature of interest: 0 °C
- viscosity at 0 °C: ca. 0.0052 kg/m·s

total pressure drop: 0.32 bar

Those pressure drops have to be taken into account when choosing the heat pumps and/or circulation pumps for the thermal source system.

The following pipe dimensions are used in the district networks source cycle:

Energy pile system (office towers):

- 32 x 2.9 mm tor thermal activation
- 50 x 4.8 mm for the horizontal connection
- 125 x 11.4 mm for the collector/distributor pipes

Thermo-active foundations (commercial building):

- 25 x 2.3 mm for the thermal base plate activation
- 25 x 2.3 mm for the horizontal connection
- 50 x 4.8 mm for the collector/distributor pipes

2.3.3 Demand oriented heat distribution

Premises and possible distribution setups

In the following, the two most efficient and practically proven ways of balancing thermal energy on a district level are described. The first variant uses a single heat pump room inside a centrally located building, from which “refined” thermal energy is distributed towards the demanding buildings around. A second variant consists of two separate (but connected) networks over which the “unrefined raw energy” is gathered and then distributed towards the heat pumps inside the single buildings.

For both kinds of networks it is possible to retain more or less constant temperature levels inside the brine circuit, if heating and cooling occur either simultaneous or alternating. But even in single sided heating or cooling mode a spreading of the thermal loads over the different sources leads to a buffering effect of peak loads.

An additional section is devoted to the extension of the supply with thermal energy from a source area to an area without geothermal sources, e.g. another district.

Variant 1 - „warm“ local heat distribution

The source systems are connected to each other via connection pieces and enter the heat pump central together via a big collector pipe. Inside, cascading reversible heat pumps operate according to the buildings' demands.

From the heat pumps isolated distribution pipes for the “refined” energy run towards all connected buildings. There exist two separate sets of pipes for the buildings with heating and cooling demand, while simply heated buildings only require one set of pipes (Fig. 37).

This way it is possible to limit the house-sided installations to one heat pump central, which in total leads to a reduced effort for installation and maintenance.

Another advantage of this solution lies in its possibilities to cover bigger thermal loads per building than would be possible for the building's own geothermal source system. It only must be assured that the maximum load of the heat pumps does not exceed the combined capabilities of the thermal sources.

As the only downside of this variant are the possible temperature losses, it is generally preferable over other variants wherever applicable. The temperature losses can relatively easily be reduced by applying thermal insulation.

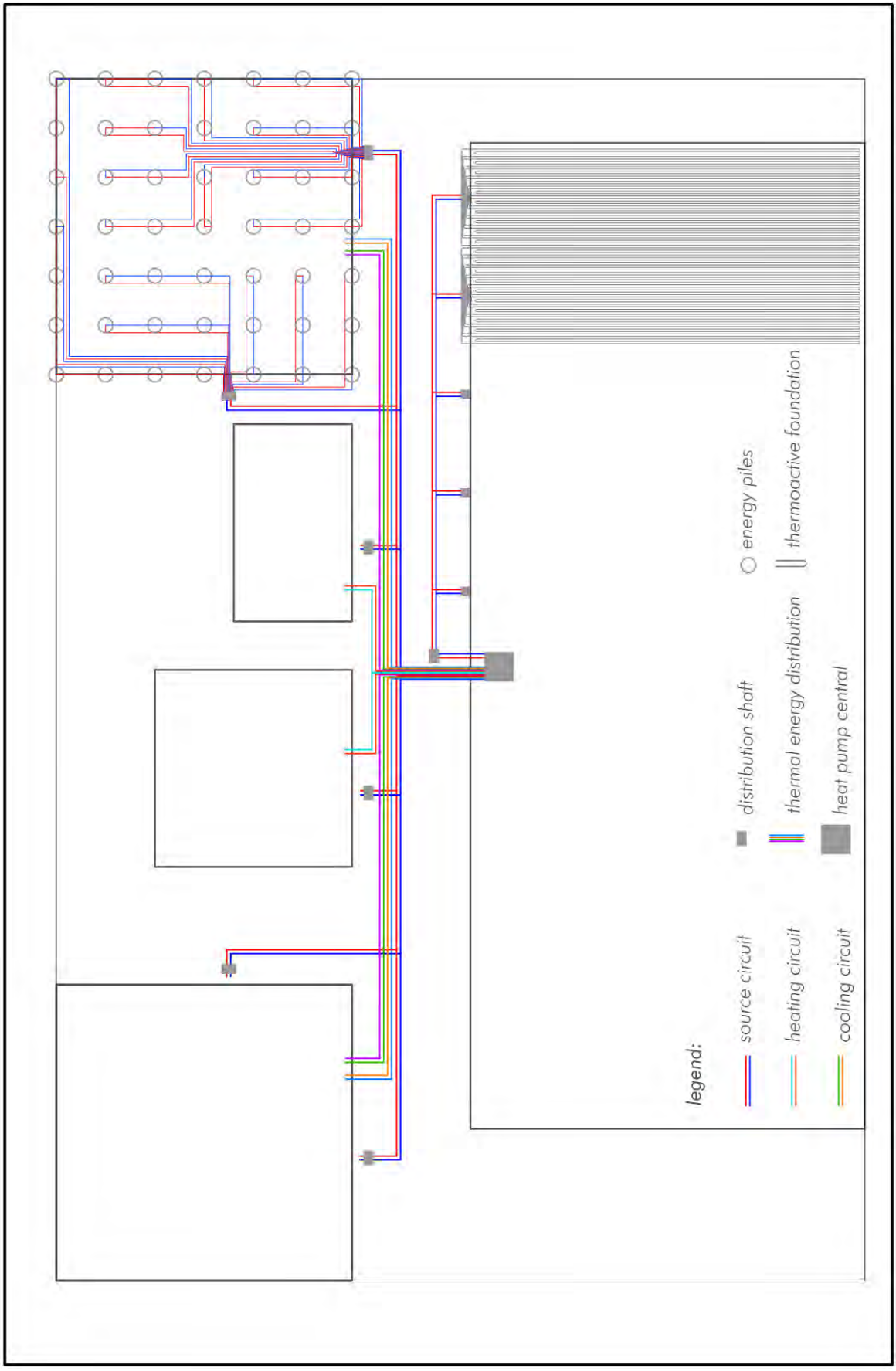

Fig. 37. piping network for variant 1 with centrally located heat pumps.

Variant 2 - „cold“ local heat distribution

The piping network for a „cold“ district thermal energy distribution is split into a source and a distribution network, which are hydraulically coupled via connection pipes (see Fig. 38). Because of this hydraulic connection of all pipes it is crucial to ensure equal pressure drops inside the source circuits (building circuits).

The heat pumps inside the separate buildings should altogether not exceed the thermal capabilities of the energy pile or thermo-active foundation field as a whole.

An advantage of this variant can be seen in the fact that, because of the overall low temperature level, the potential temperature losses over the pipe system can be kept low.

If not all heat pumps are operating, very low flow rates in the main pipes are possible for this setup, which possibly leads to relatively large temperature spreads in the brine circuit.

Distribution of thermal energy over bigger distances

There are certain upper limits to the distance between shallow geothermal source systems and energy consumers. Those depend, amongst others, on the size of the source system, the modes of operation and on the specific technology at hand. Generally, the bigger the distance between source and demand is, the more planning effort has to be put into the connection between both.

There are two major options. First, it is possible to minimize energy losses during transport. Therefore, thermal insulation of the piping should be considered. As losses generally increase with higher temperature differences, unrefined source fluid temperatures provide way better prerequisites for transport. Hence, the heat pumps should be installed close to where the energy is required.

The second option uses the relatively constant underground temperatures below the subsurface as an extension of the energy source in itself. The large diameter connection pipes can serve as a horizontal trench collector. Of course, in this case it is also necessary to have a heat pump installed at the location of the thermal energy demand. It is reasonable to install the fluid transport pipes as deep as possible to minimize the atmospheric thermal influence on the fluid temperatures. Thermal insulation is not desirable as it contradicts the base idea.

Centrally installed heat pumps for several buildings are certainly attractive due to lower installation and maintenance costs compared to individual heat pumps. However, the higher thermal losses with increasing distance can deny the good seasonal performance factors and the more economic investment cost of central heat pump installations.

Therefore, unrefined source energy should be used for medium to large distance thermal energy transport.

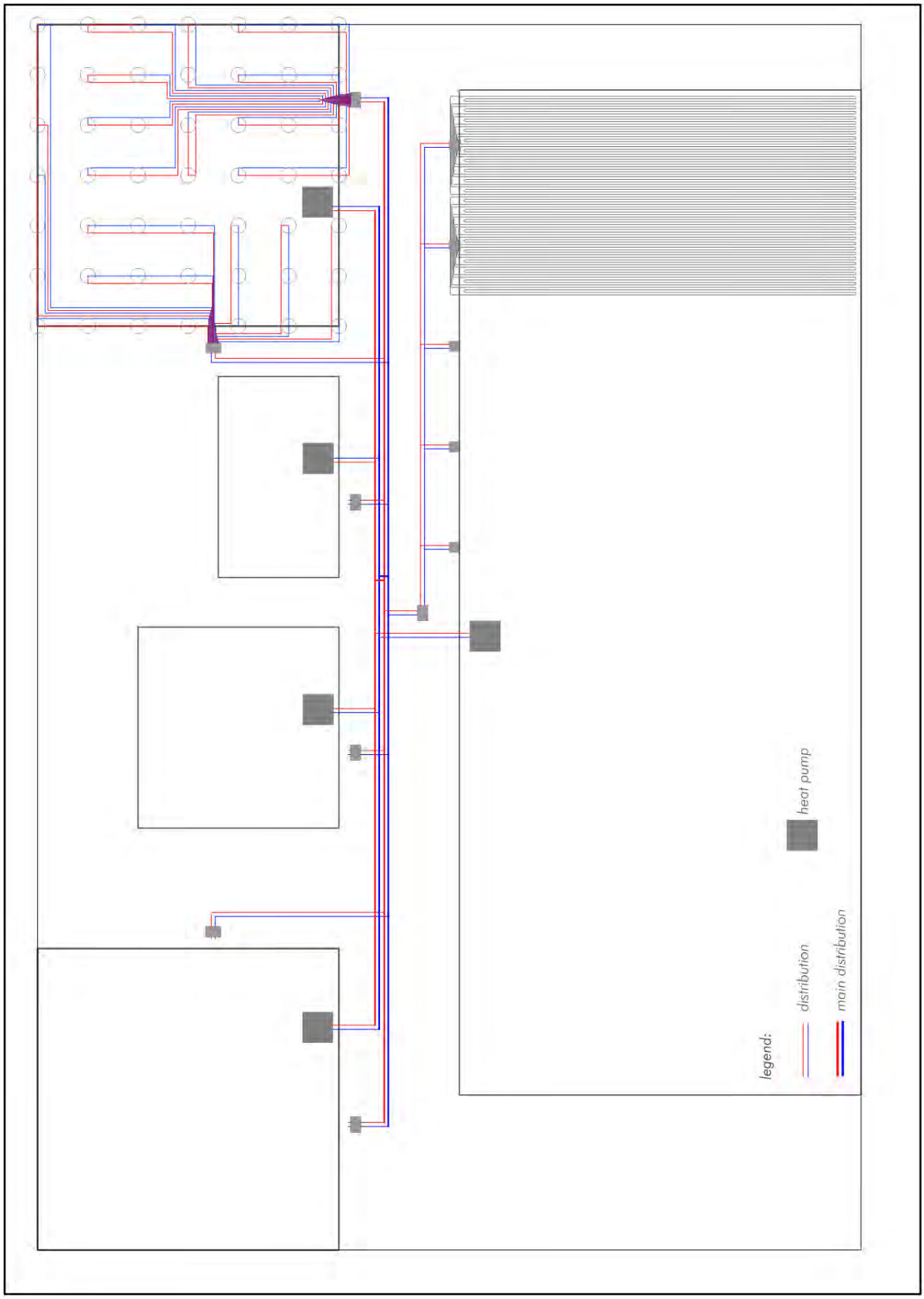

Fig. 38. Piping network for variant 2 with individual heat pumps for each building.

2.3.4 Inclusion of the district network into the E-Hub

Inclusion of a low temperature district network inside a thermal concept should be planned in the districts concept from the beginning. Technical building equipment has to consider the required low temperature levels when choosing the buildings heating and cooling systems. Furthermore possibilities to interconnect different thermal source systems have to be checked as sometimes the conditions require or encourage special technological solutions. For example, when specific buildings have a relatively high heating demand (residential buildings) but a connection to gas, a gas-absorption heat pump (maybe coupled with a gas boiler for peak loads) presents a viable option.

Additionally the geothermal source system has to be connected to the E-Hub monitoring and control systems. Therefore, the technological interfaces have to be compatible. Other than that, the necessary monitoring and control technologies (including fluid temperature monitoring, electricity and heat amount counter, the necessary electrical installations and data transfer/evaluation) already exist and are state of the art.

2.4 Loss of Structural Capacity in Piles due to thermal activation

2.4.1 Introduction

The present section illustrates and quantifies the loss of structural capacity expected in piles bearing internal pipes for thermal activation.

Thermal activation of piles strives to extract very low temperature geothermal energy from the surroundings through thermal exchange between pipes displayed inside piles and the embedding terrain. In order to implement this system, piped circuits are inserted into the pile rebar before concreting, thus effectively reducing pile section.

Different types of piles shall be described, analysing the applicability of thermal activation depending on the fabrication and installation process, and parametric studies shall be developed to examine the impact of thermal activation in structural resistance of piles in compression, tension, shear, flexure and buckling situations. The details of the parametric studies performed can be found in Annex C.

Finally, two case studies shall be presented and structural capacity shall be compared between activated and non-activated piles.

2.4.2 Pile classification

Pile type		Material	Fabrication and installation
Prefabricated	Prefabricated piles with different cross sections: full square, hollow square, hexagonal, tubular, etc.	Reinforced concrete, with or without steel shoe on point	Fabrication off site with medium to high resistance concrete. Installation by pile driving.
		Pre-stressed concrete with adherent pre-stressing, with or without steel shoe on point	Fabrication off site with medium to high resistance concrete. Installation by pile driving.
		Pre-stressed concrete with post stressed tendons, generally made of several pieces connected through pre-stressing, with or without steel or concrete shoe on point	Fabrication off site with medium to high resistance concrete. Installation by pile driving. Piece connection through pre-stressing. Tendons are stressed after driving
In situ	Displacement piles	Reinforced concrete, with shoe on casing point	Casing is closed at the bottom with a shoe, is driven into the ground to the required set or depth. Concrete is then poured into the casing and a cast-in-situ pile is formed inside. Casing is gradually removed during concreting
In situ	Displacement piles	Reinforced concrete, with gravel plug closing the bottom	Casing is closed at the bottom with a gravel plug, and is driven into the ground by hammering the plug. Concrete is then poured into the casing and a cast-in-situ pile is formed inside.

Pile type		Material	Fabrication and installation
	Extraction piles	Reinforced concrete, with retrievable casing	Casing is used as a hollow drill while interior soil is extracted by mechanical means. Once the required depth is reached, rebar is placed inside the casing and concrete is poured while casing is recovered
		Reinforced concrete, with lost casing	Casing is used as a hollow drill while interior soil is extracted by mechanical means. Once the required depth is reached, rebar is placed inside the casing and concrete is poured inside.
	Drilled piles	Reinforced concrete on drilled hole held by bentonite sludge	Excavation is held thanks to the pressure of bentonite sludge. Once required depth is reached, rebar is introduced and concrete is pumped into the hole
		Reinforced concrete on hole drilled by continuous drill with central concreting pipe	Excavation is executed with a continuous drill. Once required depth is reached, the drill is extracted while concrete is pumped through the central pipe in the drill. Rebar is introduced into the fresh concrete, not always reaching the bottom.

Table 9. Pile classification.

2.4.3 Thermal activation applicability

A succinct analysis of the different fabrication and installation procedures for piling promptly shows that some of them are either incompatible with thermal activation, or at least, highly unadvisable.

Post stressed prefabricated piles are the perfect example: not only pile driving stresses would be prone to damage the piping, but connection between different pipe sections would be a big issue, as would be the water tightness of these connections or their integrity during the pile hammering. Leakages of pipe content would undoubtedly damage both concrete and reinforcement in unpredictable ways.

To a lesser extent, all prefabricated piles bear a risk that makes thermal activation unadvisable, since pipe damage during jacking would be almost unavoidable, and leakage and corrosion would ensue. This is especially worrying in pre-stressed piles with adherent cables, since tensioned steel is more prone to accelerated corrosion, and cable breakage would lead to whiplash, tensioned concrete and pile failure.

Finally, piles drilled with continuous drill present the problem of pipe insertion into fresh concrete, which is in most cases limited to the first few meters of the pile, thus minimizing the actual energy yielding capability of the activated pile.

For the rest of the different pile types, thermal activation would represent no major problem either from a constructive point of view, or from a corrosion prevention one.

2.4.4 Spanish and European regulations

Considering pile integrity and state cannot be effectively checked, Spanish regulations limit the mechanical properties of concrete used in piles.

According to CTE (Spanish technical building regulation), piles shall be checked for the following ultimate limit states:

- Global stability
- Terrain collapse
- Pile pull out
- Horizontal terrain failure
- Pile structural limit and structural capacity

Since thermal activation pipes make no contact with the surrounding terrain, it is only to be expected that failure modes unrelated to the actual pile remain unaffected by thermal activation. Thus, only the regulations related to pile structural limit are relevant.

Said regulation state the following:

The structural limit of a pile, defined as maximum allowable axial force, shall be defined as a product of its cross section area and the capacity factor, or limit compressive stress. Said limit depends on the pile type, as shown in the following table.

Procedure	Pile type	Capacity factor (MPa)	
Driven piles	Pre/post-stressed concrete	$0,30 \cdot (f_{ck} - 0,9 \cdot f_p)$	
	Reinforced concrete	$0,30 \cdot f_{ck}$	
	Steel piles	$0,30 \cdot f_{yk}$	
	Wood piles	5	
		Soil type	
		Firm soil	rock
Bored piles	Cased	5	6
	Slurry	4	5
	Dry cast	4	5
	Drilled - no parameter control	3,5	-
	Drilled - parameter control	4	-

Table 10. Capacity factor of piles.

Bored (in situ) piles may allow a rise of 25% in the compressive stress limit if integrity control is implemented and integrity is guaranteed. Shown values for bored piles are valid for C25/30 (concrete mix designation), and may be proportionally adjusted to concrete resistance if a different concrete is used.

The structural capacity of a pile must be studied following standard structural checks for reinforced concrete as stated in EHE-08, Spanish reinforced concrete regulations compliant with Eurocode 2.

Flexure ultimate limit states in *in situ* piles shall consider concrete resistance to be no higher than 18 MPa.

Applicable European regulation, Eurocode 7, remits to Eurocode 2 for pile structural calculation. In turn, Eurocode 2 proposes a diameter reduction and a 10% raise on concrete safety factor for bored piles without permanent casing.

Thus, Spanish regulations are more restrictive than Eurocodes, since in CTE axial capacity is limited to less than 1/5 of concrete characteristic resistance, and flexural capacity is reduced to that expected of a 18MPa concrete, while Eurocodes merely reduce concrete characteristic resistance by 40%.

2.4.5 Case studies

In the present document, two representative case studies shall be analysed:

a) pile diameter 45 cm, distance of heat exchanger pipes 20 cm, 4 pipes (double-u) with 25 mm diameter (2,3 mm piping material strength) each.

b) pile diameter 80 cm, distance of heat exchanger pipes 30 cm, 6 pipes (triple-u) with 32 mm diameter (2,9 mm piping material strength) each.

a)	b)
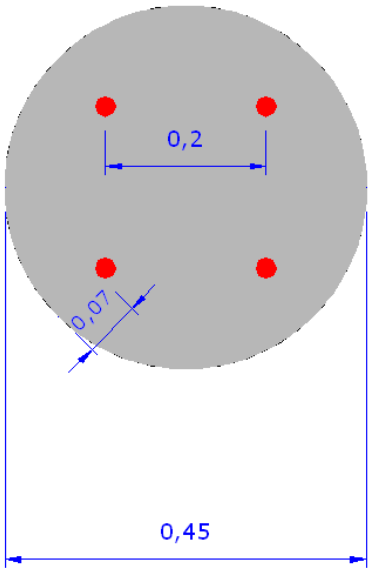	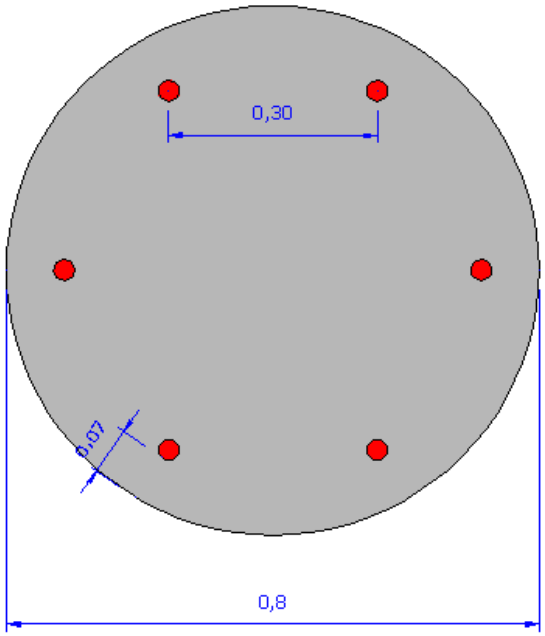

Table 11. Cross section of the case studies.

Materials used shall be standard issue: C20/25 concrete and B500 steel rebar.

2.4.6 Case study results

According to local regulations, pile structural compressive capacity is a linear function of the homogenized concrete section area. The actual capacity factor depends on the piling conditions, piling method, soil type and used concrete, and may be raised by 25% by performing cross-hole ultrasound-wave pile integrity tests.

Thus, in any case, loss of structural compressive capacity caused by the thermal activation only depends on percentage loss of sectional area due to piping.

Case A, presenting a circular section of 45 cm in diameter, standard issue rebar of 4 F16 mm rods and 4 F25 mm hollow pipes (supposed non-resistant), would experiment a loss of 1,20% structural capacity.

Case B, presenting a circular section of 80 cm in diameter, standard issue rebar of 10 F16 mm rods and 6 F32 mm hollow pipes (supposed non-resistant), would experiment a loss of 0,94% structural capacity.

On the other hand, structural tensile capacity of concrete piles depends solely on steel rebar, and thus it would be unaffected by thermal activation on either case, given that thermal activation pipes do not interfere with rebar display in the concrete section.

Shear resistance in **Case A**, assuming F8 stirrups every 0,15 m and perpendicular to the pile axis, would be of 93,78 kN for standard piles and 93,38 kN for active piles, registering a shear resistance loss of 0,43%

Shear resistance in **Case B**, assuming F8 stirrups every 0,15 m and perpendicular to the pile axis, would be of 214,4 kN for standard piles and 213,96 kN for active piles, registering a shear resistance loss of 0,21%

For **Case A,** ultimate flexural (pure flexion) moment of inactive pile is 54,21 kN·m, while ultimate flexural moment of thermo-active pile is 53,98 kN·m, so flexural loss of capacity is 0,42%.

Ultimate flexocompression of standard pile, assuming compression equal to pile structural capacity, would allow an axil force of 636,17 kN and a concomitant flexural moment of 120 kN·m, while activated pile would allow an axil force of 628,53 kN and a concomitant flexural moment of 118,50 kN·m, so flexocompressive loss of capacity in activated piles would be of 1,25%

For **Case B**, ultimate flexural (pure flexion) moment of inactive pile is 275.99 kN·m, while ultimate flexural moment of thermo-active pile is 275,62 kN·m, so flexural loss of capacity is 0,13%.

Ultimate flexocompression of standard pile in similar conditions to case A would allow an axil force of 2010,61 kN and a concomitant flexural moment of 630 kN·m, while activated pile would allow an axil force of 1991,72 kN a concomitant flexural moment of 625 kN·m, so flexural loss of capacity would be 0,79%.

Under buckling, **Case A** standard pile with 10R free length (l_0 = 2,25 m) and an axial load equal to the structural limit N=636,17 kN, maximum eccentricity is 0,1886 m. Maximum admissible moment is thus 112,59 kN·m. Active pile with an axial load equal to the structural limit N=628,53 has a maximum eccentricity of 0,1885 m. Maximum admissible moment is thus 111,24 kN·m, so buckling capacity loss is 1,20%.

Case B, under similar circumstances (l_0 = 4 m) and an axial load equal to the structural limit N=2010,61, maximum eccentricity is 0,3133 m. Maximum admissible moment is thus 588.86 kN·m. Active pile with an axial load equal to the structural limit N=1991,72 has a maximum eccentricity of 0,3138 m. Maximum admissible moment is thus 583.33 kN·m, so buckling capacity loss is 0,94%

The results are summarized in

	Case A	Case B
Compression loss	1.2%	0.9%
Tension loss	0%	0%
Shear loss	0.4%	0.2%
Flexure loss	0.4%	0.1%
Flexocompression loss	1.2%	0.8
Buckling loss	1.2%	0.9%

Table 12 below.

	Case A	Case B
Compression loss	1.2%	0.9%
Tension loss	0%	0%
Shear loss	0.4%	0.2%
Flexure loss	0.4%	0.1%
Flexocompression loss	1.2%	0.8
Buckling loss	1.2%	0.9%

Table 12. Case study results.

2.4.7 Conclusions

The effect of thermal exchange piping on the mechanical properties on regular piles is comparatively small, almost irrelevant. Even more so since structural capacity is seldom reached in any case. More often than not, the limit is set by terrain resistance.

Furthermore, piping could be used to perform ultrasound wave integrity tests, thus allowing a raise in structural capacity that overly compensates for any possible loss.

2.5 General conclusions of TAF

To sum up the results of the material testing via numerical simulations, the following conclusions can be drawn for the thermal activation of energy piles.

- Thermal effects of different piping material and pile concrete have been analysed individually as well as coupled for two different representative undergrounds and with two different methodological approaches (highly detailed, BHE boundary condition).

- The use of thermally enhanced piping material has, according to the simulation runs, no measurable influence on the thermal performance of the energy pile.

- Thermally enhanced concrete significantly increases the performance of energy piles in peak load operation, seemingly independent from the geology; the resulting effect can be as high as 25…40 %.

While reliable economic decisions can only be made for individual projects, it can generally be said that additional costs for the use of thermally enhanced concrete can pay off directly, with a performance gain to investment factor up to 1.2.

Regarding the integration of TAF at district level, the key idea for the E-Hub project is the distribution of the available energy between the network participants. The goal was defining a hydraulic piping network, in which a market-oriented distribution of thermal energy demand and supply was possible.

After taking into consideration important issues like temperature levels, transport medium, distances, etc., the most efficient and practically proven possible ways of balancing thermal energy on a district were developed.

The first variant developed uses a single heat pump room inside a centrally located building, from which "refined" thermal energy is distributed towards the demanding building around. The system can be defined as a low temperature district heating where a central heat pump is the generator.

The source systems are connected to each other via connection pieces and enter the heat pump central together via a big collector pipe. Inside cascading reversible heat pumps operate according to the building demands. From the heat pumps, insulated distribution pipes for the heating/cooling run towards all the buildings: two separate sets of pipes for the buildings with heating and cooling demand, while simply heated buildings only require one set of pipes.

The second variant consists of a piping circuit connecting all the TAFs, providing one big thermal source for the heat pumps, which are installed at building level (at least one per building). It is crucial to ensure equal pressure drops inside the source circuits (building circuits). The heat pumps inside the buildings should altogether not exceed the thermal capabilities of the TAF field as a whole.

Less piping is needed and less thermal losses are generated in this alternative, among other things, while on the other hand more heat pumps are necessary.

Both layouts will be implemented in the simulation environment developed in WP4 in order to quantify the viability of these variants. It will be particularly interesting, to analyse the integration of the TAFs with the Thermal Road Solar Collector with this tool.

Fig. 39. piping network alternatives, left: central heat pump, right: generation at building level.

Lastly, In order to quantify the loss of structural capacity expected in piles bearing internal pipes for thermal activation, a structural analysis has been performed.

	Case A	Case B
	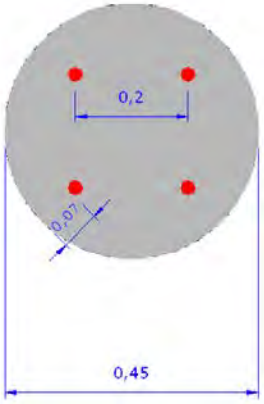	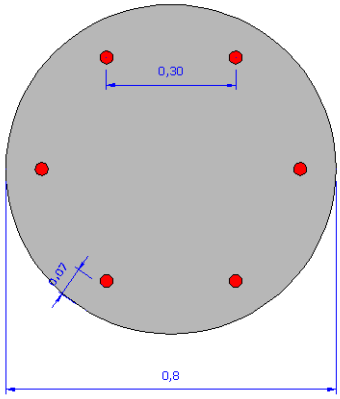
Compression loss	1,2%	0,9%
Tension loss	0%	0%
Shear loss	0,4%	0,2%
Flexure loss	0,4%	0,1%
Flexocompression loss	1,2%	0,8%
Buckling loss	1,2%	0,9%

Table 13. Case study results.

It can be seen that the effect of thermal exchange piping on regular piles is comparatively small. Even more so since structural capacity is seldom reached in any case: more often than not, the limit is set by terrain resistance.

Furthermore, piping could be used to perform ultrasound wave integrity tests, thus allowing a raise in structural capacity that overly compensates for any possible loss.

3 Thermal road solar collector

3.1 General Introduction of thermal road solar collector

A thermal road solar collector is basically a road with pipes embedded in it. Fluid running through the pipes extracts heat from the upper part of the road, which is heated by solar radiation. The thermal energy potential of a road thermal collector is lower than that of a normal solar hot water system and the quality of the energy is also lower but there are many advantages of the use of this kind of system.

Asphalt pavements can heat up to 60-70º C during solar irradiation and the available area of asphalt is so enormous that the energy potential appears to be huge. This heat can be used in many ways. Usually this energy is stored over seasons by means of aquifers, borehole heat exchangers, energy piles, etc. Besides the energy storage, another advantage of the use of a road thermal collector is also found in the maintenance of the road. The maximum temperature of the road (in summer) can be damped so that the chance of formation of ruts is reduced. In winter time, it is possible to avoid slippery roads by damping the minimum asphalt temperature. The life of the road can also be extended if the road is prevented from entering repeated cycles of icing and de-icing

Although there are additional advantages of using road thermal collectors, interest is mainly focussed on the energy potential and the application of this technology in order to reduce energy consumption in the built environment. It is of particular interest as a possible renewable system to be integrated within a district controlled by the E-Hub system

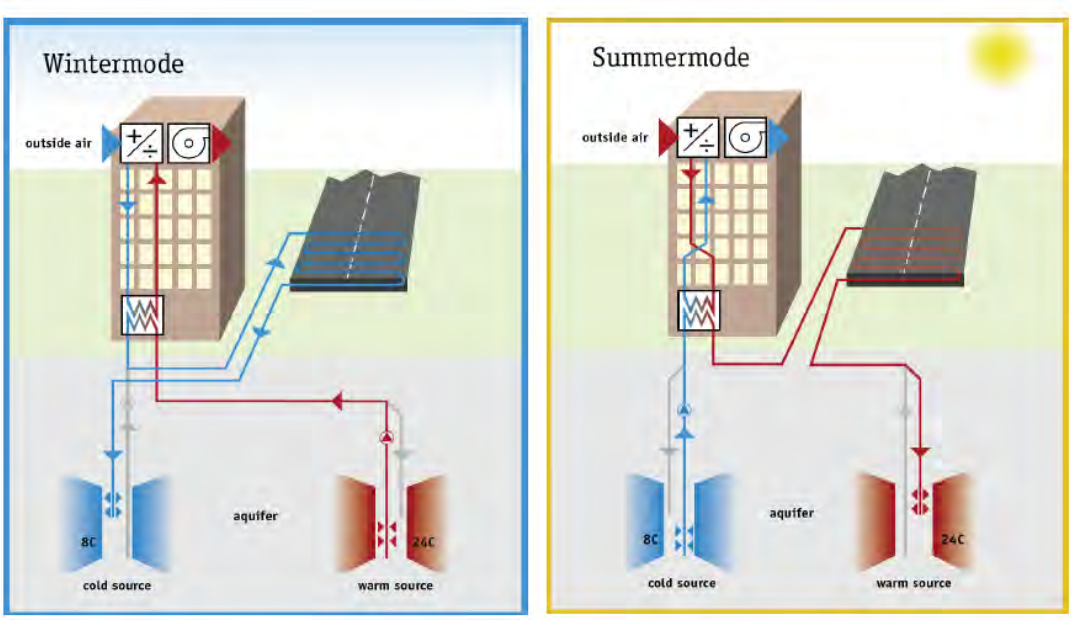

Fig. 40. Road thermal collector diagram

The quantity of energy that can be harvested from the thermal road solar collector depends on many design parameters that will be analysed in the thermal optimization section. However, the thermal design process can lead to unfeasible layouts, from a structural point of view. That is the reason why a structural analysis has been performed in order to determine which pipe configurations can guarantee that the road design will continue fulfilling all the road requirements. Lastly, an experimental confirmation of the mechanical performance of the whole system has been carried out. The overall aim of all this section is to develop an optimized design of the Thermal Road Solar Collector that could fulfil all the requirements.

3.2 Thermal optimization

3.2.1 Introduction

This section presents the results of the optimisation process of an asphalt solar collector. Some of the default parameters and data for performing this thermal optimization have been taken from the structural section which describes the structural implications of burying pipes in a traditional asphalt road.

The influence of the following parameters will be studied:

1. Pipe spacing
2. Pipe diameter
3. Pipe depth
4. Pipe material
5. Thermal conductivity of layer beneath the pipe array (insulation layer)
6. Infrared reflectivity of asphalt surface

The study is based on simulations realised with TRNSYS[1]; a dynamic simulation software widely used in the energy industry (see Annex E). Parameters 1 to 3 will be studied with two different weather data sets: London and Madrid, whereas parameters 4 to 6 will be studied only with the London weather data set.

The aim of these studies is to present the **annual collection rate** (kWh/m^2/yr) for each value of each parameter.

3.2.2 Structural layout

A standard Polish road composition fulfilling all the standards and regulations, was provided by Mostostal, a construction company, for the structural analysis that will be shown in the next section. In order to be consistent, the same composition was used for the thermal optimization. The thermal properties for each layer involved in this typical build-up of an asphalt road are the following:

Thermal properties	Thickness (cm)	K (W/mK)	Cp (J/kg K)	ro (kg/m3)
Wearing asphalt course	5	1.21	900	2250
Binding asphalt course	8	1.21	900	2250
Asphalt base course	10	1.21	900	2250
Aggregate base	20	1.137	960	2390
Subgrade (Original Soil)	1000	1.21	840	1960

Table 14. Thermal properties for each layer of an asphalt road, from the top down.

[1] For more information on TRNSYS, refer to http://sel.me.wisc.edu/trnsys/

We have made the assumption that the layer below the “Aggregate base” (“Subgrade”) would be composed on the made-up ground, and we have used the properties of clay, a soil material very common in the UK.

3.2.3 Description of the TRNSYS model

The process of optimising an asphalt collector system can become an impossible task if the context and the boundaries of the study are not defined. Some of the critical variables are:

- Geographical location (weather type)
- Type of heat sink (ground storage, hot water cylinder, swimming pool)
- Size of heat sink
- Control parameters
- Soil type
- Annual heat demand from the building

All of these will have a dynamic influence on the actual collection yield of an asphalt collector. This is why, in practice, the optimisation process is done on a case-by-case basis, to suit the specific requirements of each project.

Weather data and inlet water temperature

In the first three studies, we will use both **London** and **Madrid** weather data set to compare the performance of an asphalt collector under different climate conditions. In the other studies, only the London weather data set will be used for simplicity.

Besides, we have decided to fix the temperature of the water entering the collector so as to simulate an “infinite sink” linked to the collector. This temperature will be the annual average of the ground temperature for the location, i.e. **10°C** for London and **14°C** for Madrid.

Fluid type

The fluid used in the simulations is a mix of water and monoethylene glycol with a concentration of 25%, for a -14°C freeze protection. The fluid properties are:

- Specific heat capacity: 3.795 kJ/kg/K
- Density: 1052 kg/m^3
- Thermal conductivity: 0.48 W/m/K
- Viscosity: 0.00520 kg/m/s

Collection period

The collection period will start at the beginning of April (2160h) and finish at the end of October (7296h)

Reference configuration

We have selected a common reference collector configuration, which features in all the studies mentioned above. This reference configuration uses the following default values:

	Variables	Values
1	Pipe depth	90 mm
2	Pipe length	100 m
3	Pipe material	PEX-a (thermal conductivity = 0.4 W/m/K)
4	Pipe external diameter	25 mm
5	Pipe spacing	250 mm
6	Flow rate per pipe	0.15 l/s
7	Asphalt short-wave absorption coefficient	0.9
8	Asphalt long-wave emissivity coefficient	0.9

Table 15. Reference configuration - default values.

In each study, only the parameters that are varied will be specifically mentioned, the others will have their default value (as above).

Description of the collector component

In order to achieve an acceptable simulation run time, we set the number of pipes in the array to 1 only, with adiabatic boundaries located half way through the spacing distance (see Fig. 41).

This assumes that the pipe is part of an “infinite” series of parallel pipes, with no boundary effect on the “front” and “back” sides. In these simulations we will discount the boundary effects.

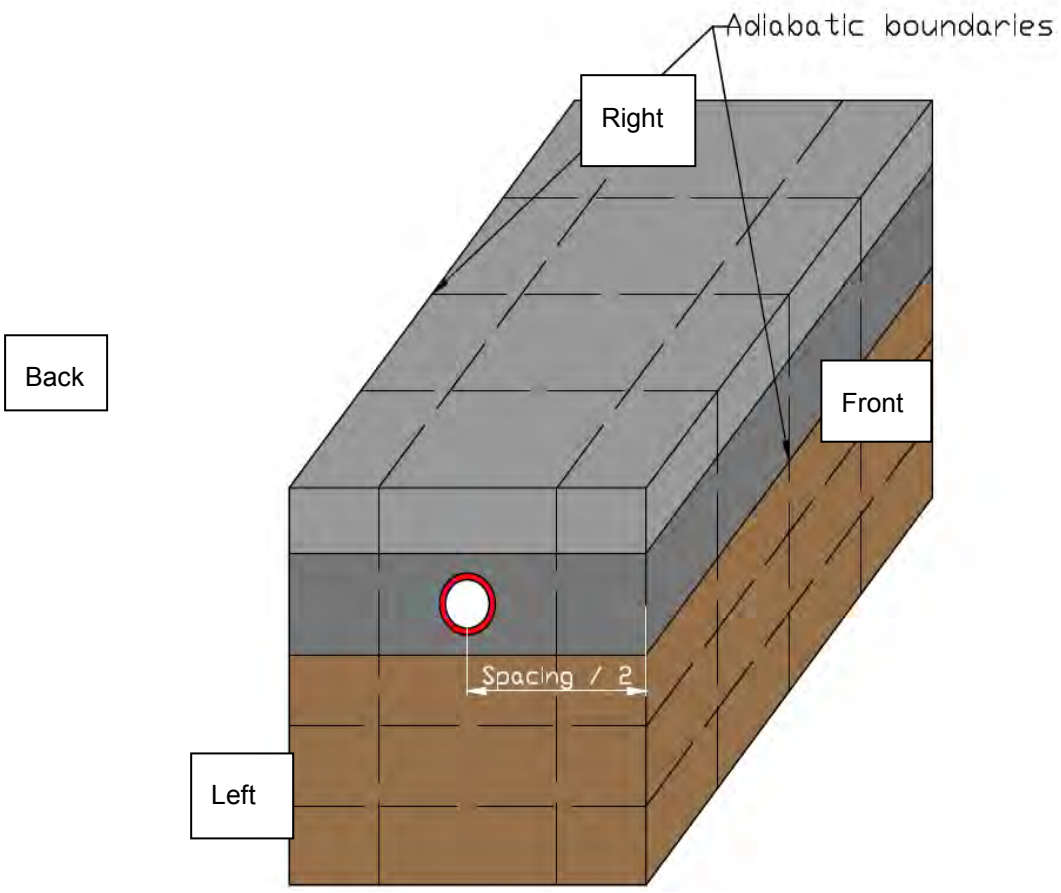

Fig. 41. Representation of the collector in TRNSYS.

3.2.4 Parameter 1 – Pipe spacing

Pipe spacing		London		Madrid	
Spacing (mm)	**Collector area (m2)**	**Heat transferred (kWh)**	**Heat transferred (kWh/m2)**	**Heat transferred (kWh)**	**Heat transferred (kWh/m2)**
100	10	2399	240	3675	368
150	15	3037	202	4640	309
200	20	3535	177	5391	270
250	25	3863	155	5881	235
300	30	4071	136	6204	207
350	35	4240	121	6459	185
400	40	4371	109	6633	166
450	45	4470	99	6781	151
500	50	4549	91	6899	138

Table 16. Pipe spacing study (pipe length = 100 m.).

As the heat collection rate has been studied for a given pipe length of 100 m., increasing the pipe spacing increases the collection area and therefore the total energy.

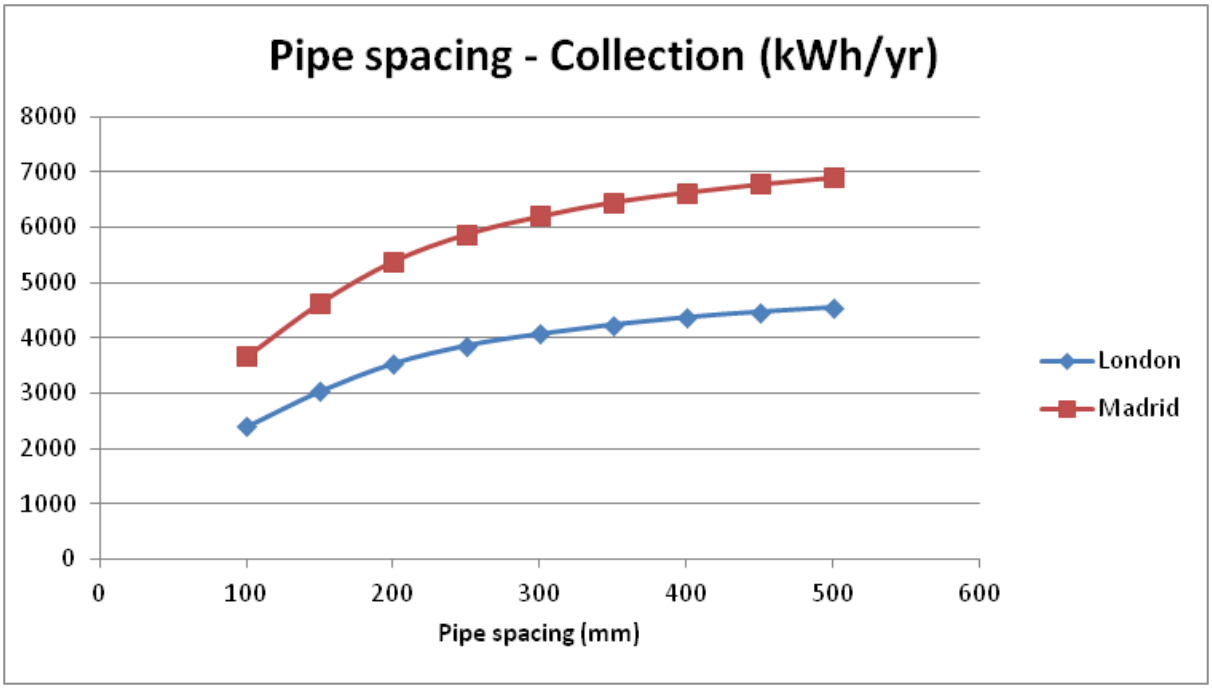

Fig. 42. Pipe spacing study – Collection per 100 metres of pipe length.

If the rate is calculated per square meter of road, the less the pipe spacing, the more the collection per unit area:

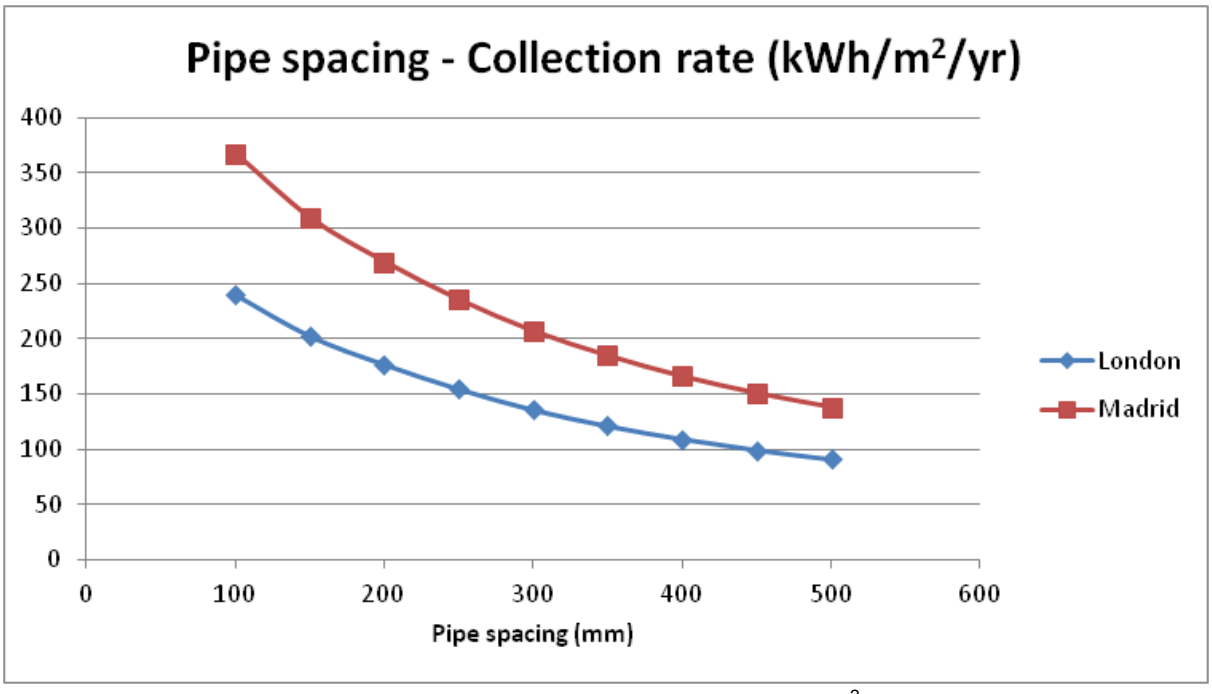

Fig. 43. Pipe spacing study – Collection rate per m^2 of road.

Fig. 43 shows a decreasing collection rate with an increase of the pipe spacing. This trend is explained by the fact that there is less pipe length per unit of area when the pipe spacing is increased, leading to a decrease of collection rate when the pipe spacing increases. Based on ICAX experience, a spacing of **250mm** is a good value, balancing collection rate and installation costs, from a thermal point of view.

3.2.5 Parameter 2 – Pipe diameter

The pipe diameter values for this study are 20mm, 25mm, 32mm and 40mm. These are the standard pipe sizes for PEXa. With a selected pipe spacing of 250mm and a collector pipe length of 100m, the collector area was fixed to 25 m^2.

Pipe diameter	London		Madrid	
Diameter (mm)	Heat transferred (kWh)	Heat transferred (kWh/m2)	Heat transferred (kWh)	Heat transferred (kWh/m2)
20	3521	141	5367	215
25	3863	155	5881	235
32	4781	191	7316	293
40	4998	200	7668	307

Table 17. Results - Pipe diameter study.

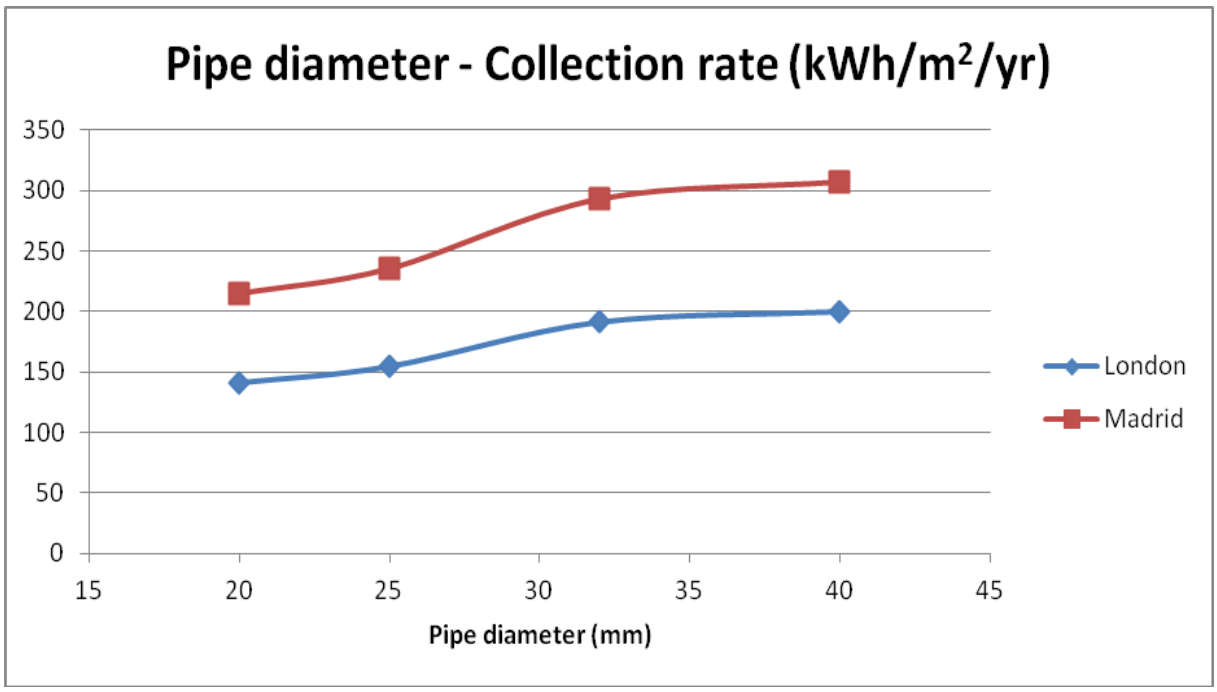

Fig. 44. Collection rate - Pipe diameter study.

Fig. 44 shows an increase in collection rate with the pipe diameter. The increase between the values at 25mm and 32mm is due to the fact that the flow regime is laminar in the 20mm and 25mm diameter pipes tests and turbulent in the 32mm and 40mm diameter pipes. A turbulent regime creates a greater heat transfer coefficient between the fluid and the pipe wall. In this scenario, we have selected the flow

rates for each pipe diameter so as to be within an acceptable range of linear pressure drop (Pa/m) in relation to pumping costs. Because the fluid contains glycol which is more viscous than water, the flow rate for the smaller diameters cannot be high enough to ensure a turbulent regime, without creating unacceptable pressure drops. Table 18 shows the different flow rates selected and the corresponding pressure drop and flow rates. In reality, the transition between laminar and turbulent flow does not occur in a step fashion, but for the sake of modelling, we have selected a Reynolds = 2300 as a frontier between laminar and turbulent regime.

OD (mm)	Pipe wall thickness (mm)	ID (mm)	Flow rate per pipe (l/s)	Linear pressure drop (Pa/m)	Reynolds (-)
20	1.9	16	0.08	283	1272
25	2.3	20	0.15	275	1894
32	2.9	26	0.30	274	2949
40	3.7	33	0.55	274	4346

Table 18. Pipe diameter study - Flow rates and pressure drops.

Based on ICAX experience, **25mm pipework** is a good compromise between installation costs and collection yield, from a thermal point of view.

3.2.6 Parameter 3 – Pipe depth

We have varied the pipe depth, starting from 40mm up to 200mm, in order to obtain a trend. Even if the structural results can suggest that the minimum structural depth recommended is higher than 40mm, it is still interesting to include shallow depths in case future construction materials can allow pipes to be buried at these depths.

Pipe depth	London		Madrid	
Depth (mm)	Heat transferred (kWh)	Heat transferred (kWh/m2)	Heat transferred (kWh)	Heat transferred (kWh/m2)
40	4545	182	6953	278
50	4343	174	6639	266
60	4232	169	6468	259
70	4118	165	6295	252
80	3959	158	6047	242
90	3852	154	5881	235
120	3540	142	5405	216
150	3236	129	4934	197
200	2853	114	4344	174

Table 19. Results - Pipe depth study.

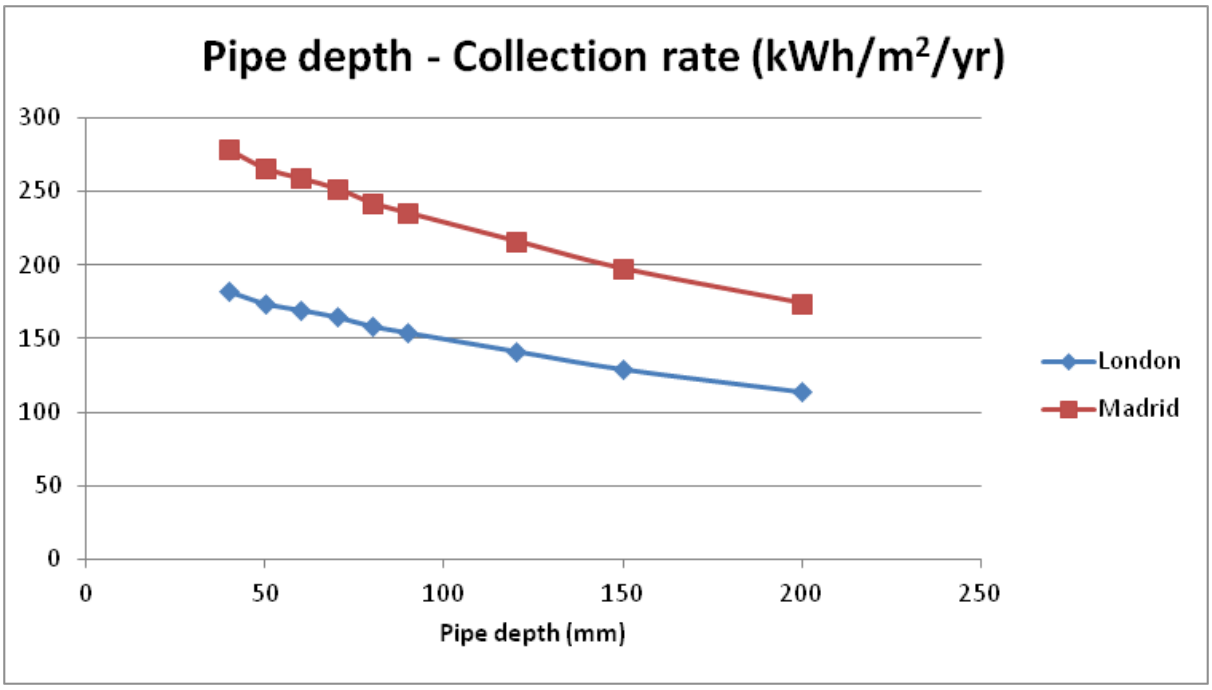

Fig. 45. Collection rate - Pipe depth study.

This study shows that the collection rate decreases with the pipe depth, this is explained by the fact that the grade of temperature decreases as the heat absorbed at the surface gets more and more diffuse as it travels down the collector. Therefore, heat exchanges with a pipe buried deeper are less efficient than with a pipe buried closer to the surface. According to the structural restrictions that will be shown in the structural analysis, a depth of **90mm** seems to be the minimum depth able to withstand the load. Therefore the best position from a thermal point of view.

3.2.7 Parameter 4 – Pipe material

The default pipe material is cross-linked polyethylene PEX-a, it can withstand higher temperatures (up to 90°C) and is much stronger than standard MDPE pipes. Its thermal conductivity is 0.4 W/m/K. The other materials considered for this potentially high temperature application are carbon fibres and stainless steel.

Pipe material	**London**				
Pipe material	**Thermal conductivity (W/m/K)**	**OD (mm)**	**Pipe wall thickness (mm)**	**Heat transferred (kWh)**	**Heat transferred (kWh/m2)**
PEX-a	0.4	25.0	2.3	3863	155
Stainless steel	16	26.7	2.9	4155	166
Carbon fibres	1.4	25.0	1.4	4085	163

Table 20. Results - Pipe material study.

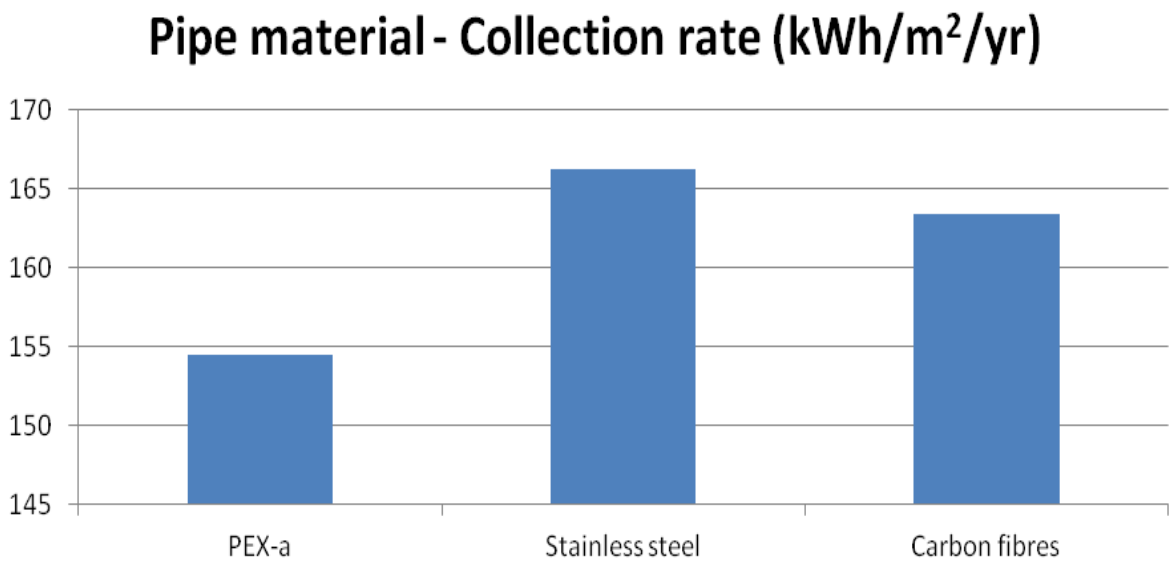

Fig. 46. Collection rate - Pipe material study.

This study shows that when the conductivity of the pipe material is closer to that of the surrounding soil, heat transfer will be more effective and therefore yield a greater annual collection rate. It can also be seen that materials with a thermal conductivity value higher than the surrounding soil (such as stainless steel in this case) does not increase the yield significantly. In this instance, carbon fibres and stainless steel seem to be relevant alternatives to PEX-a in terms of thermal performance. However, more information such as cost, structural issues and practicalities of installation will play a part in the selection of the material.

3.2.8 Parameter 5 – Thermal conductivity of the aggregate base layer

The purpose of this study is to see the influence of the thermal conductivity of the aggregate base layer on the annual collection rate. We have used two values of entering water temperatures (**10°C** and **20°C**) to see if working with warmer fluid creates a need for a more insulative aggregate base layer.

Insulation layer	**London**			
Inlet temperature (°C)	**10**		**20**	
Aggregate thermal conductivity	**Heat transferred (kWh)**	**Heat transferred (kWh/m2)**	**Heat transferred (kWh)**	**Heat transferred (kWh/m2)**
1.137	3863	154.5	939	37.5
1.0	3853	154.1	939	37.6
0.8	3855	154.2	942	37.7
0.6	3856	154.2	944	37.8
0.4	3862	154.5	951	38.0

Table 21. Results - Thermal conductivity of aggregate base layer.

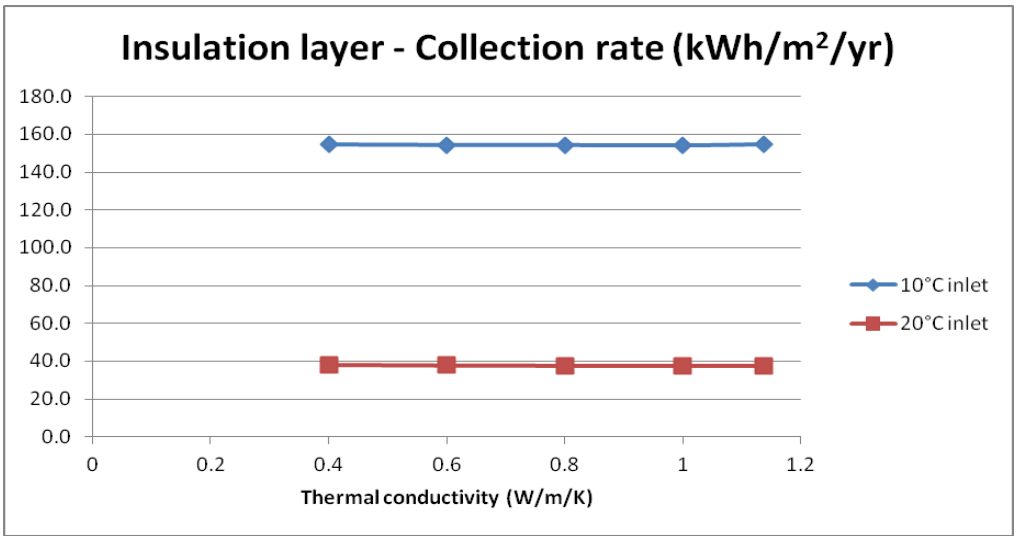

Fig. 47. Collection rate - Thermal conductivity of aggregate base layer.

This study shows that there is almost no difference in the annual collection rate when the conductivity of the aggregate base layer is decreased. This shows that most of the heat absorbed at the top surface is transferred to the fluid, and therefore there is no need for improving the insulative characteristic of the aggregate base layer.

Furthermore, it can be seen that the collection rate relating to inlet water temperature of **20°C** is about four times lower than that with **10°C** inlet water temperature. This shows that it is essential to define what the heat sink is in reality so that the simulation outputs a realistic collection rate for each situation.

3.2.9 Parameter 6 – Infrared emissivity of asphalt surface

The purpose of this study is to see the influence of the asphalt infrared (IR) emissivity.

Asphalt IR emissivity	London	
Asphalt IR emissivity	**Heat transferred (kWh)**	**Heat transferred (kWh/m2)**
0.9	3863	155
0.8	4053	162
0.7	4265	171
0.6	4501	180
0.5	4755	190
0.4	5022	201
0.3	5310	212
0.2	5626	225
0.1	5966	239

Table 22. Results - Asphalt IR Emissivity.

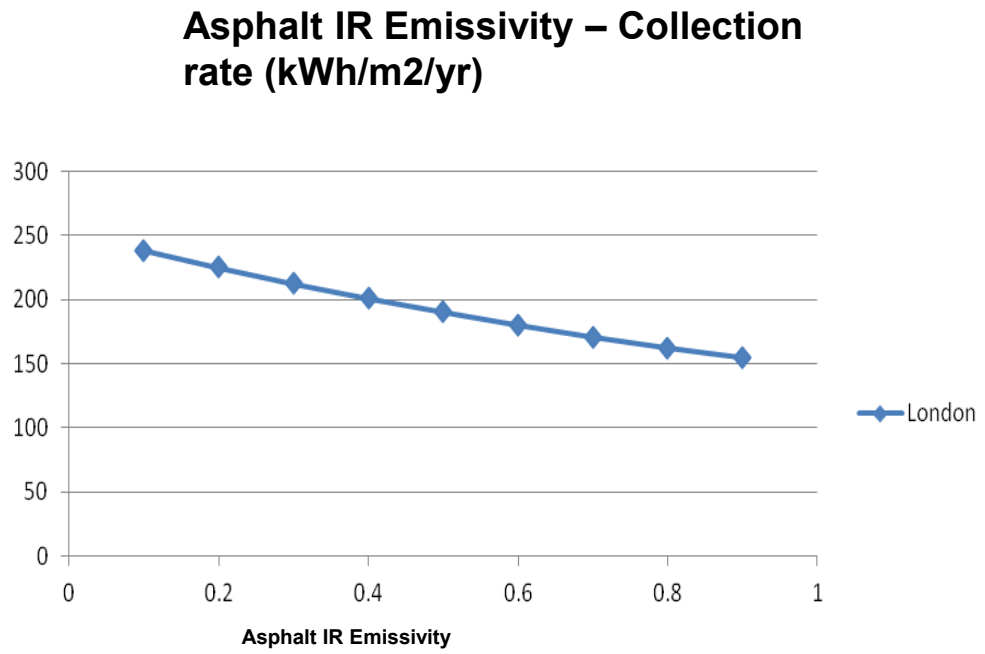

Fig. 48. Collection rate – Asphalt IR Emissivity.

If a coating material with a lower than 0.9 emissivity value can be applied, it could bring useful benefit to the collection rate, as it will reduce the losses due to IR emission from the surface to the surroundings. We can see that the increase of collection rate with the diminution of the emissivity value is fairly linear.

3.2.10 Conclusion

The studies presented in this section focus on the influence of several parameters over the annual collection rate. From these results, it could be relatively easy to select an optimal configuration based on thermal performances only. However, in practise, the final selection will be different in each situation as capital cost and installation times will have a significant influence over it. Additionally, the collection rates presented in this report are only valid in this particular context, where the fluid entering the collector remains at a constant 10°C, and with the given soil types and layout involved. Connected to a “real” sink like a ground-storage borehole system, this collection rate is likely to go down, since “thermally charging” a ground storage system will result in a gradual increase of the return temperature to the collector.

3.3 Structural simulations

3.3.1 Introduction

The work presented in this text contains a structural analysis of a buried pipe system: road plus buried pipes. An extensive study of the loads, stresses and strains supported by the system has been done in order to develop the current document.

To provide a better understanding of the study that has been carried out, the load theory used to develop the different analysis is presented in Annex F. In this section, the different loads imposed upon the road, the traffic load (live load) and the dead load corresponding to weight of the road layers, is explained in detail.

To develop the road analysis contained in this document, an important software research was done in order to choose a suitable structural software. Finally, the civil structural software ALIZE was chosen to perform the analysis.

The main aim of the results presented in the document will be to assess, from the structural point of view, what are the suitable positions of the buried pipe system. For this reason, different types of analysis have been done to obtain the design critical parameters of the system.

This document focuses on the fatigue damage analysis of the system, by establishing the maximum number of cycles, or years of lifespan of the buried pipe system. The inputs necessary to determine the maximum number of cycles came from the results obtained with Alize software.

It should be noticed that, with the aim to provide an added value to the performed studies and to improve its properties as thermal collector, an epoxy resin layer has been placed on top of the road. This reinforcement is aimed to improve the structural properties of the road in a way that enables the positioning of the buried pipes closer to the surface of the road, hence increasing the heat transfer capability.

3.3.2 Load theory

The load theory used to develop the analyses presented in the next sections of the document, is detailed in Annex F/Load theory. The aim of presenting this load theory is getting a better understanding of the results obtained from these analyses.

The load theory presented describe theoretically the load cases that have been used to perform the different types of analyses. These load cases have been combined to compose the load hypothesis that have been imposed to the road. It has to be noticed that the simulation software ALIZE takes into account the dead load due to the weight of the different layers of the road, by default.

It should be also noticed that the outcomes presented in the next sections of the document correspond to the most unfavourable load hypothesis.

3.3.3 Behaviour limits

As occurs with every constructive work, there are certain limitations which should not be exceeded in the design of the system road and buried pipes. For this reason, a quality design is endorsed by technical criteria which allow a long term service life of this system as a whole and of their single components. Annex F/ Behaviour limits presents several factors to take into account at the time to get a proper design of the system.

3.3.4 Simulations of structural strength

With the goal of assessing the structural integrity of the road composition and the buried pipe system, a battery of simulations using ALIZE software was carried out. Some concepts must be cleared at this point in order to understand the scope of these simulations and the magnitudes involved.

The physical and mechanical properties of the materials used for the implementation of the road composition and the pipe system have a crucial role in its durability. For this reason, the simulations have been divided in three meteorological seasons: winter, summer and spring-autumn. The properties of the materials, Elastic modulus and Poisson coefficient, will be different in each one of these seasons.

In order to take into account the effect of the buried pipe system on the road layers, the structural properties of the layer containing the pipe system have been reduced, as a function of the percentage of the cross area occupied by the pipes.

Although many pipe depths are possible from a theoretical point, from a constructive point of view the pipes must be contained within just one layer of the road material.

Taking all these into consideration, five case studies have been developed in order to analyse the different possible layouts. The five case studies have been considered to take place for each one of the defined meteorological seasons.

The five case studies are:

- Base case
- Base case plus buried pipes in wearing asphalt course (depth equal to 0.0375 m)
- Base case plus buried pipes in binding asphalt course (depth equal to 0.09 m)
- Base case plus buried pipes in asphalt base course (depth equal to 0.14 m)
- Base case plus buried pipes in the fourth layer (depth equal to 0.24 m)

Approach, Tools

The methodology followed for performing the structural simulations utilizes the road design software ALIZE.

The strategy followed for this software, to obtain the outcomes to be analysed for our purpose, considers the following assumptions:

- Steady state
- Computing stresses created by traffic loads on these types of pavement structures.
- Theoretical core of the program lies in the solution to the problem of an isotropic linear elastic multi-layer.
- Complementary pavement design assistance feature in accordance with the precepts of the rational LCPC-SETRA method.
- A parametric sweep of the selected physical magnitude, in this case the layout in different layers.

An example of a cut of the road with the pipe system simulated is shown in the following figure:

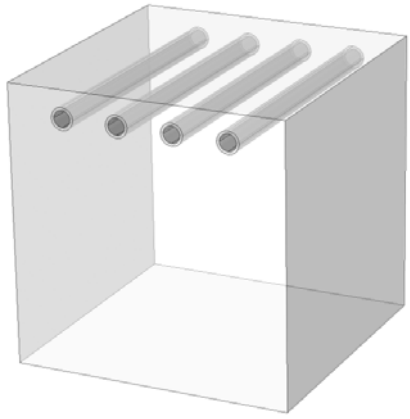

Fig. 49. Snapshot of the model of the pipe system.

For the dimensional requirements of the model, in accordance with the ICAX group, the following parameters for the pipe system have been fixed, while varying the pipe depth:

- Pipe outer diameter: 25 mm
- Pipe width: 2.3 mm
- Horizontal spacing: 250 mm

Once the characteristics of the simulation have been defined, the choice of the materials of the pipe system is established. The chosen pipe material is cross-linked polyethylene (PE-Xa), whose properties are in terms of the regulation DIN 16892/16893:

	Young modulus (MPa)	Poisson coefficient	Density (kg/m^3)	Yield strength (MPa)
PE-Xa	630	0.41	940	23

Table 23. Mechanical properties of the PEX used in the simulations.

Some of the properties of the pipe material (PE-Xa) are its wide range of working temperatures and its extremely high strength, which make it a good candidate for the conditions in the pipe environment.

The selected design of the road matches with the configuration of the typical road in Poland and it has been designed for a medium traffic intensity, 336 – 1000 axis, and 100 KN / lanes/day. Below these lines, it will be presented the composition of the selected road and their material characteristics. It should be noticed that, these materials characteristics will have different values in each one of the meteorological seasons.

Layers	Thickness (cm)
Wearing asphalt course	5
Binding asphalt course	8
Asphalt base course	10
Aggregate base	20
Subgrade	-

Table 24. Road composition (cm) from top to bottom.

Type of asphalt mixture	Winter		Spring – Autumn		Summer	
	E (MPa)	v (Poisson)	E (MPa)	v (Poisson)	E (MPa)	v (Poisson)
Wearing course	19300	0.25	10300	0.3	2800	0.4
Binding course	18800	0.25	10100	0.3	3000	0.4
Base layer	18100	0.25	9600	0.3	3000	0.4
Aggregate base	400	0.3	400	0.3	400	0.3
Subgrade	100	0.3	100	0.3	100	0.3

Table 25. Materials characteristics during the seasons of the year.

Conditions

The simulations were done considering the mechanical stress and strains present in the structures. The exterior thermal conditions have been taken into account by means of the different mechanical properties of the road materials as a function of the seasons of the year.

The following boundary conditions were used by the civil structural program to perform its internal calculations:

- Base: fixed.
- Lateral confinement: Roller (no deformations occur in the perpendicular direction to the roller surface).
- Front/back sides (sides perpendicular to the direction of the pipes): symmetry.
- Upper face: free, inward.
- Inner diameter of the pipes: constant pressure of 2 bar corresponding to the driving of the water.
- Upper face condition for the load: boundary load according with the load theory presented in the section two of this document.

3.3.5 Road Results

Fatigue analyses.

In this section, it will be presented the results from the fatigue analyses. These outcomes will be classified according to the three different seasons, with the aim to show the influence of the exterior conditions on the materials properties, and consequently on the fatigue failure of the element.

In the first three tables of this section it will be presented the millions of cycles that define the lifespan of the road for each configuration. It has to be noticed that these outcomes have been calculated considering constant values of the properties during each period.

The fourth table presents the estimated lifespan of the road for each layout, performed taking into account the duration of each meteorological season along the years.

It has to be said that the inputs used to develop this analysis, and the four tables presented in this section, come as a result of the points contained in sections from Annex F.

As it is reflected in Annex F/Behaviour limits, there are two different types of fatigue damage, the fatigue damage created by tangential stresses and the fatigue damage created by vertical stresses.

The millions of cycles of the bitumen (tangential stresses) will be calculated by means of the strain of the fiber located at the bottom of the bituminous layer. The millions of cycles of the square of land will be calculated by means of the upper fiber of the square of land layer.

It should be emphasized that, the last column of the first three tables presents the years of useful life of the material, taking into account that the constant value of the material properties along the year, whereas the real outcome in years and millions of cycles will be presented in the fourth table of this point section. This table was developed taking into consideration the following duration for each season:

- Winter: 20%
- Spring – Autumn: 50%
- Summer: 30%

It has to be noticed that although the water flow will help (in principle) to have less extreme asphalt temperatures, this effect has been neglected in the simulations.

Case studies	Layers thicknesses (cm)	Tangencial deformation (mm)	Vertical deformation (mm)	Millions of cycles of the Bitumen	Millions of cycles of the square of land	Years of useful life (Bitumen)	Years of useful life (Square of land)
Base case	5+8+10+20	-0.0474	0.0965	426.29	243.70	129.77	74.19
Pipes in Wearing Asphalt	2.5-pipes-8+10+20	-0.0484	0.0994	384.04	219.25	116.91	66.74
Pipes in Binding Asphalt	5+4-pipes-4+10+20	-0.0477	0.0975	413.06	234.89	125.74	71.50
Pipes in Asphalt Base	5+8+5-pipes-5+20	-0.0495	0.0995	343.22	218.47	104.48	66.50
Pipes in Aggregate base	5+8+10+10-pipes-10	-0.0473	0.0955	430.82	252.93	131.15	77.00

Table 26. Fatigue damage (winter).

Case studies	Layers thicknesses (cm)	Tangential deformation	Vertical deformation	Millions of cycles of the Bitumen	Millions of cycles of the square of land	Years of useful life (Bitumen)	Years of useful life (Square of land)
Base case	5+8+10+20	-0.072	0.142	53.828	61.215	16.39	18.63
Pipes in Wearing Asphalt	2.5-pipes-8+10+20	-0.061	0.166	124.806	35.523	37.99	10.81
Pipes in Binding Asphalt	5+4-pipes-4+10+20	-0.072	0.1436	52.351	58.962	15.94	17.95
Pipes in Asphalt Base	5+8+5-pipes-5+20	-0.0743	0.1459	45.046	55.711	13.71	16.96
Pipes in Aggregate base	5+8+10+10-pipes-10	-0.0714	0.1406	54.968	63.578	16.73	19.35

Table 27. Fatigue damage (Spring - Autumn).

Case studies	Layers thicknesses (cm)	Tangencial deformation (mm)	Vertical deformation (mm)	Millions of cycles of the Bitumen	Millions of cycles of the square of land	Years of useful life (Bitumen)	Years of useful life (Square of land)
Base case	5+8+10+20	-0.135	0.269	2.258	6.297	0.687	1.917
Pipes in Wearing Asphalt	2.5-pipes-8+10+20	-0.104	0.312	8.506	3.702	2.589	1.127
Pipes in Binding Asphalt	5+4-pipes-4+10+20	-0.140	0.277	1.924	5.627	0.586	1.713
Pipes in Asphalt Base	5+8+5-pipes-5+20	-0.139	0.274	1.973	5.842	0.601	1.778
Pipes in Aggregate base	5+8+10+10-pipes-10	-0.134	0.265	2.361	6.581	0.719	2.003

Table 28. Fatigue damage (Summer).

Regarding the different kind of stresses, the more restrictive ones have been used to provide an estimation of the lifespan of the road.

Case studies	Layers thicknesses (cm)	Millions of cycles winter	Millions of cycles Spring - Autumn	Millions of cycles Summer	Total years of useful life
Base case	5+8+10+20	243.70	61.215	6.297	**24.729**
Pipes in Wearing Asphalt	2.5-pipes-8+10+20	219.25	35.523	3.702	**19.094**
Pipes in Binding Asphalt	5+4-pipes-4+10+20	235.75	58.962	5.627	**23.842**
Pipes in Asphalt Base	5+8+5-pipes-5+20	220.04	55.711	5.842	**22.410**
Pipes in Aggregate base	5+8+10+10-pipes-10	234.89	60.452	6.198	**24.068**

Table 29. Total years of useful life.

The computational analysis determine that the road lifespan decreases considerably when placing the pipes embedded in the wearing asphalt.

It has to be noticed that the thermal conditions of the asphalt

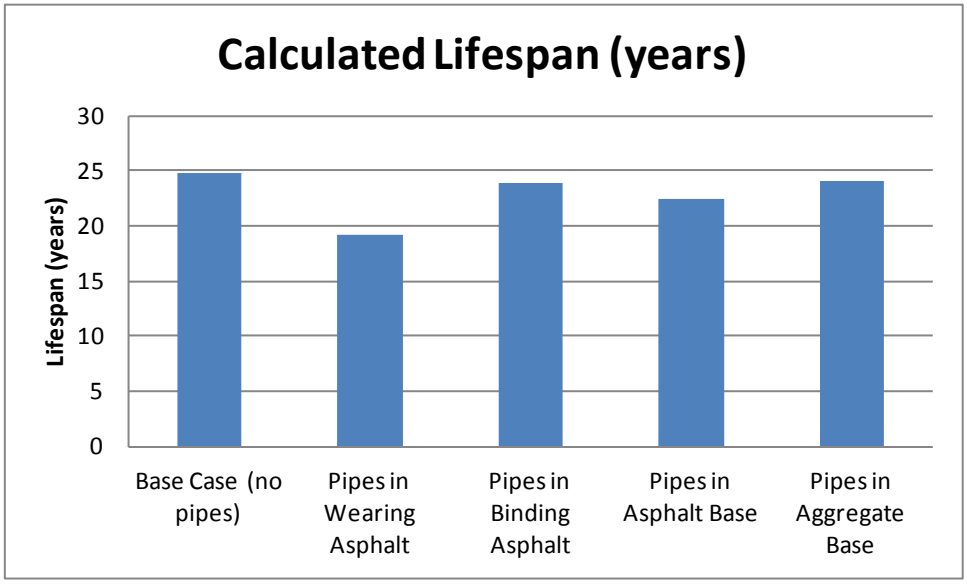

Fig. 50. Total years of useful life.

3.3.6 Tests with resin

In the following section, the study of the mechanical stress of the system will be done adding a fine layer of resin on top of the road. For this analysis a mix of the resin G 11-CR and granular material was considered. An epoxy resin is a polyepoxide resin which hardens when mixed with a catalyst agent or hardener. Epoxy resins appear frequently as products of a reaction between bisphenol A and epichlorohydrin. Epoxy resins commonly consist of two components which are premixed before being used; when mixed react causing the solidification of the resin. The main characteristics of these resins are:

- Optimal wetting and adhesion.
- Good electrical insulation.
- Good mechanical strength.
- Resist moisture.
- Resist the corrosive attack.
- Withstands high temperatures
- Excellent chemical resistance
- Excellent adhesive properties.

Nowadays this kind of resins is used in grouts for repairing rigid pavements due to their mechanical properties.

The main mechanical characteristics of this layer are the followings:

- Tensile strength: 65 ± 5 MPa
- E (Tensile): 2200 ± 300 MPa
- Elongation at rupture: 5.3 ± 0.2 %

The main purpose here is to determine the effectiveness of the G 11-CR epoxy resin layer to improve the structural behaviour of the road. The aim is to place the buried pipe system closer to the surface of the road, to improve the heat transfer capabilities. In this section, the same kind of analyses already done will be performed again, but this time adding the resin layer on top of the road.

Fatigue analyses

In this section, it will be presented the results from the fatigue analyses. These outcomes will be classified according to the three different seasons, with the aim to show the influence of the exterior conditions on the materials properties, and consequently on the fatigue failure of the element.

In the first three tables of this section it will be presented the millions of cycles that define the lifespan of the road for each configuration. Notice that these outcomes have been calculated considering constant values of the properties during each period.

The fourth table presents the estimated lifespan of the road for each layout, performed taking into account the duration of each meteorological season along the years.

It has to be said that the inputs used to develop this analysis, and the four tables presented until now in this section, come as a result of the points contained in previous sections.

As it was reflected previously, there will be two different types of fatigue damage, the fatigue damage created by tangential stresses and the fatigue damage created by vertical stresses.

The millions of cycles of the bitumen (tangential stresses) will be calculated by means of the strain of the fiber located at the bottom of the bituminous layer. The millions of cycles of the square of land will be calculated by means of the upper fiber of the square of land layer.

It should be emphasized that, the last column of the first three tables presents the years of useful life of the material, taking into account that the constant value of the material properties along the year, whereas the real outcome in years and millions of cycles will be presented in the fourth table of this

point section. This table was developed taking into consideration the following duration for each season:

- Winter: 20%
- Spring – Autumn: 50%
- Summer: 30%

Case studies	Layers thicknesses (cm)	Tangencial deformation (mm)	Vertical deformation (mm)	Millions of cycles of the Bitumen	Millions of cycles of the square of land	Years of useful life (Bitumen)	Years of useful life (Square of land)
Resin + Pipes in Binding Asphalt	Resin + 5+4-pipes-4+10+20	-0.0476	0.0973	417.41	236.62	1143.60	648.28
Resin + Pipes in Asphalt Base	Resin + 5+8+5-pipes-5+20	-0.0494	0.0993	346.71	220.04	949.89	602.86
Resin + Pipes in Aggregate base	Resin + 5+8+10+10-pipes-10	-0.0472	0.0953	435.40	254.83	1192.88	698.17

Table 30. Fatigue damage (winter, Resin).

Case studies	Layers thicknesses (cm)	Tangential deformation	Vertical deformation	Millions of cycles of the Bitumen	Millions of cycles of the square of land	Years of useful life (Bitumen)	Years of useful life (Square of land)
Resin + Pipes in Binding Asphalt	Resin + 5+4-pipes-4+10+20	-0.072	0.1432	52.715	59.552	16.05	18.13
Resin + Pipes in Asphalt Base	Resin + 5+8+5-pipes-5+20	-0.0742	0.1455	45.350	56.259	13.81	17.13
Resin + Pipes in Aggregate base	Resin + 5+8+10+10-pipes-10	-0.0712	0.1402	55.744	64.228	16.97	19.55

Table 31. Fatigue damage (Spring - Autumn, Resin).

Case studies	Layers thicknesses (cm)	Tangencial deformation (mm)	Vertical deformation (mm)	Millions of cycles of the Bitumen	Millions of cycles of the square of land	Years of useful life (Bitumen)	Years of useful life (Square of land)
Resin + Pipes in Binding Asphalt	Resin + 5+4-pipes-4+10+20	-0.135	0.270	2.241	6.165	0.682	1.877
Resin + Pipes in Asphalt Base	Resin + 5+8+5-pipes-5+20	-0.139	0.273	2.001	5.942	0.609	1.809
Resin + Pipes in Aggregate base	Resin + 5+8+10+10-pipes-10	-0.134	0.264	2.396	6.688	0.730	2.036

Table 32. Fatigue damage (Summer, Resin).

Regarding the different kind of stresses, the more restrictive ones have been used to provide an estimation of the lifespan of the road.

Case studies	Layers thicknesses (cm)	Millions of cycles winter	Millions of cycles Spring - Autumn	Millions of cycles Summer	Total years of useful life
Pipes in Binding Asphalt	5+4-pipes-4+10+20	236.62	59.552	6.165	**24.033**
Pipes in Asphalt Base	5+8+5-pipes-5+20	220.04	56.259	5.942	**22.503**
Pipes in Aggregate base	5+8+10+10-pipes-10	254.83	64.228	6.688	**25.902**

Table 33. Total years of useful life when adding a resin layer on top.

The computational analysis determines that the road lifespan increases (lightly) when adding the resin layer on top of the road. As the pipe positioning in the wearing asphalt is quite critical, it has been left out of this resin analysis. The experimental tests that will be presented in the following section will explore the possibilities of placing the pipes in the upper layer of the road.

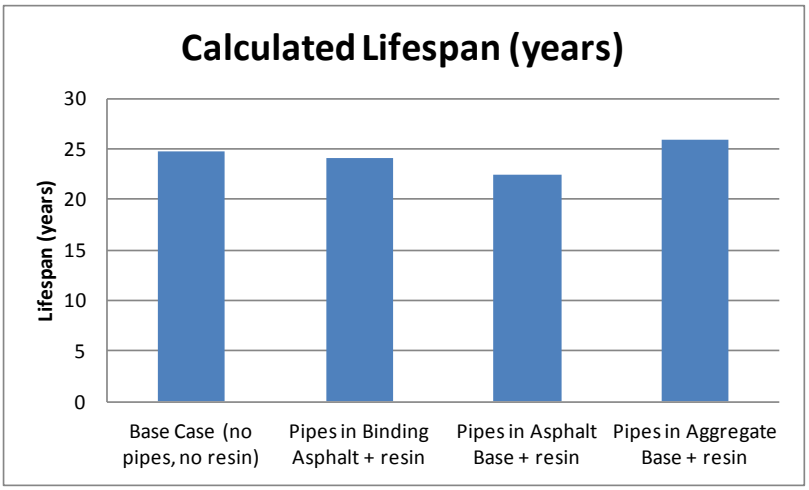

Fig. 51. Total years of useful life when adding a resin layer on top.

3.3.7 Conclusions

The structural behaviour of the system: road + buried pipes has been analysed, taking into consideration different layouts of the piping. The road considered is a typical Polish road that has been defined by Mostostal, according to their experience and of course it is a type of road that fulfils the Polish/European regulations. The road characteristics have been designed to withstand a determinate traffic intensity.

The main criterion to establish the most suitable depth/layout to locate the buried pipe system is that the expected lifespan of the road has to be higher than twenty years. For this reason, the depth of 0.09 m (in the middle of the asphalt binding course) seems to be the most suitable place for the system.

It should be noticed that, although the depth of 0.035 m, at the lowest part of the wearing course, has a lifespan close to 20 years, it has been decided to discard this layout due to the fact that in the analysis performed, only one distress model (the most important one) has been taken into account and just with one distress model the road does not fulfil the minimum lifespan. It is for sure that when taking into consideration the simultaneous effects of several distress models, the road lifespan would be even lower.

As it can be seen in the presented outcomes from the fatigue damage, the depths from 0.09 m to 0.33 m show a lifespan higher than 20 years. However the smaller depth (0.09 m) is the place where, logically, the buried system would perform better from a thermal point of view.

With the goal of improving the structural behaviour of the road and being able to locate the buried pipe system closer to the surface of the road, an epoxy resin layer was placed on the top of the surface of the road. When this fine layer of resin (with aggregates) is applied, a redistribution of loads occurs. As it can be seen in the presented outcomes, this resin layer confers a significant improvement on the structural behaviour of the road, prolonging its lifespan. The proof of this is that, just one millimetre of this resin on the top of the road provides a significant improvement of its structural properties, as can be seen in the tables.

According to the results, it can be concluded that it might be possible to locate the buried pipe system closer to the surface of the road, by adding an epoxy resin layer. However, additional and more complex studies/test are necessary to determine if a specific epoxy resin layer can provide enough structural reinforcement to place the piping embedded in the wearing asphalt course. It has to be noticed that this position seems to be unsuitable when not using a resin layer on top.

3.4 Experimental confirmation of minimum pipe depth to fulfil structural requirements of pavement

3.4.1 Introduction

The aim of this chapter is to study the mechanical performance of pipes system and assess its usability for thermal road solar collectors. The tests conducted in this task are specified in Table 34.

For purpose of this task Mostostal Warszawa provided two recipes of asphalt mixtures – one type was stone mastic asphalt SMA 11 45/80-55 KR 3-6 and the second one was asphalt concrete AC 16W 35/50 KR 3-6. Solintel delivered resin and hardener for Ultra-Thin resin layer along with an instruction how to prepare the layer. Commercially available Rauway Stabil was used as an example of pipe that can be put inside a pavement.

A summary of the tests carried out is given in Table 34 below.

	Test case description	Assumed number of variants
1	Resistance to indirect tensile stress	Three variants - with pipes (two different compaction methods) and without pipes
2	Influence of the pipe system on the rigidity module on cylindrical samples	Three variants - with pipes (two different compaction methods) and without pipes
3	Frost resistance	Two variants - with pipes and without pipes
4	The Marshall test - stability, deformation.	Two variants - with pipes and without pipes
5	Determination of resistance to permanent deformation	Three variants - options with pipes(at bottom and top of the layer) + comparative samples without inserts
6	Definition of the base rigidity module and resistance to fatigue with 4-point bending method	Three variants - options with pipes(at bottom and top of the layer) + comparative samples without inserts
7	Roughness test	1 option including 3 samples
8	Checking adhesion of the abrasive layer made of resin with the lay of mineral and asphalt mix - 2 tests per sample	Tests on 2 samples

Table 34. Scope of tests.

Samples for particular tests were prepared in the number corresponding to the variants specified in Table 34. Samples were marked with white paint for the purpose of clear identification.

3.4.2 Indirect Tensile Stress test ITS

The test verified resistance to indirect tensile stress of mineral-asphalt samples of asphalt concrete AC16W 35/50 and SMA 11 PmB 45/80-55. The test was performed according to PN-EN 12697-23.

The principle of this method is that, the tested cylindrical specimen is brought to the specified test temperature, placed in the compression testing machine between the loading strips, and loaded diametrically along the direction of the cylinder axis with a constant speed of displacement until it breaks. The indirect tensile strength is the maximum tensile stress calculated form the peak load applied at break and the dimensions of the specimen.

The test was conducted for samples without an insert in the form of a tube and with a tube.

For each mix, the following were prepared: 3 Marshall samples without a tube, 3 samples with a tube formed with a bolt filling the inside of the tube and compacted without the bolt and 3 samples with a bolt during forming and compacting samples.

The application of a filling bolt resulted directly from observation of a filling tube deformation when compacting the samples in Marshall's tamper in spite of the fact that the tube had smaller length than roll sample thickness (reserve for compacting). The use of a filling bolt was supposed to provide an answer to a question whether filling the tube will substantially affect the result of Indirect Tensile Stress test. Diameter of the bolt was selected so that the difference between its diameter and the internal diameter of the tube was 1mm. It was supposed to enable slight deformation of the tube under the effect of side pressure when compacting in a manner similar to filling the tube with hardly compressible liquid. The samples were compacted at the temperature consistent with the temperature specified in corresponding recipes for SMA and AC, with power of 2x75 strokes. Test results are specified in Table 35 and in Table 36.

Fig. 52. Tube preparation (overlaying with binder) intended for being placed in the sample.

Fig. 53. Samples of asphalt concrete prepared for ITS tests.

Fig. 54. SMA 11 samples prepared for ITS tests.

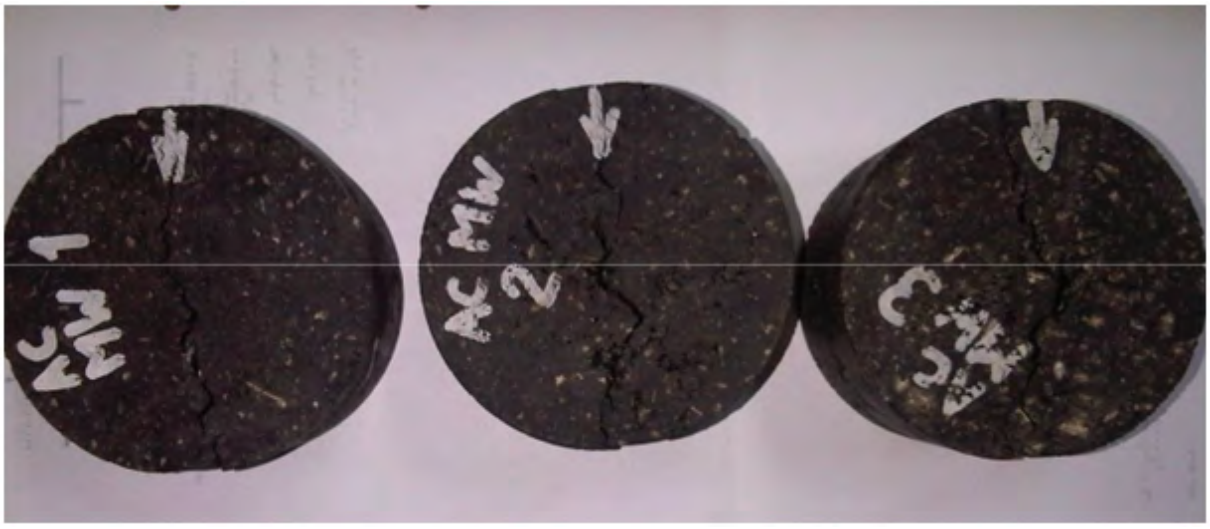

Fig. 55. The course of cracks of asphalt concrete.

Fig. 56. RB1 Sample after testing – cracks along load axis and fracture samples without tubes after ITS tests.

Fig. 57. Visual appearance of the rear part of asphalt concrete samples after ITS tests. The upper row is RB1-3 samples, the lower - RBB1-3.

Fig. 58. SMA samples before the ITS test. The left row - samples without a tube, middle - RB1,2,6 samples compacted with a bolt, on the - right RBB1,2,7 samples compacted without a bolt.

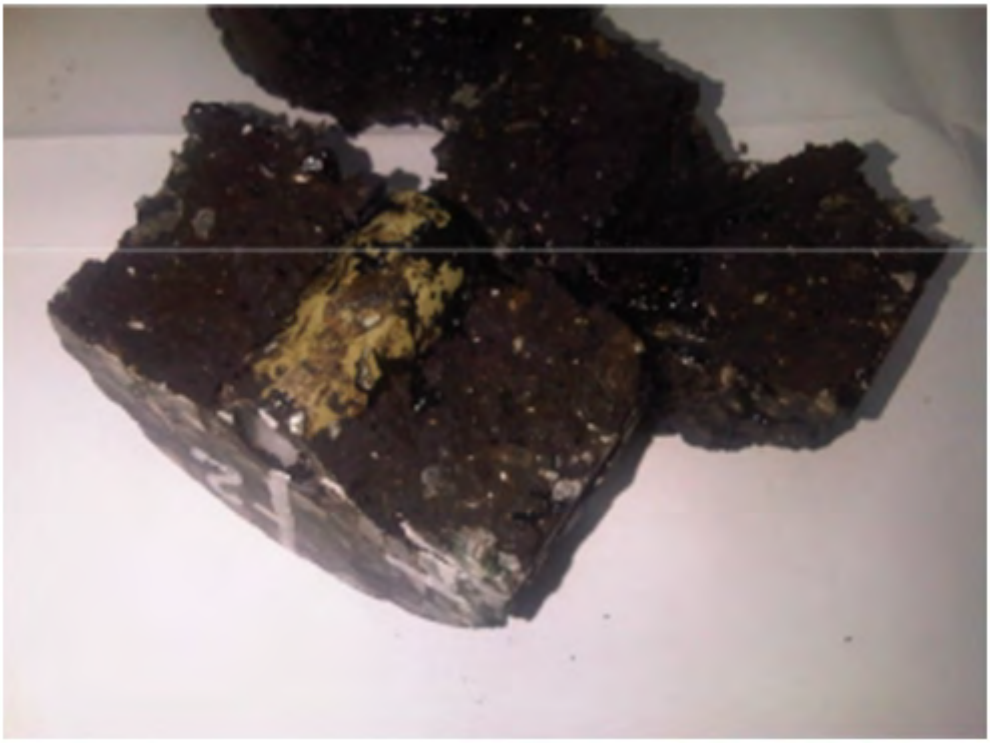

Fig. 59. RB1 sample fracture.

Larger deformations of tubes in samples compacted without the bolt was observed as compared to those compacted with a filling bolt (Fig. 58).

Sample type	Designation of the sample	Average height [mm]	Average diameter [mm]	Force of load [kN]	Stress [MPa]	Average stress [MPa]
AC without a tube	AC MW 1			19,499	1,891	1,91 (100%)
	AC MW 2			20,113	1,893	
	AC MW 3			21,091	1,941	
AC formed and compacted with a bolt	AC MW RB 1	51,4	101,75	15,180	1,847	1,84 (96%)
	AC MW RB 2	56,1	101,65	16,302	1,819	
	AC MW RB 3	56,25	101,70	16,615	1,847	
AC formed with a bolt and compacted without a bolt	AC MW RBB 1	51,0	101,6	15,654	1,923	1,93 (101%)
	AC MW 2 RBB 2	52,1	101,8	16,151	1,939	
	AC MW RBB 3	52,0	101,6	15,898	1,916	

Table 35. ITS test and results for AC16W mix.

Sample type	Symbol of sample	Height mean [mm]	Diameter average mm]	Force of load [kN]	Stress [MPa]	Average stress [MPa]
SMA without a tube	SMA 1	72,1	101,6	22,903	1,998	2,087
	SMA 2	71,2	101,6	22,706	1,990	
	SMA 3	61,2	101,7	22,232	2,274	
SMA formed and compacted with a bolt	S1 RB	49,2	101,7	11,944	1,520	1,485 (71%)
	S2 RB	49,2	101,6	11,350	1,446	
	S3 RB	49,2	101,6	11,690	1,489	
SMA formed with a bolt and compacted without a bolt	S1 RBB	44,1	101,7	11,216	1,592	1,612 (77%)
	S2 RBB	47,8	101,8	11,858	1,683	
	S3 RBB	46,0	101,7	11,471	1,561	

Table 36. ITS test and results for SMA 11 mix.

The results obtained in ITS test are surprising. The decrease of ITS in samples made of asphalt concrete and compacted without a bolt is very low 4%. Samples compacted with the bolt don't show any decrease in ITS results.

On the other hand, stone mastic asphalt samples show a very big decrease in ITS results. Both specimens groups, compacted with and without a bolt, show a significant decrease (respectively 29% and 23%) in comparison to the samples without a tube.

It's difficult to point out the reason for this. It is considered that a tensile strength in asphalt mixtures is mainly determined by the type of asphalt used. Modified asphalt is a material with a much higher tensile strength than the standard asphalt used. The opposite result obtained in a mixture containing SMA, based on modified asphalt, indicates that the introduction of the tube interfered with the construction of a mineral structure. The study indicates that in the case of SMA mixture impact on the shape of the mineral structure determines the strength, not the type of asphalt used.

3.4.3 Determination of the rigidity module on cylindrical samples

Before the test all samples were marked with perpendicular diameters and then in 4 places sample height of the sample was measured and its diameter and volumetric density was determined. Before the test samples were conditioned at the temperature of tests for 4 hours. Sample temperature measurement was made on the control sample on its surface and inside. A frame was mounted on the sample with displacement sensors (Fig. 60) . The frame was fastened perpendicularly to the direction of the used load. In order to adjust the value of force, which will enable obtaining appropriate value of displacement at least 10 preliminary pulses were made. Then 5 test pulses were performed with value of displacement registration and corresponding rigidity module. As the result arithmetic mean was assumed. After completion of this test the sample was rotated about 90 degrees and the test was performed. If the difference between the average from the second measurement does not exceed+ 10%, -20% of the value of the first tests, the assumed result was the average value from two tests.

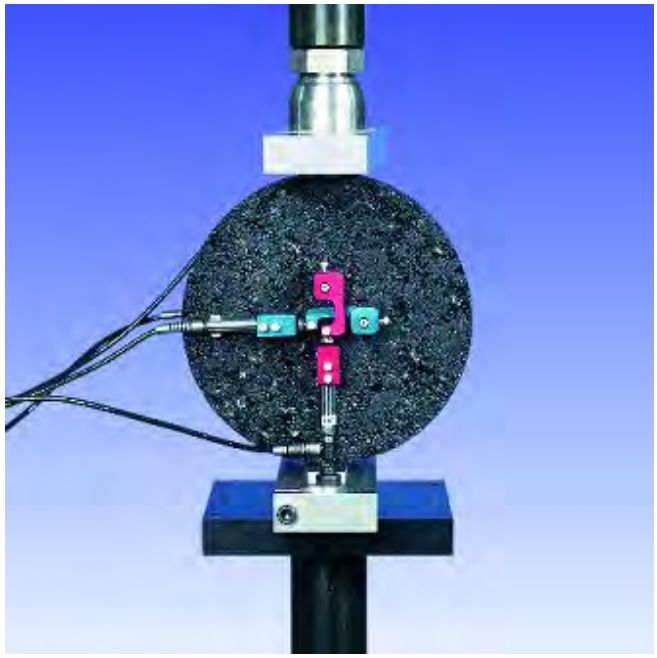

Fig. 60. A scheme of sample placing.

The results obtained are shown in the next tables.

Sample marking	Dimensions of samples						Test temperature											
							2.0 oC				10.0 oC				20.0 oC			
	Height			diameter			the obtained values of rigidity module				the obtained values of rigidity module				the obtained values of rigidity module			
	measured		average	measured		average	SM	SM 90o	SM of the sample	SM of the set	SM	SM 90o	SM of the sample	SM of the set	SM	SM 90o	SM of the sample	Sm of the set
	[mm]	[mm]	[mm]	[mm]	[mm]	[mm]	[MPa]	[MPa]	[MPa]	[MPa]	[MPa]	[MPa]	[MPa]	[MPa]	[MPa]	[MPa]	[MPa]	[MPa]
normal samples																		
AC1	65,2	65,5	65,4	101,6	101,6	101,6	15206	14928	15067		9450	9394	9422		3175	2995	3085	
	65,3	65,6		101,6	101,7													
AC 2	66,6	66,3	66,2	101,7	101,6	101,6	14940	14160	14550	15005	9184	9238	9211	9253	3652	3594	3623	**3406**
	66,0	66,1		101,6	101,6													
AC 3	61,2	61,3	61,3	101,6	101,7	101,7	15426	15368	15397		9076	9173	9125		3580	3440	3510	
	61.5	61,3		101.7	101.6													
samples with a tube compacted with a steel bolt																		
AC1 RB	44,4	44,6	44,4	101,6	101,7	101,7	7753	7539	7646		4652	4551	4602		2728	2611	2670	
	44,3	44,1		101,7	101,6													
AC2 RB	48,5	48,6	49,0	101,6	101,7	101,6	7956	7829	7893	7846	4008	4163	4086	4325	2237	2326	2282	**2488**
	49,3	49,5		101,5	101,6													
AC3 RB	46,1	45,9	46,1	101,6	101,7	101,6	8062	7933	7998		4321	4250	4286		2598	2423	2511	
	45.6	46.9		101.5	101.6													
samples with a tube compacted without a steel bolt																		
AC1 RBB	48,6	50,0	49,2	101,8	101,7	101,7	7721	7327	7524		4568	4287	4428		2410	2376	2393	
	49,1	49,1		101,7	101,7													
AC2 RBB	49,2	49,4	48,9	101,8	101,8	101,8	7856	7798	7827	7802	4395	4150	4273	4222	2650	2585	2618	**2500**
	48,2	48,6		101,8	101,6													
AC3 RBB	47,6	47,1	46,1	101,8	101,6	101,7	7990	8120	8055		4035	3897	3966		2534	2445	2490	
	47.6	48.2		101.7	101.7													

Table 37. Rigidity module test for AC 16 W.

Sample marking	Dimensions of samples						Test temperature							
							2.0 oC				10.0 oC			
	Height			diameter			the obtained values of rigidity module				the obtained values of rigidity module			
	measured		average	measured		average	SM	SM 90o	SM of the sample	Sm of the set	SM	SM 90o	SM of the sample	SM of the set
	mm	[mm]	[mm]	[mm]	[mm]	[mm]	[MPa]	[MPa]	[MPa]	[MPa]	[MPa]	[MPa]	[MPa]	[MPa]
samples without a tube														
SMA 1	72,2	72,1	72,1	101,6	101,6	101,6	14786	14149	14468	14367	6690	6395	6543	**7089**
	72,2	72,0		101,6	101,7									
SMA 2	71,7	70,6	71,2	101,7	101,6	101,6	13586	14170	13878		7361	6683	7022	
	71,6	71,0		101,6	101,6									
SMA 3	61,0	61,0	61,2	101,6	101,7	101,7	15136	14375	14756		8102	7300	7701	
	61,6	61,3		101.7	101.6									
samples with a tube formed in a taper with a steel bolt														
S1 RB	49,2	49,4	49,2	101,6	101,7	101,7	6653	6439	6546	6424	3644	3660	3652	**3437**
	48,2	50,0		101,7	101,6									
S2 RB	48,6	50,0	49,2	101,6	101,7	101,6	6353	6088	6221		3412	3490	3451	
	49,1	49,1		101,5	101,6									
S6 RB	48,5	48,6	49,2	101,6	101,7	101,6	5996	7015	6506		3391	3023	3207	
	50.3	49.5		101.5	101.6									
samples with a tube formed in a taper without a steel bolt														
S1 RBB	44,4	43,9	44,1	101,8	101,7	101,7	7213	6441	6827	6297	3918	3767	3843	**3465**
	44,0	44,1		101,7	101,7									
S3 RBB	47,6	47,3	47,8	101,8	101,8	101,8	5927	5769	5848		3422	2986	3204	
	47,8	48,3		101,8	101,6									
S7 RBB	46,0	45,7	46,0	101,8	101,6	101,7	6640	5789	6215		3433	3262	3348	
	45.6	46.8		101.7	101.7									

Table 38. Rigidity module test for SMA 11.

We can observe approximately 50% reduction in the static rigidity module of roll samples with a tube as compared to samples without a tube, both in the case of asphalt concrete and grit mastic SMA.

3.4.4 Frost resistance

Test was made accordingly to Polish standards specified in “Wymagania Techniczne 2:2010”. Test of frost resistance was conducted on cylindrical samples prepared as for a test in the Marshall apparatus. A set of samples of SMA mix and AC16W with tubes insert was prepared and comparative samples without an insert. One group comprised of samples of "the dry set" – comparative and the second of "the wet set".

Two sets of samples were prepared for the test: "dry", not subjected to freezing cycle and "wet", which was kept in water at increased temperature and frozen. For each set 3 samples were made. The samples were compacted 2x35 strokes in the Marshall's tamper. The samples were measured (height and diameter) and volumetric density was determined. Then, they were divided into two sets of similar dimensions and volumetric densities. The difference between dimensions should not be greater than 5 mm, and between the densities 15 kg/m3 (0.015g/cm3). The samples from the "dry" set were placed on an even surface and kept in a room temperature (ca. 20◦C). The samples from the "wet" set were inserted to a vacuum chamber and soaked with water. This activity was performed under reduced pressure 6.7kPa, for the period of half an hour. After this time the pressure was gradually increased to the level of atmospheric pressure and left in water for the next 30 minutes. After this time the samples were taken out of water and the dimensions were measured again. Samples were rejected if they changed their volume by more than 2%. Then, the samples were placed in water bath at the temperature of 40◦C for a period of 68 to 72 hours. After taking the samples out of water bath avoiding excessive water dripping, they were tightly wrapped in foil of "stretch" type and put into a plastic bag containing 10ml of water and tightly closed. Samples prepared in that way were put into a cooling chamber at the temperature of - 18◦C and kept for 16 hours, counting from the moment of the cooler reaching this temperature. After taking the samples out of the freezer, they were put into water bath with the temperature of 60◦C and after defrosting bags and foil were removed. The samples were stored in the bath for 24 hours from the moment of the first placement of the samples in water after taking them out of cooling chamber. Before the indirect tensile stress test of the sample tests temperature reached 25◦C. Samples were kept in this temperature for the period of 2 hours. The prepared samples were pressed in the Marshall press and their indirect tensile stress strength was determined. The resistance of samples to frost was defined by comparing average strength of samples from wet to average strength of samples from the dry set in accordance with the formula:

$$ITSR = 100 \cdot \frac{ITSw}{ITS_d}$$

where:

ITSw – average indirect tensile strength determined for wet samples

ITSd – average indirect tensile strength determined for dry samples.

Fig. 61. Roll samples AC16W for testing frost resistance after formation the Marshall tamper.

Fig. 62. A batch of samples for frost resistance testing during soaking in water with the temperature of 40 and 60^{0}C.

Fig. 63. Samples prepared for freezing.

Sample marking	Properties of samples							Test results				
	Height			diameter			volumetric density	maximum force	value ITS	ITS of the set	I TSR	set
	measured		average	measured		average						
	[mm]	[mm]	[mm]	[mm]	[mm]	[mm]	[g/cm3]	[kN]	[MPa]	[MPa]	[%]	
concrete asphalt samples with a tube												
AC16M01	65,1	65,3	65,4	101,8	101,9	101,8	2,346	14,671	1,403	1,370	80,3	wet set
	65,8	65,4		101,9	101,6							
AC16M02	63,0	63,3	63,2	101,6	101,6	101,6	2,345	13,874	1,376			
	63,3	63,3		101,5	101,5							
AC16M03	65,3	66,0	65,8	101,6	101,6	101,6	2,333	13,965	1,330			
	66,0	65,7		101,6	101,7							
AC16M04	62,0	63,1	63,0	101,6	101,6	101,6	2,329	17,202	1,711	1,706		dry set
	63,7	63,0		101,7	101,5							
AC16M05	57,3	57,2	57,2	101,8	101,6	101,7	2,330	15,520	1,698			
	57,4	57,0		101,6	101,8							
AC16M06	60,3	59,9	60,2	101,8	102,0	101,9	2,331	16,468	1,709			
	60.1	60.3		101.9	101.8							
concrete asphalt samples without a tube												
AC16M08	62,3	62,0	62,0	101,8	101,7	101,7	2,408	20,494	2,069	2,155	87,9	wet set
	61,7	61,9		101,6	101,8							
AC16M09	69,0	68,6	69,1	101,6	101,6	101,6	2,400	24,843	2,253			
	69,1	69,8		101,6	101,4							
AC16M10	69,0	68,4	68,7	101,4	101,4	101,4	2,401	23,434	2,142			
	68,4	69,0		101,7	101,2							
AC16M07	73,4	73,2	73,2	101,6	101,5	101,6	2,396	26,574	2,275	2,453		dry set
	73,1	73,1		101,7	101,6							
AC16M11	63,6	63,7	63,9	101,3	101,8	101,6	2,394	26,261	2,575			
	63,9	64,2		101,6	101,8							
AC16M12	67,4	67,8	67,6	101,8	101,8	101,8	2,383	27,134	2,510			
	67,7	67,3		101,7	101,8							

Table 39. Frost resistance tests results. Concrete asphalt samples.

Sample marking	Properties of samples							Test results				
	Height			diameter			volumetric density	maximum force	value ITS	ITS of the set	I TSR	Set
	measured		average	measured		average						
	[mm]	[mm]	[mm]	[mm]	[mm]	[mm]	[g/cm3]	[kN]	[MPa]	[MPa]	[%]	
SMA samples with a tube												
SMA M8	75,0	74,8	75,2	101,6	101,2	101,5	2,510	15,522	1,295	1,239	93.4	wet set
	75,4	75,5		101,5	101,5							
SMA M10	70,2	70,3	69,9	101,6	101,4	101,5	2,514	14,050	1,261			
	69,1	70,0		101,5	101,5							
SMA M11	58,8	59,3	59,4	101,4	101,6	101,6	2,507	11,343	1,197			
	59,6	59,7		101,8	101,7							
SMA M9	67,5	68,2	67,8	101,3	101,4	101,4	2,493	13,325	1,234	1,326		dry set
	68,3	67,3		101,4	101,5							
SMA M12	72,0	72,6	72,5	101,5	101,4	101,4	2,502	17,253	1,494			
	72,9	72,3		101,4	101,3							
SMA M7	65,0	65,5	65,6	101,6	101,6	101,6	2,499	13,101	1,251			
	65.9	66.0		101.6	101.5							
SMA samples without a tube												
SMA M1	67,4	67,3	67,5	101,7	101,6	101,7	2,558	16,499	1,530	1,590	92.4	wet set
	67,5	67,8		101,7	101,6							
SMA M3	59,1	59,3	59,0	101,6	101,6	101,6	2,555	14,455	1,535			
	59,0	58,5		101,7	101,6							
SMA M4	66,1	65,8	65,6	101,8	101,6	101,8	2,556	17,874	1,704			
	65,0	65,3		101,8	101,8							
SMA M2	65,0	65,7	65,5	101,4	101,6	101,6	2,551	17,082	1,634	1,720		dry set
	65,9	65,2		101,5	101,7							
SMA M5	59,7	59,6	59,8	101,6	101,7	101,6	2,540	16,421	1,721			
	60,1	59,9		101,7	101,5							
SMA M6	65,5	65,5	65,3	101,6	101,7	101,7	2,542	18,865	1,806			
	65.2	65.1		101.8	101.6							

Table 40. Frost resistance tests results. SMA samples.

Minimum ITSR values according to the guidelines WT-2 are: for AC16W – 80% and for SMA 90%. These requirements were met by the tested samples.

3.4.5 Test of rut formation

A rut is a sunken track or groove made by the passage of vehicles. A test is necessary to determine the behaviour of the road regarding rut formation. This test was conducted by means of a "small" wheel tracker (model B) – test in the air according to PN-EN 12697-22. The samples had the form of perpendicular slabs with the horizontal dimensions of 305x400 mm. The mineral-asphalt mix was compacted using the steel roller method, in accordance with PN-EN 12697-33 in the temperature of 140^0C for asphalt concrete and 145^0C for stone mastic asphalt (SMA) mix. Samples were formed in two phases – first the SMA mix, given that in samples with inserts in the mix of asphalt concrete, the previously prepared tubes coated with a binder layer were placed, and then a layer of resin and aggregate 0/8mm was applied on the samples. Such grain size of aggregate is recommended by the manufacturer of the resin – and for such grain size, it stated the suggested consumption of resin and hardener. Because of a visible lack of connection between the aggregates and resin a 50% addition to the quantity of resin was made. To increase the stiffness of the resin-aggregate layer it thickness was increased to 10mm. It was accomplished by laying resin and aggregate in two layers. The second layer was made with double amount of resin then suggested in recipe. In this way, 6 samples were prepared: 2 without tubes (marking M1 and M2), 2 with tubes at the top part of the SMA layer (M4 and M6) and 2 with tubes at the bottom SMA layer (M3 and M7). In each sample 2 tubes were installed at the surface, running throughout the whole width of the mould, in the perpendicular direction to the rut formation. The distance between tubes is 100mm and they were located symmetrically relative to the transverse axis of the sample. Such spreading of samples can guarantee a possibility of verification of behaviour of inserts under the effect of the wheel load on the rut meter. The view of the sample with inserts is shown in Fig. 64 and a more detailed view of the surface can be seen in Fig. 65, Fig. 66 and Fig. 67.

Thickness of the SMA mix layer for each sample is specified in Table 41.

Then, samples were subjected to the wheel tracking test. Before its commencement, the samples were conditioned at the temperature of 60^0C. 10000 cycles or achieving the rut depth of 20mm were set. During the course of wheel tracking test, temperature in the working chamber was controlled, and the rut depth was measured. Then, calculations were conducted as to inclination of the rut formation chart WTSAIR, the average proportional rut depth PRDAIR and the average rut depth RDAIR. The results have been shown in Table 41.

Fig. 64. Sample M3 before the rut formation test.

.

Fig. 65. Sample 1 after laying the 1st aggregate layer on resin.

Fig. 66. Laying the 2nd aggregate layer after application of resin on the 1st layer.

Fig. 67. Sample ready for rut formation test.

Designation of the sample	Thickness of SMA + 2x aggregate 0/8 on resin (core thickness of SMA/core thickness with layers of aggregate on resin) [cm]	Inclination of the rut formation chart WTSAIR [-]	Average proportional rut depth PRD_{AIR} of the whole sample /brought to SMA [%]	Rut depth RD_{AIR} [mm]	Number of rut formation cycles [-]
M1 without inserts	46,2/61,2	0,038	4,4 / -	2,62	10000
M2 without inserts	44,4/61,2	0,044	3,8 / -	2,30	10000
M3 inserts from the bottom	48,4/62,2	0,032	3,4 / -	2,02	10000
M4 inserts from the top	47,8/60,4	0,050	5,0 / -	3,01	10000
M6 inserts from the top	50,5/64,4	0,052	3,1 / -	1,99	10000
M7 inserts from the bottom	49,0/61,6	0,052	3,8 / -	2,32	10000

Table 41. Rut formation test results

Below, there are charts of growth and profile of ruts for particular samples.

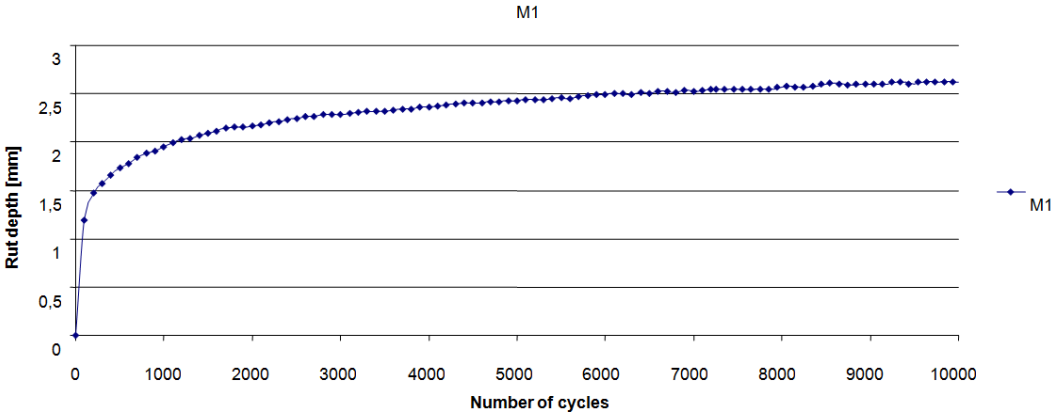

Fig. 68. Chart of rut growth for sample M1

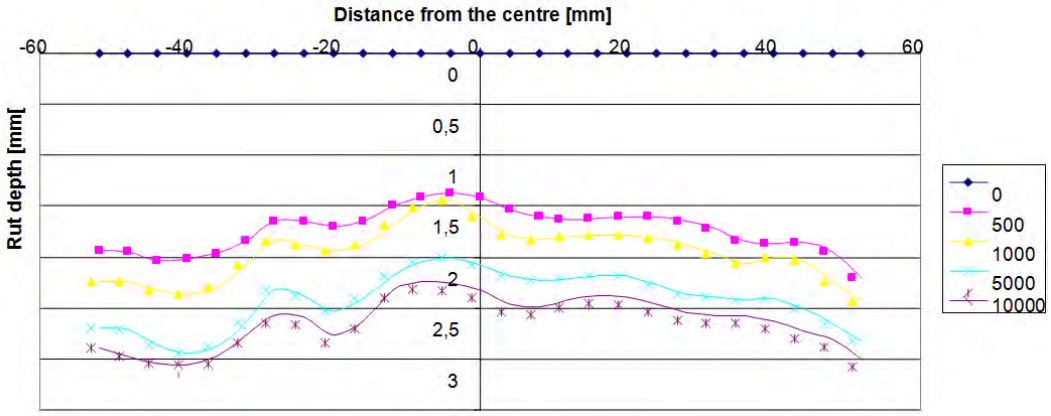

Fig. 69. Chart of rut profile for sample M1

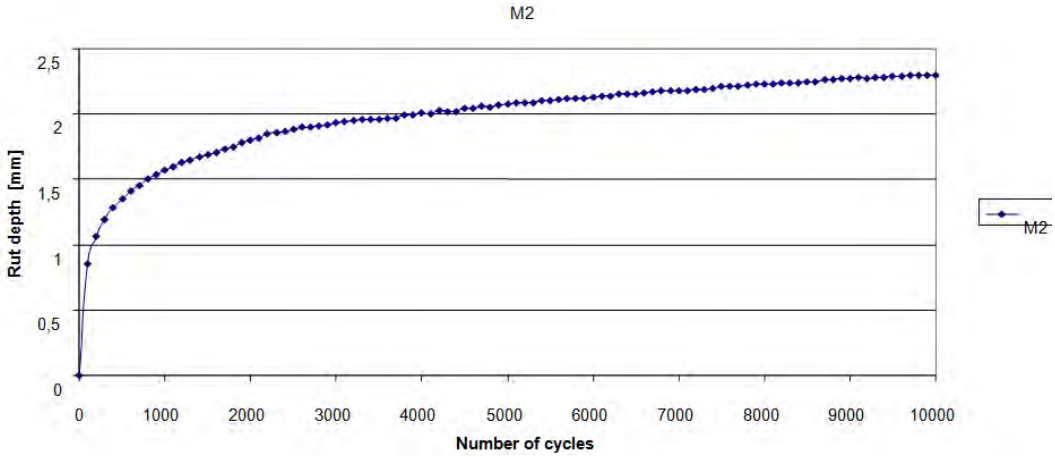

Fig. 70. Chart of rut growth for sample M2

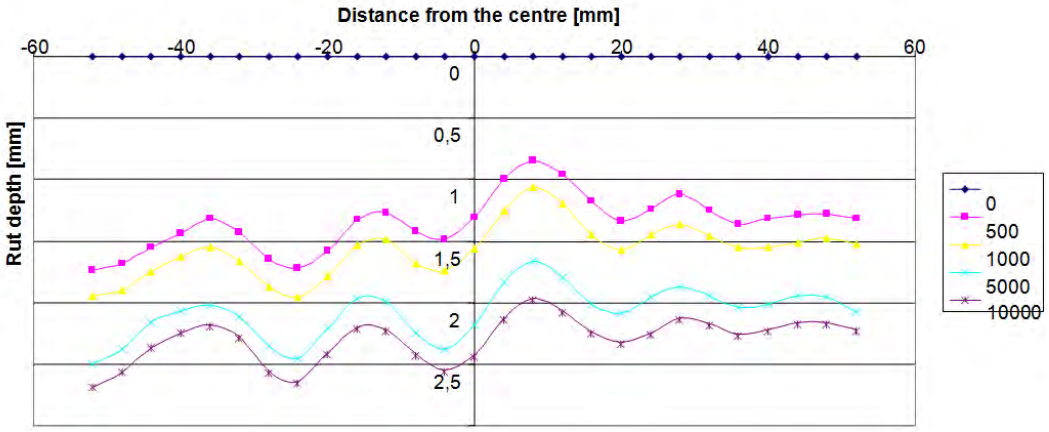

Fig. 71. Chart of rut profile for sample M2

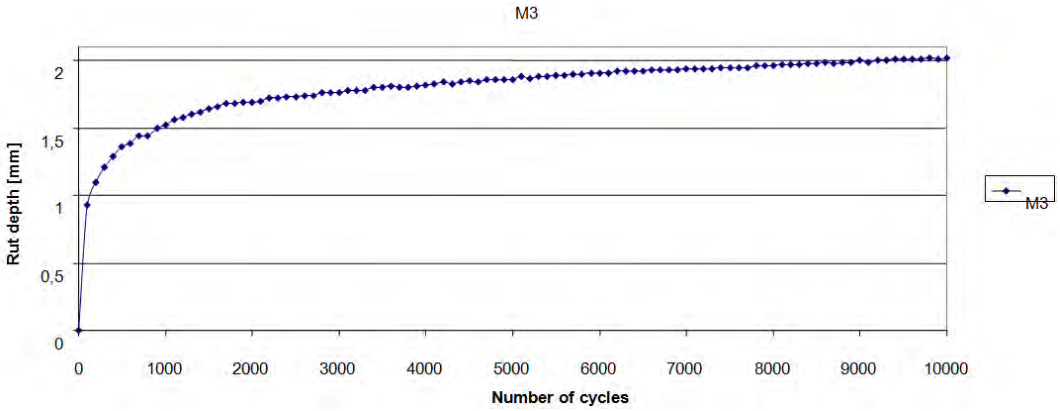

Fig. 72. Chart of rut growth for sample M3

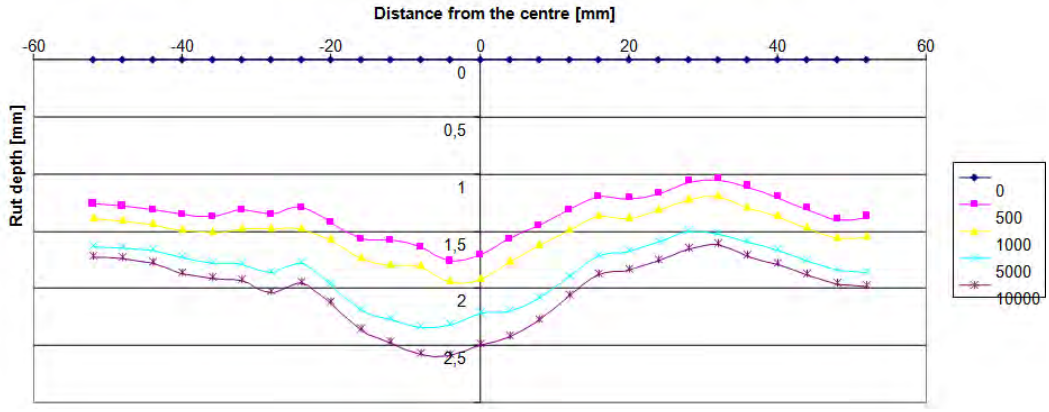

Fig. 73. Chart of rut profile for sample M3

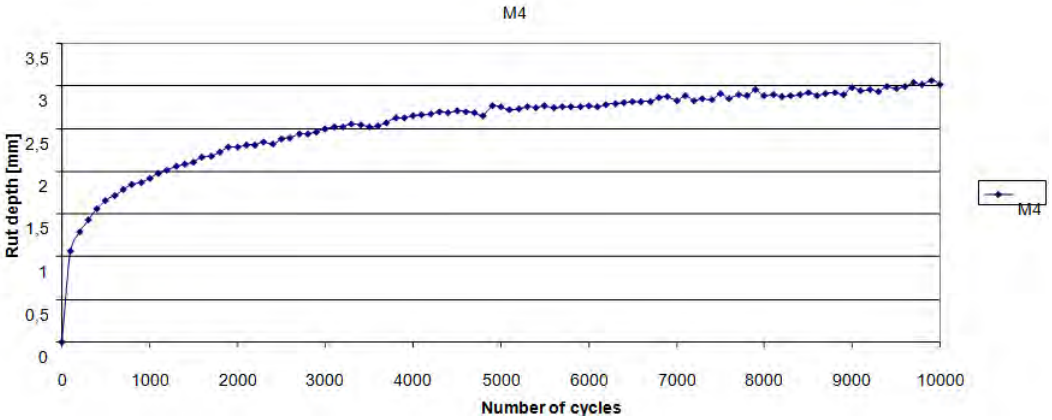

Fig. 74. Chart of rut growth for sample M4

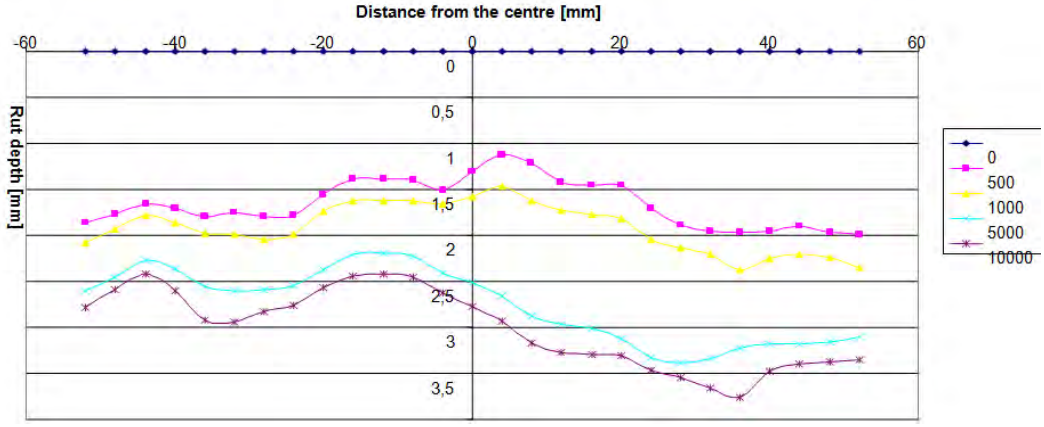

Fig. 75. Chart of rut profile for sample M4

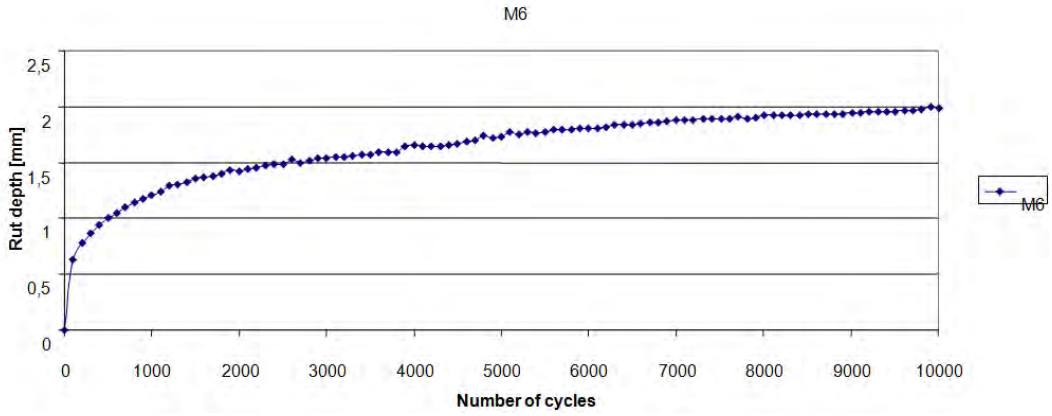

Fig. 76. Chart of rut growth for sample M6

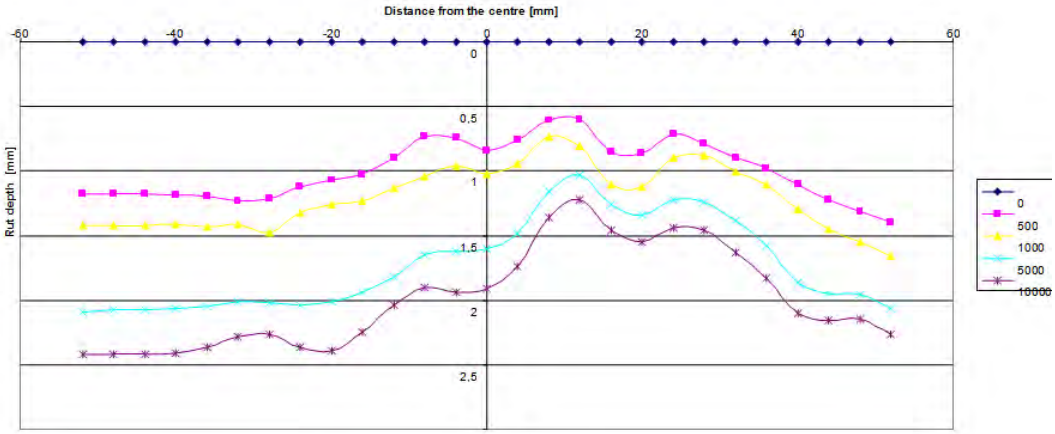

Fig. 77. Chart of rut profile for sample M6

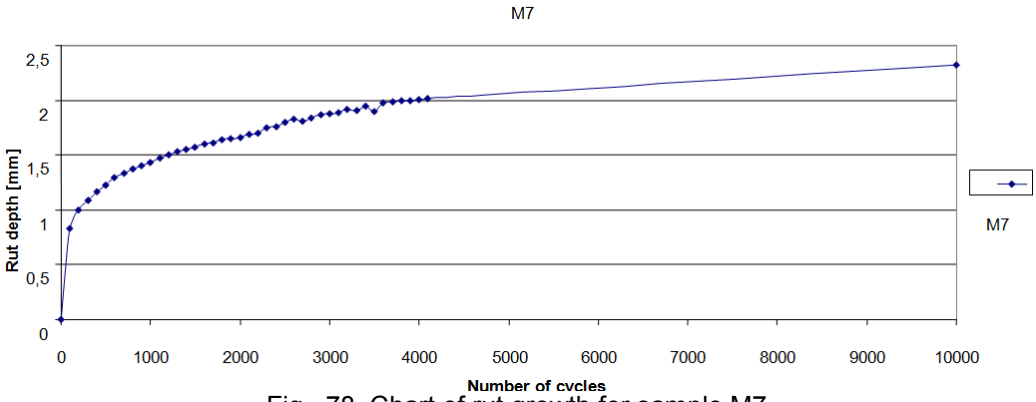

Fig. 78. Chart of rut growth for sample M7

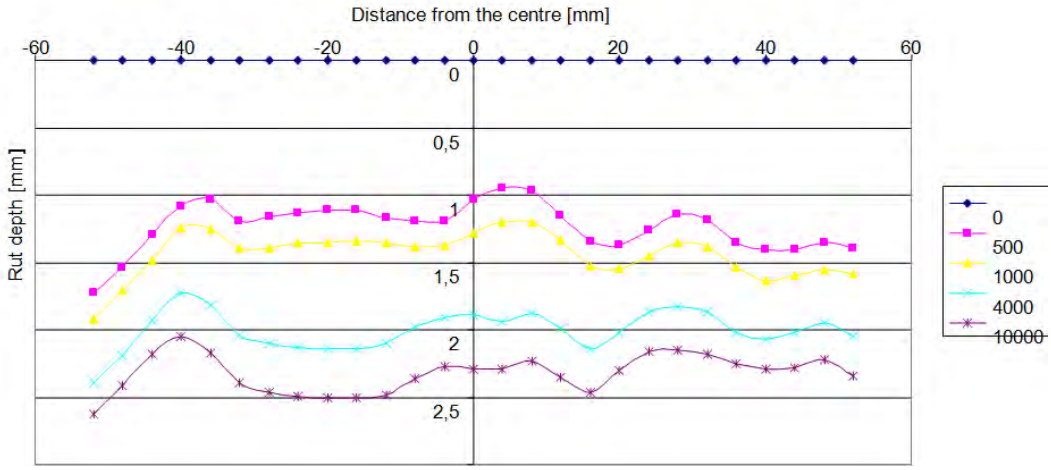

Fig. 79. Chart of rut profile for sample M7

Small flattening of tubes was observed in consequence of compaction of the abrasive layer with a roll.

No significant deformations in tubes were observed under the wheel of the tracking device.

The beneficial impact of the mineral and resin layer on reduction in rut formation test was observed for sample M3 (pipes at the bottom), while the sample with pipes located at the top had the greatest rut depth. This proves insufficient rigidity of the mineral and resin layer covering the tubes located directly under it.

The layers with pipes put at top, even with a double resin layer couldn't fulfil requirements specified in Polish standards regarding their durability to deformations.

Only samples that were made with inserts of the pipes in the bottom of the SMA layer could have been used in roads specified as KR3-KR4. The rigidity of a resin layer was insufficient to put more axis number load (specified as KR5-KR6) on such prepared layer.

3.4.6 Testing resistance to fatigue and the rigidity module with a four-point bending method

Testing by means of a four point bending method consists in causing load of the beam with the nominal dimensions of 50x63x380mm cut-out from the prepared sample of mineral and asphalt mix. Samples were tested in two positions of tubes: at the upper surface of the sample, as well as the lower surface of the sample. In connection with the above, samples with inserts made of tubes and comparative samples without tubes were prepared. Tubes were spread in the gauge of 10cm, 3 per sample.

Samples were moulded in the compactor for the rut meter. Before embedding, the tubes were coated with binder (Fig. 80). The tests were conducted at the temperature of 10^0C. Before a test, samples were conditioned at the test temperature for 4 hours. Altogether, 12 samples were made.

Samples:

- of series BR/z had no inserts, two samples without resin layer (1;2) and two samples with resin layer (3;4),

- of series R1/x had inserts at the top,

- of series R2/y – inserts at the bottom.

The test was conducted in the multifunctional machine UTM-25 (see next figures) which chamber enables maintaining the test temperature. Load frequency of 10Hz was applied. Before each, a series of preliminary impulses with the frequency of 1, 2, 5,10 and 1 Hz were made, 100 impulses for each frequency.

After the 100th cycle the initial rigidity module of the examined beam was determined. Then, the proper test was performed, determining the parameters of its interruption at the moment when the rigidity module decreased by over 50% of the primary module. Then in accordance with the research procedure, fatigue strength was deemed exhausted. Trials were assumed according to the controlled shift on the sample of up to 100 deformation units.

Fig. 80. Tubes coated with binder before installation in the mineral-asphalt mix.

Fig. 81. Samples R1/1 and R1/2 before the test.

Fig. 82. Addition to the test using four point bending method.

Fig. 83. Beams coated with resin – prepared for applying the aggregate.

Fig. 84. Beams with 2 layers of aggregate on resin.

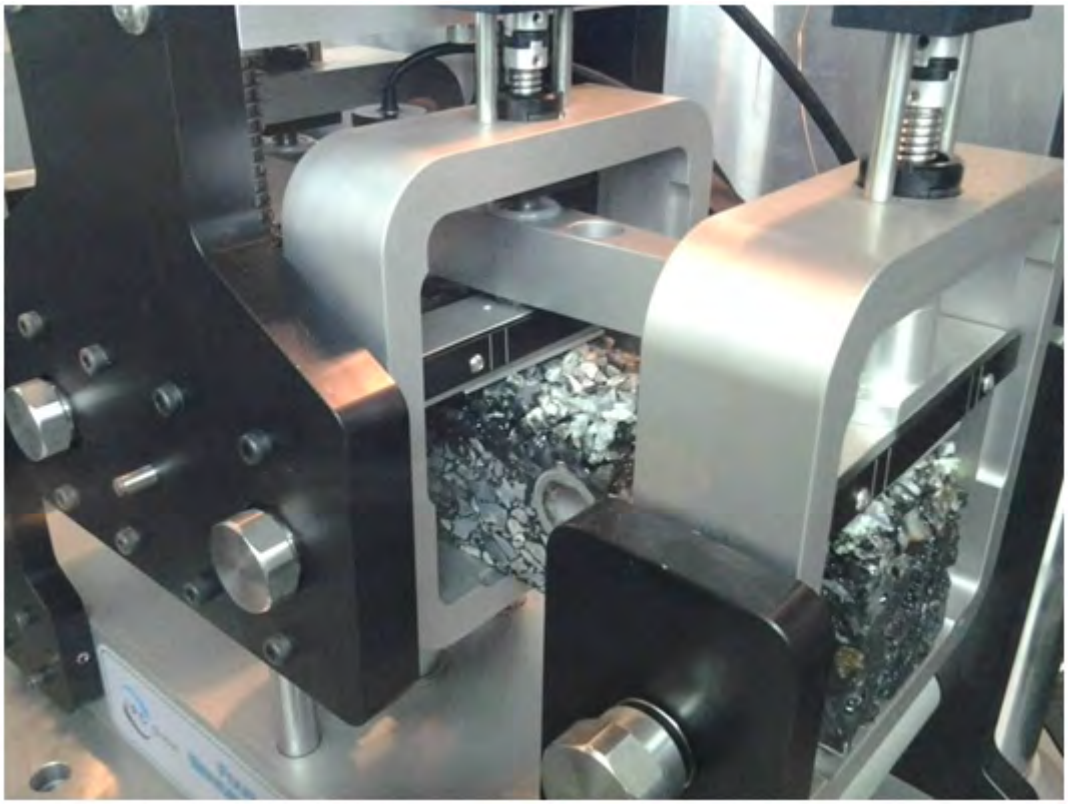

Fig. 85. Beam R1/1 during the test - tubes at the top part of the beam.

Fig. 86. Sample R2/2 prepared for the test.

Test conditions for the results in the Table 42 and Table 43: temperature: + 10^0C and deformation amplitude 50$\mu\varepsilon$.

Sample symbol	Rigidity module [MPa]				
	1Hz	2Hz	5Hz	10Hz	1Hz
BR1/1	4334	5383	7000	8429	4291
BR1/2	4205	5220	6767	8110	4172
BR1/3	3943	4540	5477	6246	3907
BR1/4	3740	4308	5203	5929	3731
R1/1	Cracking of slab	-	-	-	-
R1/2	3652	4220	4987	5595	3659
R1/3	4479	5119	5947	6562	4466
R1/4	4526	5137	5942	6641	4539
R2/1	1753	1931	2207	2453	1759
R2/2	1668	1874	2123	2364	1683
R2/3	1780	1963	2267	2558	1793
R2/4	2713	3023	3518	3875	2789

Table 42. Initial test of the rigidity module with the four point bending method

Sample symbol	Rigidity module [MPa]		Fatigue damage%
	After the 100th cycle	After 1 million cycles	
BR1/1	8152	6408	21,4
BR1/2	7603	6155	19,0
BR1/3	5991	5593	6,6
BR1/4	6388	5337	16,5
R1/2	6471	5436	16,0
R1/3	6576	5465	16,9
R1/4	7065	5829	17,5
R2/1	2510	2308	8,0
R2/2	2463	2339	5,0
R2/3	2276	1903	16,4
R2/4	3911	3578	8,5

Table 43. Final test of the rigidity module with the four point bending method.

As a result of the conducted tests, the following were diagnosed:

- value of the dynamic rigidity module in the test with the 4-point bent beam method - at the level of 84.8-101.8% for samples with tubes at the bottom of the sample and approximately 40% with tubes at the top of the sample in comparison to samples without tubes, and the initial value of the rigidity module of the samples with tubes at the top was at an average level of approximately 30% of the rigidity module of samples without inserts,
- smaller fatigue damage of samples with mineral and resin layers with pipes than in samples without inserts.

Although Polish national standard do not specify the requirements regarding stiffness for this type of mixture (SMA), the rigidity module of a layers with the lowest fatigue damage is too low to be considered as proper and durable solution for KR 3-6 road pavement. However, it should be also

noted that this method assumes isotropy of the tested material- which is clearly in the case of pipes inside of samples not met.

3.4.7 Tests of roughness

Roughness check was made by means of determination of the friction coefficient using the BRST method – by defining the value of friction between the rubber slipper, and the pavement. The pendulum reflects the conditions of the slip of a wheel moving at the speed of 50÷60 km/h on the roadway surface.

Sample symbol	Friction value in the temperature of 13.5 ° C		Mean
	In the 1st direction	In the 2nd direction	
PR M6 over the inserts	80 65 77 93 78 85	91 68 82 88 84 82	85,5 66,5 79,5 90,5 81 83,5
PR M6 next to the inserts	88 98 93 80 98 88	72 78 78 78 88 81	80 88 85,5 79 93 84,5
PR M2	65 84 87 80 80 82	88 83 93 72 78 82	76,5 83,5 90 76 79 82

Table 44. Measurement of friction using the BRST method.

During the tests, pulled out aggregate grains from the abrasive layer was noticed – on average 6 grains at each test. No impact of the location of the test on the obtained roughness results was observed.

3.4.8 Checking adhesion of abrasive layer of resin to the mineral and asphalt mix

The test was performed with the use of a Proceq Dyna Tester device, with pull-off method (Fig. 87). The test was performed for 2 samples. On each sample, 4 disks were stuck with epoxy glue: 2 over the inserts and 2 beyond the inserts.

Fig. 87. Test of adhesion with the pull-off method.

The adhesion test results are shown in Table 45.

Sample symbol	Pull-off force value [kN]			
	Disk 1 (over the insert)	Disk 2 (above the insert)	Disk 3	Disk 4
PR M6 over the inserts	2,0	1,7	1,6	1,4
PR M2	1,2	1,4	1,6	1,3

Table 45. Results of adhesion test with the pull-off method.

Results of adhesion test proved poor sticking of aggregate to the SMA slab through the layer with epoxy resin with hardener. It should be pointed out that the slab surface was covered with resin mixed with hardener in the quantity 1.5-times higher than recommended for aggregate with the grain size of 0/8mm. Other option is to use more even asphalt mixture, like asphalt concrete for an example.

3.4.9 Conclusions

The following features of SMA (and in some tests AC) samples with and without pipes were studied:

- The resistance to permanent deformation.
- The rigidity module.
- The rigidity module on cylindrical samples.
- The resistance to fatigue.
- The roughness.
- The adhesion of abrasive layer made of resin with the lay of mineral and asphalt mix.
- The frost resistance.
- The resistance to indirect tensile stress.

The placing of the tubes was made accordingly to the best possible thermal situation obtained in simulation done in 3.1. Lateral spacing was 10 cm and diameter of tubes was 2 cm.

The tests checked if it is possible to put the tubes as close as it is possible to the surface of road. To increase the rigidity of the road construction was tested with the use of a mineral and resin layer as the top course. As the asphalt top layer, the wearing course, SMA was chosen. Stone mastic asphalt is a type of mixture that is widely known and used in the whole of Europe as a durable type of pavement on heavy traffic roads. Even though national standards in road construction can be different, still these tests can be useful from structure point of view.

The tests proved small impact of the mineral and resin layer on the endurance and durability characteristics of the pavement.

A clear positive effect of application of this layer was a limitation of rut formation. No significant deformations in tubes under the wheel of the rut meter were observed. The beneficial impact of the mineral and resin layer on reduction in rut formation test was observed for sample with inserts from the bottom, while the sample with inserts from the top had the greatest rut depth. This proves insufficient rigidity of the mineral and resin layer covering the tubes when they are located directly under it. The layers with pipes put at top, even with a double resin layer couldn't fulfil requirements specified in Polish standards regarding their durability to deformations.

Only samples that were made with inserts of the pipes in the bottom of the SMA layer could have been used in roads with medium traffic specified as KR3-KR4 (up to 1000 of 100 kN equivalent of single axle load per lane per twenty four hours (ESAL100)). Naturally this type of mixture with pipes at the bottom of wearing course can also be used on roads with even lower traffic - KR1-2. The rigidity of a resin layer was insufficient to put more axis number load (specified as KR5-KR6 (more than 2000 per day of ESAL100) on such prepared layer.

If we decide to increase the lateral spacing of the tubes or to decrease their diameter we can suspect that we will obtain a more durable pavement. Of course, the efficiency of such thermal collector system will be lower.

However, adhesion of the resin layer to the base is insufficient. Because of this, studied technology of resin layer can't be safely used in any of EU countries. Obtaining a uniform abrasive layer, with good adhesion to the base, and, at the same time the proper thickness requires changing a technology or a resin. In the tests, this layer was made of broken aggregate with grain size of 0-8mm. Such maximum grain size was accepted by the manufacturer of the resin. In order to obtain selected thickness, two aggregate layers were laid on resin (along with compacting), which could have been an indirect cause for low adhesion of the mineral and resin layer to the base and the mutual adhesion of aggregate grains.

It is also possible to completely abandon the idea of aggregate and resin layer and just increase the depth of tubes. We will significantly increase durability of the road by placing the tubes in the lower

layers of road construction – in the bonding course or even deeper in the asphalt base course. On the other hand it will also decrease the efficiency of the thermal collector system

3.5 General conclusions of Thermal Road Solar Collector

The thermal studies performed in this report focus on the influence of several parameters over the annual collection rate. From these results, it has been obtained that placing the pipes at a depth of 4-5 cm from the surface (lower part of the wearing asphalt) instead of placing them at 9 cm (middle of the binding asphalt course) increases the thermal performance of the road solar collector (See Fig. 45) but it has to be feasible from a structural point of view.

If the heat collected per meter of pipe wants to be maximized, the pipes do not have to interact thermally with each other. As can be seen in Fig. 42, when the lateral spacing is over 400-500 mm., the heat collected per meter of pipe starts being a constant that does not increase (much) with this variable. It can be considered that pipes are thermally independent when lateral spacing is over 400-500 mm.

As an example, the annual heat collected per meter of pipe (20 mm of diameter, PEX) will be shown in the following graph for London and Madrid (considering providing inlet water at the ground average temperature), for a fixed lateral spacing of 500 mm. One case (traditional) considers that the pipes are located in the middle of the second layer (binding asphalt course) and the other considers that the piping system is at the lower part of the wearing course, (in this case with an additional resin layer with aggregates, on top of the road).

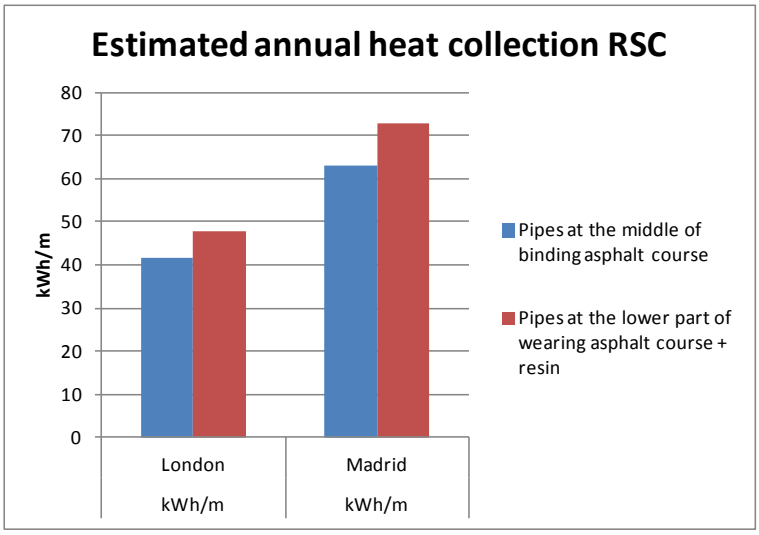

Fig. 88. Estimated road solar collector thermal yield per meter of pipe (lateral spacing = 500 mm).

The results show typical collection rates that can be expected for this configuration an also the quantification of placing the piping system closer to the surface (approximately **+15.5%** of thermal yield).

If the heat collected per square meter of road wants to be maximized, the pipe lateral spacing has to be reduced as it is logical (see Fig. 43). The structural tests have checked that a lateral spacing of 100 mm, a pipe diameter of 20 mm and placing the pipes on the wearing course can be a valid configuration in roads with medium traffic specified as KR3-KR4 (up to 1000 of 100 kN equivalent of single axle load per lane per twenty four hours (ESAL100)). In order to quantify the improvement the following cases are shown now:

- Reference: lateral spacing 250 mm, pipework 25 mm diameter, middle of the binding asphalt course.
- Case 1: lateral spacing 100 mm, pipework 20 mm diameter, middle of the binding asphalt course.
- Case 2: lateral spacing 100 mm, pipework 20 mm diameter, lower part of the wearing course.

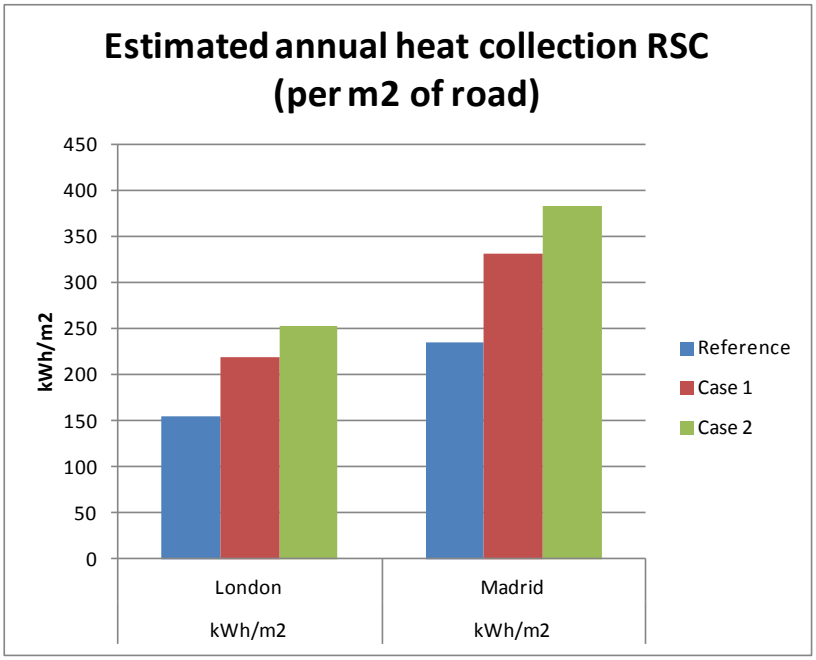

Fig. 89. Estimated road solar collector thermal yield for m2 of road.

The so called Case 1, improves the thermal yield of the reference case by 41%. This configuration has been tested from a structural point of view and as it has been already said, it can be used in roads with medium traffic.

The Case 2 is a further step that places the pipes closer to the surface, by adding a resin on top of the road that increases the structural strength. It improves the thermal yield of the reference case by 63%. However, it has been observed in the test that adhesion of such a layer to the base is insufficient in the test that have been performed and up to now, this has to be solved before implementing this layout in a real road.

Annex A: GRT runs results to test TAF measures

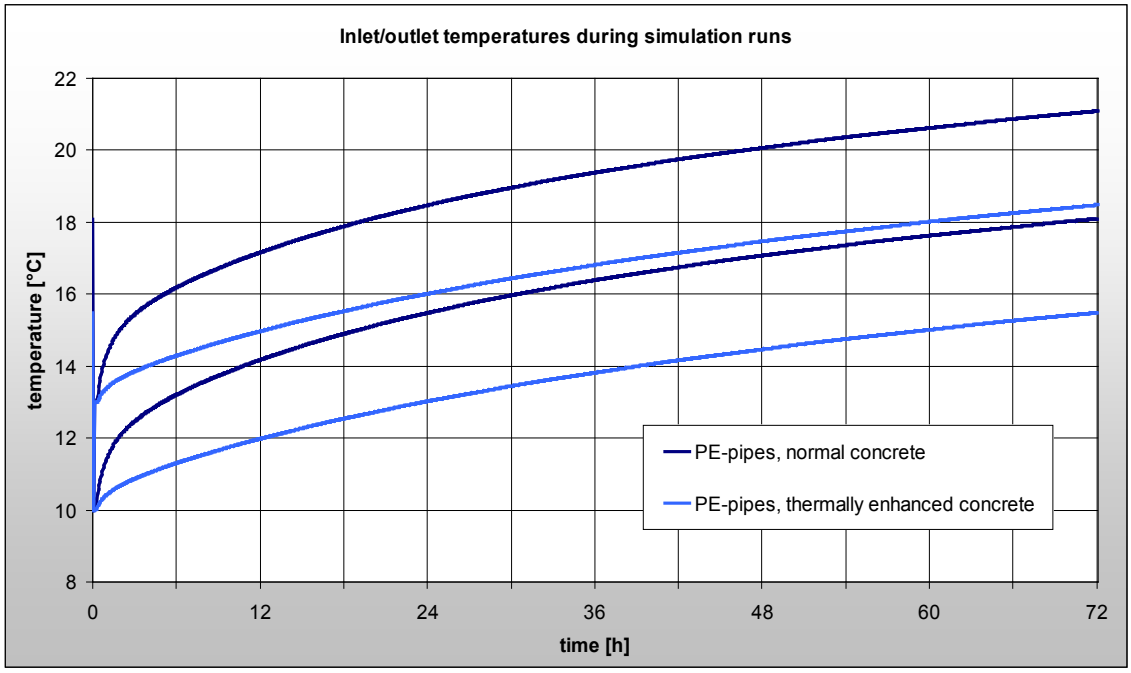

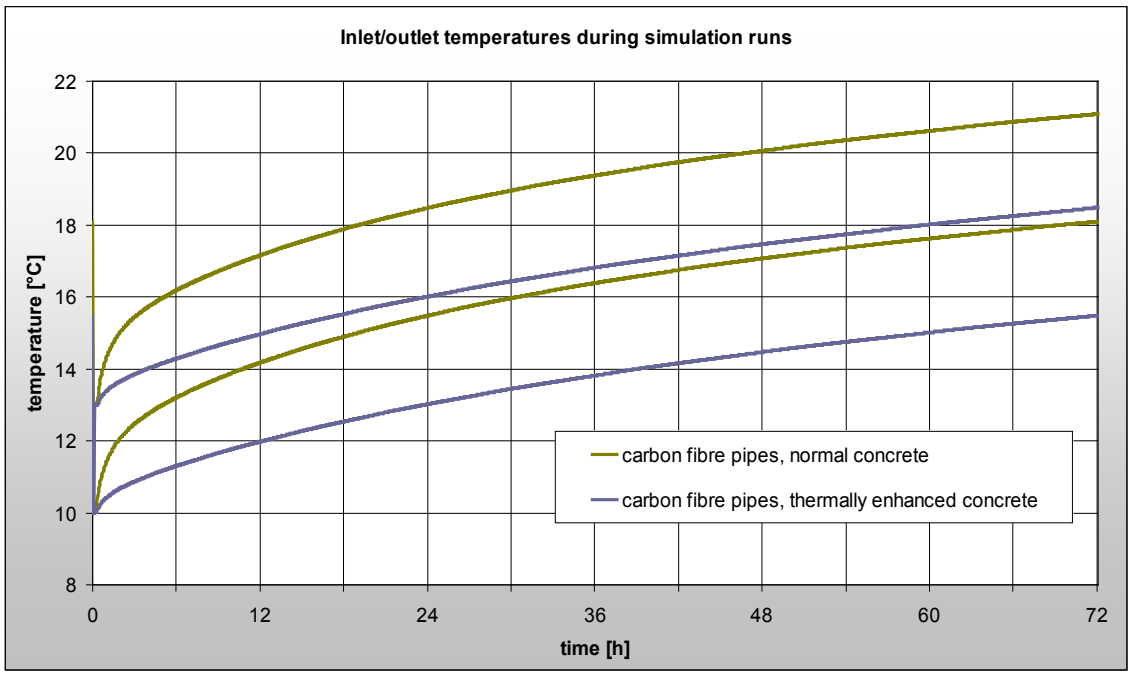

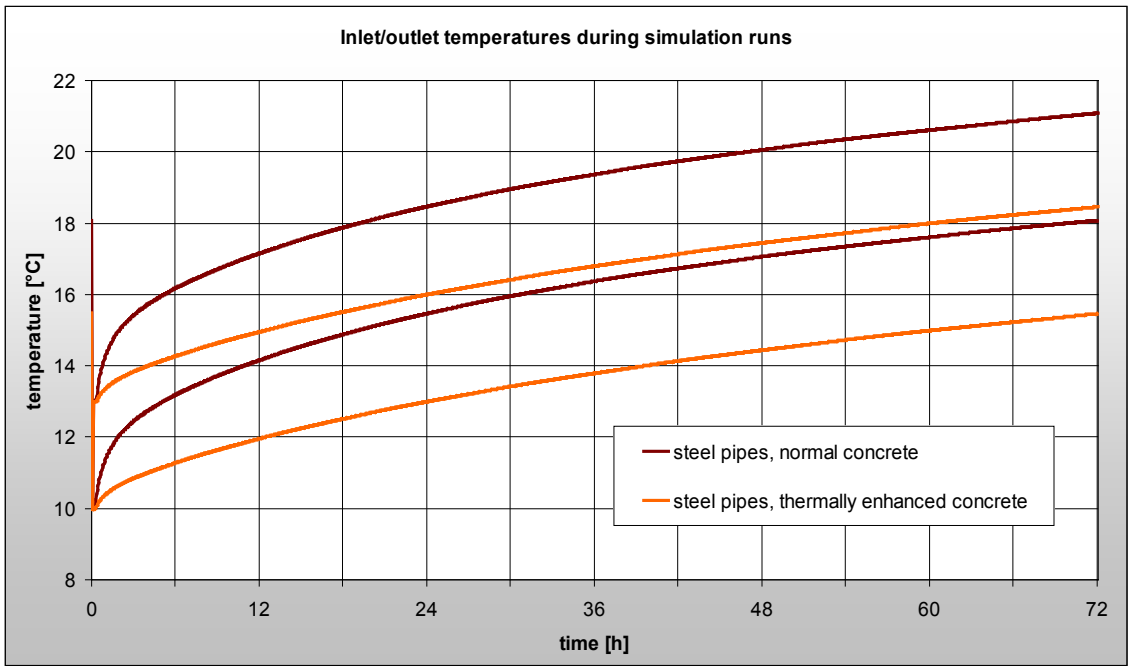

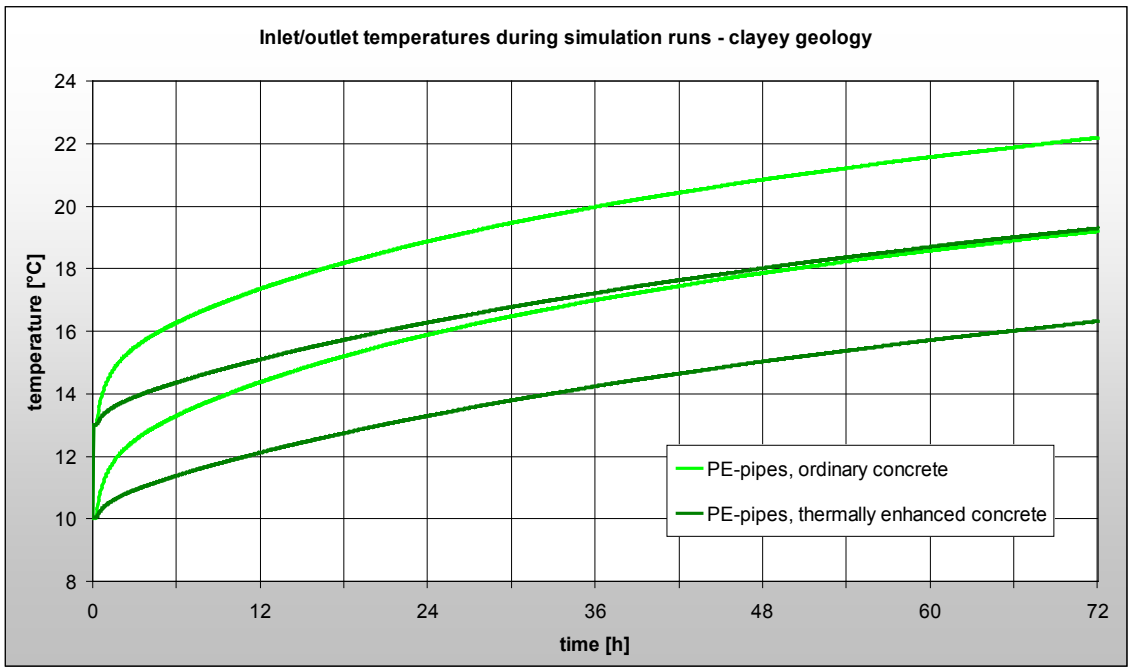

Fig. 90. The diagrams above show the inlet and outlet temperatures of the heat exchanger pipes which were monitored during the simulation via observation points. a) shows the simulated temperatures inside PE-pipes (runs 1 & 4), b) displays the temperatures in carbon fibre heat pipes (runs 2 & 5), in c) temperatures inside steel pipes are presented (runs 3 & 6) and in d) the temperatures in PE-pipes for a clayey geology (runs 7&8).

Annex B: Basic considerations for the design of a district network to interconnect thermo-active foundations

Temperature levels in the underground

For TAF and other near surface geothermal source systems the temperature levels on the source site are usually in the range of “normal” underground temperatures. Up to about 20 m in depth from the surface, climatic boundary conditions such as air temperature, solar irradiation and precipitation are the main influencing parameters (Fig. 91). Beneath that depth, heat from inside the earth dominates the thermal regime. The temperature levels of usually about 10 - 15 °C (undisturbed, mid-European) can be used for heating via heat pumps and for cooling either via heat pumps or in a so called “passive” cooling mode without compressor/vaporiser operation.

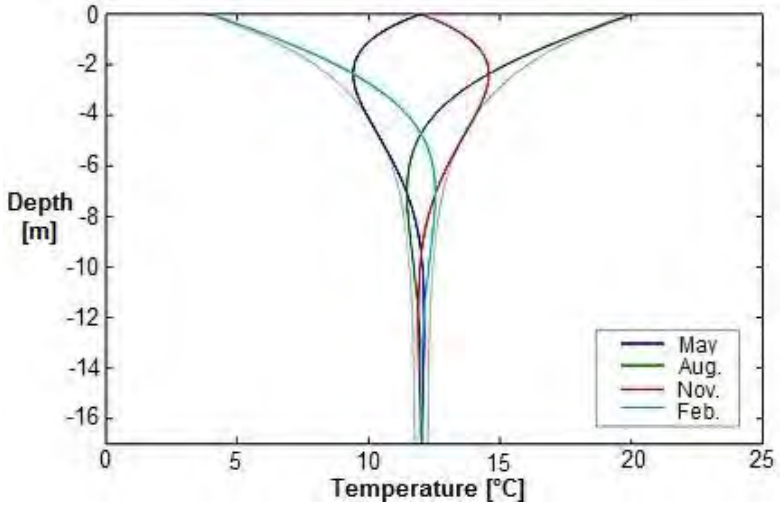

Fig. 91. Temperature-depth distribution in the underground, depending on the time of the year (for mid-European climate).

Heat carrier fluid

The heat transport from the TAF to the heat pump is realized via a circulating heat carrier fluid. The fluid consists mainly of water, which is most often mixed with antifreeze fluid to prevent formation of ice crystals in the so called “brine circuit”.

Antifreeze fluid is usually based on ethylene-glycol and contains additives to inhibit corrosion and incrustation of pipes, heat exchangers etc. A typical antifreeze concentration is about 25% which results in a freezing point of the heat carrier fluid between - 10 and - 15 °C.

In TAF-installations which are mainly used for cooling purposes or if authorities prohibit the use of antifreeze materials inside the brine circuit, pure water can be used as well. Those geothermal systems generally lack the potential for a most efficient heating operation and should therefore be avoided if a maximal yield of energy from the underground is aimed at.

The hydraulic properties (density, viscosity) of heat carrier fluid vary with the concentration of antifreeze inside the fluid and with its temperature (Fig. 92). Viscosity and density generally increase with higher concentrations of antifreeze in the brine and with descending temperatures. This aspect becomes fairly important when specifying hydraulic parameters of a geothermal source system and dimensioning its hydraulic connection to the heat pump/heat exchanger.

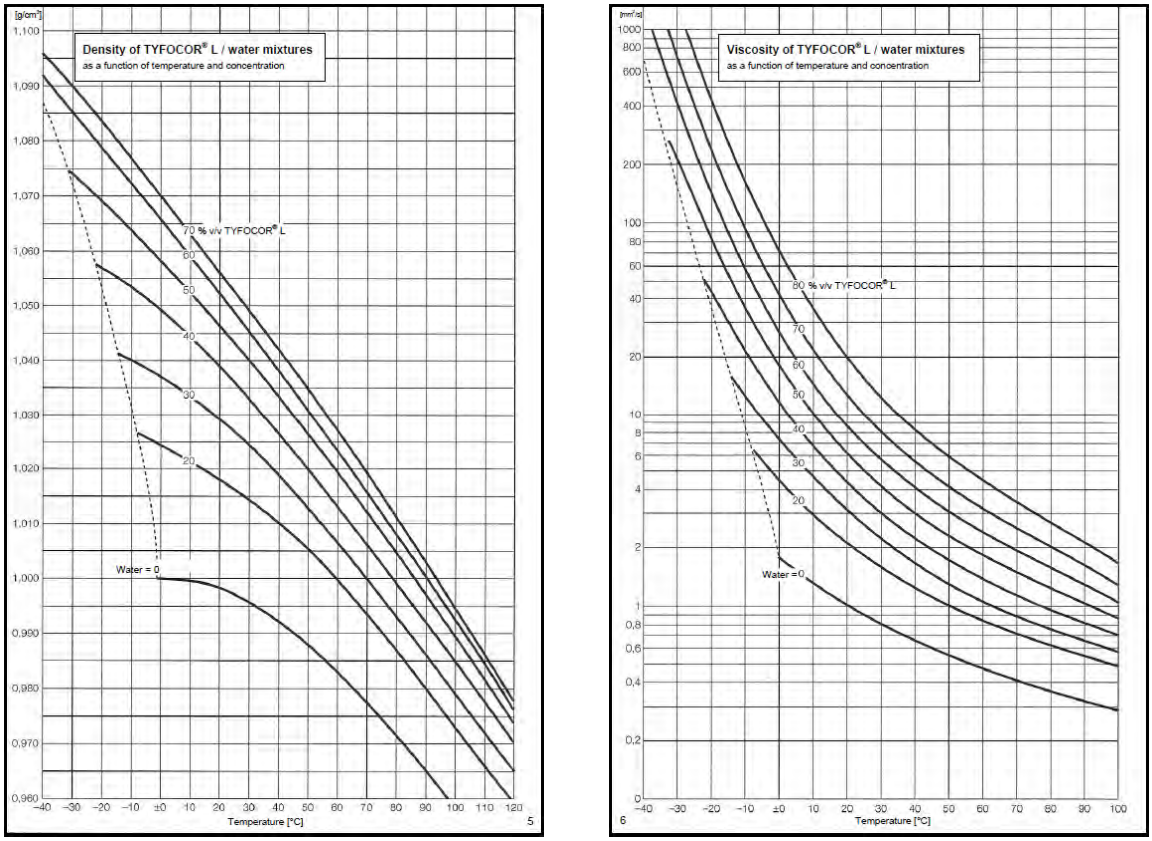

Fig. 92. Material properties (density/viscosity) of a typical heat carrier fluid in dependence of concentration and temperature (Source: TYFOROP Chemie).

Piping and connection material

The thermal activation of foundation parts is generally realized by polyethylene (PE) or (much rarer) by polypropylene (PP) pipes. Those have to meet different criteria in terms of pressure resistance and crack propagation resistance. Typical outer dimensions for heat exchange tubes are either 25 mm or 32 mm. Smaller diameters are only used in capillary tube mats. Examples of thermally activated foundation parts are shown in Fig. 93.

Fig. 93. left: thermal activation of a base plate in the harbour area of Hamburg, Germany, piping material: PE-RC, 25 mm; right: thermally activated foundation piles in Rostock, Germany, piping material: PE-Xa, 25 mm.

The immediate connection of the individual sources (energy piles, collector pipes, capillary mats) to the hydraulic distribution is usually realized with the next bigger pipe diameter. An impression of hydraulic connection pipes shows Fig. 94.

Fig. 94. Two examples for hydraulic connection of energy piles; **left:** Stade, Germany; **right:** Rostock, Germany.

The hydraulic connection pipes lead to a header (inside a central collector/distributor shaft) by means of flow and return lines (examples see Fig. 95). The header serves multiple purposes inside the piping distribution network in that it a) connects the individual circuits to bigger collecting pipes, b) allows for a hydraulic adjustment via volumetric flow rate setters (Fig. 96), c) is one of the main access points for maintenance works, d) allows the shutoff of individual circuits and e) contains outlets for venting.

Fig. 95. left: collector/distributor shaft; right: header pipe with 9 individual circuits attached; both images taken in Stade, Germany.

Fig. 96. Example of a
volumetric stream setter, source: taconova.com.

The diameter with which the pipes continue from the collector/distributor towards the heat pump or a possible further distribution network depends on the volumetric stream of the heat carrier fluid, which is determined by the dimension and number of the individual geothermal sources as well as by the required power on the building site.

Thermal energy central

The thermal energy central usually is designed by building services engineers and therefore is only mentioned for the sake of completeness.

Inside the thermal energy central, there usually have to be a variety of individual installations securing and supervising the proper system functionality which include:

- A heat pump, alternatively a passive heat exchanger and a separate circulation pump,

- Insulated pipes, connecting the thermal source to the heat pump/heat exchanger,

- A surge tank and venting possibilities,

- Filling pressure monitoring,

- An energy management/monitoring system consisting of different sensors inside the brine circle, heat pump and heating cycle. The E-Hub management software has to be set up onto this monitoring system.

Annex C: Parametric study to estimate the pile capacity loss due to thermal activation

In this annex, a parametric study shall be developed to appraise the structural capacity loss due to thermal activation for all five expectable failure modes of a concrete longitudinal element: compression, tension, shear, flexure and buckling.

Pipe area shall be considered non-resistant.

The following variables shall be used:

R := pile radius

r := distance from the pile axis to the pipe axis

A_p := pipe area

A_s := rebar area

d_s := rebar concrete cover

d_p := pipe concrete cover

E_c := concrete Young's modulus

E_s := steel Young's modulus

l_0 := unrestrained buckling pile length

f_{cd} := maximum concrete (compressive) stress

f_{yd} := rebar steel yield stress

Compression

The compressive capacity of a reinforced concrete cross section is linearly dependent of the homogeneous cross section area. Thus, in a standard situation, the structural compressive limit of a reinforced concrete pile may be expressed as:

$$N_{cd} = \left[\pi \cdot R^2 + \left(\frac{E_s}{E_c} - 1\right) \cdot A_s\right] \cdot f_{cd}$$

While in case of thermo-active piles, the structural compressive limit could be expressed as:

$$N_{cd} = \left[\pi \cdot R^2 + \left(\frac{E_s}{E_c} - 1 \cdot A_s\right) - A_p\right] \cdot f_{cd}$$

Loss of capacity, in percentage, would thus be expressed as:

$$\frac{100 \cdot A_p}{\pi \cdot R^2 + \left(\frac{E_s}{E_c} - 1\right) \cdot A_s}$$

Tension

The tensile capacity of a reinforced concrete cross section is linearly dependent of the rebar area, since concrete is considered to present no tensile resistance in ULS. Thus, tensile resistance would not be affected by thermal activation as long as **the distance between bars and pipes is enough to guarantee rebar adherence**.

Tensile capacity would thus be expressed in both cases as:

$$T_{cd} = A_s \cdot f_{yd}$$

Shear

The shear capacity of a reinforced concrete cross section depends on the compressive capacity of the struts and the tensile capacity of the ties in the strut-and-tie internal model.

Compressive capacity of the struts may be expressed as:

$$V_{u1} = K \cdot f_{1cd} \cdot b_0 \cdot d \cdot \frac{cotg\ \theta + cotg\ \alpha}{1 + cotg^2 \alpha}$$

Where:

f_{1cd} := $0{,}60\ f_{cd}$

b_0 := $2 \cdot \sqrt{2 \cdot R \cdot d_s - d_s^2}$

K := $1 + \frac{\sigma'_{cd}}{f_{cd}}$

s'_{cd} := $\frac{N_d - A_s' \cdot f_{yd}}{A_c}$

N_d := Axial stress

A_s' := rebar compressed area

d := 1,6·R

θ := angle formed by the struts and the pile axis

a := angle formed by the stirrups and the pile axis

Loss of capacity due to thermal activation pipes could be estimated by reducing shear area $b_0 \cdot d$ in an amount equivalent to the area of pipes inside the strut.

Tensile capacity of ties is expressed as the sum of two components, representing the capacity of stirrups (V_{su}) and concrete (V_{cu}):

$$V_{su} = 0.85 \cdot z \cdot sen\alpha \cdot (cotg\alpha + cotg\theta) \cdot A_\alpha \cdot f_{yd}$$

Where:

z := 1,44R

A_a := stirrup area per length unit

$$V_{cu} = \left[\frac{0,15}{\gamma_c} \cdot \xi \cdot (100 \cdot \rho_l \cdot f_{cv})^{1/3}\right] \cdot \beta \cdot b_0 \cdot d$$

Where:

g_c := material safety factor for concrete (1,5)

x := $\left(1 + \sqrt{\frac{200}{d}}\right) \leq 2$

r_l := $\frac{A_S}{b_0 \cdot d} \leq 0,02$

f_{cv} := Concrete effective shear resistance. Equals f_{ck} with a limit of 15 MPa

b := $\frac{2 \cdot cotg\theta - 1}{2\ cotg\theta_e - 1}$

Q_e := $29+7 \cdot e_x$

e_x := $\frac{\frac{M_d}{z} + V_{rd} - 0,5 \cdot N_d}{2 \cdot E_S \cdot A_S} \cdot 1000 \geq 0$

Loss of capacity due to thermal activation pipes could be estimated by reducing shear area $b_0 \cdot d$ in an amount equivalent to the area of pipes inside the tie.

Flexure

The flexural capacity of a reinforced concrete cross section depends on the compressive capacity of concrete, the tensile capacity of rebar, and the geometric disposition of these materials. Thermal activation of piles modifies the geometry of the cross section, thus reducing its flexural capacity.

Section analysis of a concrete element under flexure is by no means a simple matter that may be expressed by a couple of formulas and thus easily parameterized. The parabolic laws that govern concrete stress in ultimate states, united to the 5 different failure hypotheses, make it unadvisable. This is especially true of circular piles, which add to the calculation the complication of variable width and radially distributed rebar. For the same geometry distribution, different concrete qualities present different ultimate bend angles, and the combination of axial and flexural stresses complicates it even more.

Thus, it is only reasonable to recommend the use of specific section analysis software to calculate the capacity loss associated to thermal activation in flexure.

Buckling

As stated in the previous paragraph with flexure, given that buckling analysis results in augmented eccentricity of axial forces (that is, greater flexure), complete parameterization is also pointless.

Nevertheless, parameterization of augmented eccentricity is possible, for piles with mechanical slenderness lower than 100. Said eccentricity may be expressed as:

$$e_a = (1 + 0{,}24) \cdot \left(\varepsilon_y + 0{,}0035\right) \cdot \frac{h + 20 \cdot e}{h + 10 \cdot e} \cdot \frac{l_0^2}{50 \cdot i_c}$$

With:

e_a := augmented eccentricity

e := first order eccentricity, $\frac{M_d}{N_d}$

i_c := radius of gyration of the concrete section

e_y := yielding strain of rebar steel

h := cross section height, 2·R

The effect of the thermal activation pipes reduces the radius of gyration, as the concrete section would be equivalent to a circle from which a slender corona has been removed.

Since the radius of gyration is equivalent to:

$$i_c = \sqrt{\frac{I_c}{A_c}}$$

And due to the pipes the area is reduced by A_p and the inertia is reduced by $A_p \cdot r^2$, the new radius of gyration is:

$$\sqrt{\frac{\frac{\pi \cdot R^4}{4} - A_p \cdot r^2}{\pi \cdot R^2 - A_p}}$$

The radius of gyration reduction causes a raise in the augmented eccentricity:

$$e_{a,p} = e_a \cdot \sqrt{1 + \frac{A_p}{R^2} \cdot \frac{R^2 - r^2}{\pi \cdot R^2 - A_p}}$$

Thus raising flexural stresses and reducing section capacity.

Annex D: Temperature graph - Optimal configuration

The graph below shows the inlet temperature to the collector (blue curve) and the outlet temperature of the collector (red curve), over the simulation period (April to October) for the optimal configuration. With a constant inlet temperature of 10°C, the maximum outlet temperature achieved is about 15°C

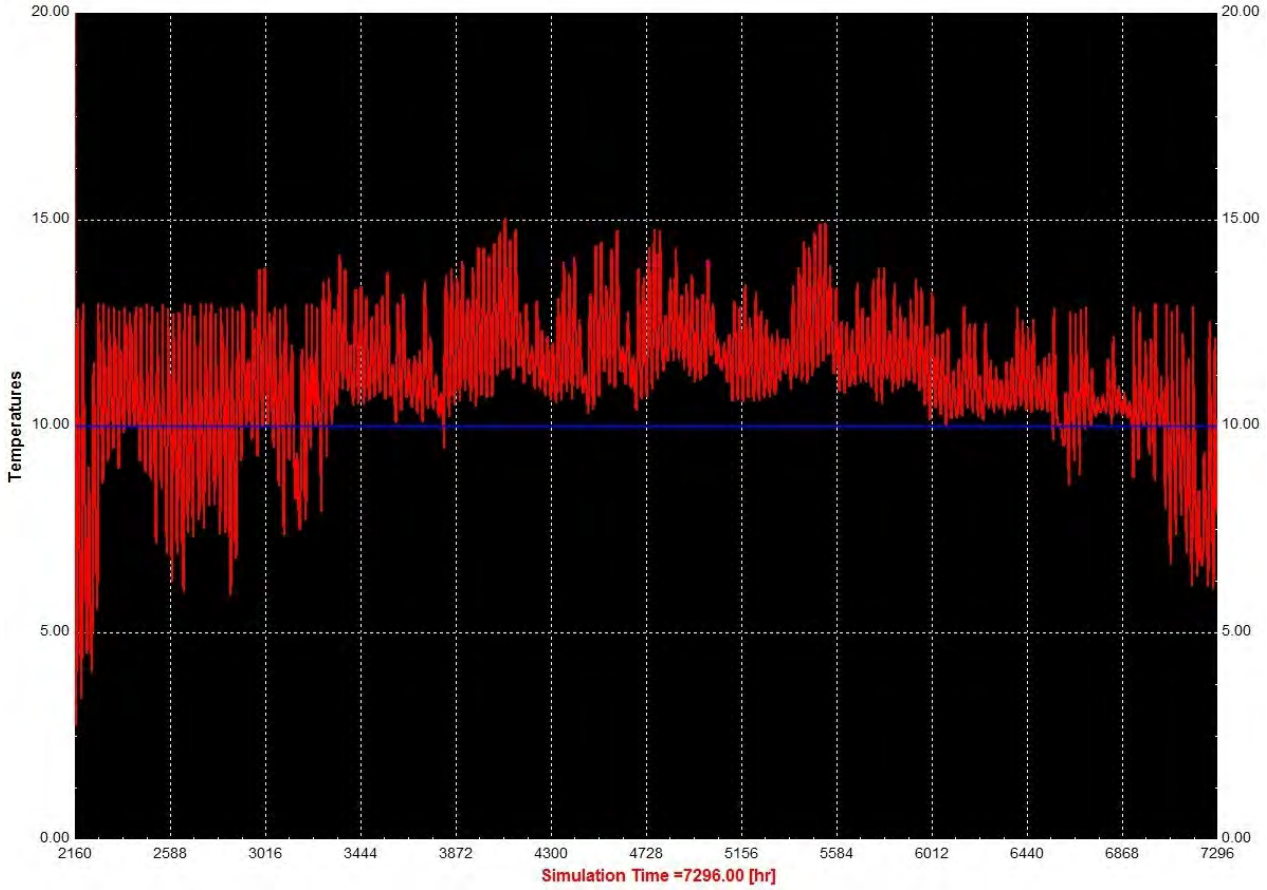

Annex E: Trnsys Description

TRNSYS has been created by the University of Wisconsin Solar Energy Laboratory and is still in a continuous development process, with many versions released in the past years. Many add-on components are developed by Thermal Energy Systems Specialists (TESS), whose founder Jeff Thornton used to work for the TRNSYS development program in the Solar Energy Laboratory. Below is a description from TESS, summarising the main benefits of using this tool:

"TRNSYS is a transient systems simulation program with a modular structure. It recognizes a system description language in which the user specifies the components that constitute the system and the manner in which they are connected. The TRNSYS library includes many of the components commonly found in thermal and electrical energy systems, as well as component routines to handle input of weather data or other time-dependent forcing functions and output of simulation results. The modular nature of TRNSYS gives the program tremendous flexibility, and facilitates the addition to the program of mathematical models not included in the standard TRNSYS library. TRNSYS is well suited to detailed analyses of any system whose behaviour is dependent on the passage of time. TRNSYS has become reference software for researchers and engineers around the world. Main applications include: solar systems (solar thermal and photovoltaic systems), low energy buildings and HVAC systems, renewable energy systems, cogeneration, fuel cells."

Graphical interface

A good feature of this software is that is includes a friendly interface called "TRNSYS Studio" from which the simulation file can be edited. The TRNSYS Simulation Studio, developed by the "Centre Scientifique et Technique du Batiment" in Sophia Antipolis, France, was added to the TRNSYS package in 1996. Its functions include creating and editing input files, creating new components, generating HTML based documentation, displaying listing and output files, plotting results, offering online help, running parametric simulations, and providing shortcuts for several repetitive tasks such as Fortran and C++ compiling and linking.

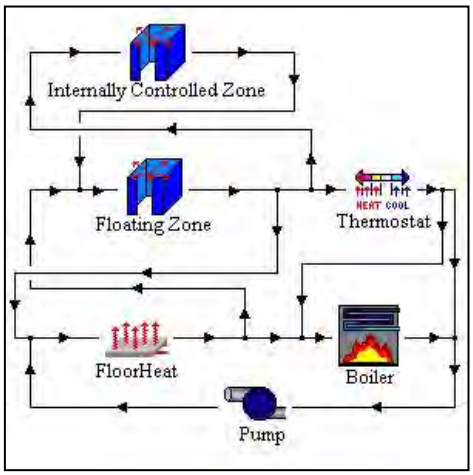

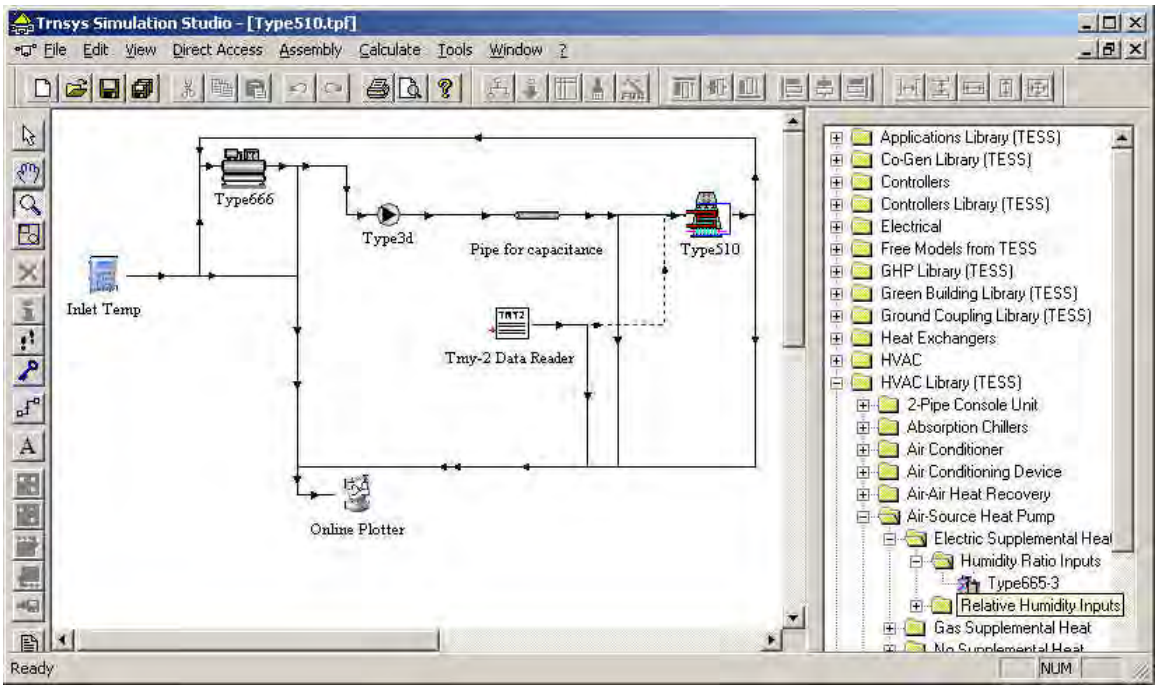

The figure above shows the Simulation Studio Assembly Panel used to create and work with TRNSYS simulations. This main window contains many descriptive icons with lines connecting them to form a system. Each icon represents a different component (e.g. pump, solar collector, steam trap, etc.). The user drags the necessary icons into the Assembly Panel from the directory structure on the right. The user then creates links between components that share information. The lines connecting the icons represent the pipes and wires that connect the physical components. While several connections are possible between two components, just one link is displayed. To view or change the input and output connections, the user clicks on the link itself to view a detailed window. A series of tools around the top and left borders of the Assembly Panel window allow the user to place icons onto the working area, connect the icons as necessary, run the simulation, access the editor, access the spreadsheet and plotting packages, and perform many other functions.

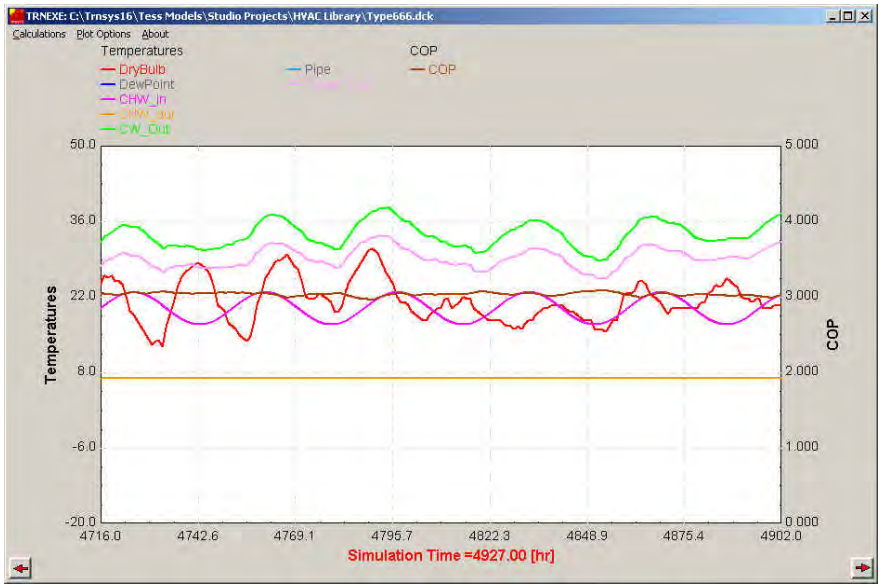

Annex F: Structural simulations of the Thermal Road Solar Collector

Load Theory

In this section, the load theory used to develop the analyses presented in the next sections of the document, is shown. The aim of presenting this load theory is obtaining a better understanding of the results from these analyses.

The next points describe theoretically the load cases that have been used to perform the different types of analyses. These load cases have been combined to compose the load hypothesis that have been imposed to the road. It has to be noticed that the simulation software ALIZE takes into account the dead load due to the weight of the different layers of the road, by default.

It should be also noticed that the outcomes presented in the next sections of the document correspond to the most unfavourable load hypothesis.

Relative effects of different axle loads

For pavement design, but also to determine the pavement wear effect of different tires, the pavement wear effects of different axle loads have to be determined. Generally this is described by a Load Equivalency Factor (LEF), where an axle load is said to be equivalent (producing equal pavement wear) to a number of applications of a reference (standard) axle load. The most well-known of such a LEF is the so called “fourth power law” which is expressed mathematically as follows:

$$\frac{N_{ref}}{N_x} = \left(\frac{W_x}{W_{ref}}\right)^4$$

Where:

Wx and Wref are axle loads

Nx and Nref are the corresponding number of load applications.

The exponent 4 in the fourth power law was found in the AASHO Road Test, carried out in USA between1958-1960. It must be understood that the fourth power law includes all distress modes.

Note that the fourth power law was derived from measurements on heavy vehicles. To apply the law also on light vehicles, such as passenger cars, would imply a vast extrapolation outside the range of vehicle loads used in the AASHO experiments.

It should to be noticed that, in the performed analyses the values from the reference variables came from the analysis program ALIZE and they were integrated by default in the program.

Dynamic axle loading

When a vehicle is not moving, the vertical (axle, wheel and tire) loads it imparts on the pavement, due to the force of gravity, are constant. These are the static loads. When the vehicle is moving along a road, however, unevenness of the road will cause the vehicle to move up and down. This will cause a dynamic variation of the loads on the pavement, above and below their static values.

The magnitude of this dynamic variation depends also on the vertical dynamics of the vehicle, including such factors as the mass and stiffness distribution of the vehicle structure, payload mass distribution, suspension and tires, and on the road surface’s longitudinal profile and the speed of the vehicle. The variation generally increases with both speed and nature road unevenness.

The magnitude of dynamic loads is mostly expressed as the Dynamic Load Coefficient (DLC), defined by the ratio of the RMS (root mean square) dynamic wheel load to the mean wheel load. The RMS of the dynamic wheel load is essentially the standard deviation of the probability distribution of the total

wheel load. The mean value reflects the static wheel load. So, the DLC is the coefficient of variation of the total wheel load.

- 5 − 10% for well-damped air suspensions and soft, well-damped steel leaf suspensions.
- 20 − 40% for less road-friendly suspensions.

Dynamic loading increases pavement wear. Because of the power-law dependency of pavement distress on axle loads, the loads above the static load increase the pavement wear more than the decrease in wear due to the loads below the static load.

Besides load magnitude, also frequency content is important for pavement wear. Most heavy vehicles have dynamic wheel loads either in the 1.5 − 4 Hz range, associated with bounce (up/down) and pitch (rotating forward/backward) motions of the vehicle body, or in the 8 − 15 Hz range, associated with axle-hop vibration. Axle hop vibrations are more significant if the pavement is rough and the vehicle speed is higher than approximately 40 km/h.

As stated before, the wheel characteristics (vertical spring compliance and damping) influence the dynamic vehicle loads. Therefore, these should be considered when establishing pavement wear effects of different wheels.

Effects of different axles: single axles, tandem axles and tri-axles

Tandem axles and tri-axles generally cannot be treated by summation of the effects of their constituting individual axles, because of two reasons:

- The load spreading of thick pavements may be such that the responses (stresses and strains) due to neighbouring axles in a tandem or tri-axle configuration may substantially increase the responses under the axle considered. Due to the non-linearity of the performance relations, such increased responses will lead to much more pavement wear than the summed responses of individual axles.
- Due to the visco-elastic nature of bituminous materials, stresses and strains caused by an axle load need some time to relax after the axle has passed. When another axle arrives within that period, some residual stresses and strain will still be present, which may compound with the stresses and strains caused by the new axle, resulting in higher total values. The effects of this mechanism are not well understood.

For axle load limitations, this is reflected in maximum allowed tandem axle (and tri-axle) loads which are less than twice (or three times) the allowed single axle load. (Two axles at more than 1.8 m spacing are not considered a ‘tandem axle’ but a ‘double axle’ and are treated as two single axles.)

For pavement design purposes, the loads of tandem axles and tri-axles are mostly converted to a number of “equivalent standard axle loads” (Nesal) by summing the contributions of the individual axles. These individual contributions are then calculated using the Load Equivalency Factor described in Section 2.1, resulting in:

$$N_{esal} = \sum_{1}^{nr\ of\ axles} \left(\frac{W_{axle}}{W_{standard\ axle}} \right)^4$$

Wheel specific effects

The current trend (in Europe) is smaller wheel diameter and higher wheel pressure. A smaller wheel diameter enables lower vehicle floors, which increases the volume that is possible to transport. A higher wheel pressure might have a positive effect on fuel consumption. Also, wide single wheels are beginning to replace the traditional dual wheels which can be explained by a lower weight, reductions in fuel consumption, and a lower cost of wheel wear. Although beneficial for transporters, the effect of

these trends might be an increase to road wear since they imply a smaller contact area between a wheel and the road. This area, henceforth called “footprint” is an important road wear factor. The larger the footprint, the less the load distributed on every road area unit. The difference in road wear between single and dual wheels is thus not caused by the differences in wheel types as such.

Single wheels are normally used on axles with loads below 8 ton, while dual wheels are the most common for axle loads above 8 ton. However, there exist wide base single wheels exist for axle loads of more than 10 ton. The use of single or dual wheels also depends on the axle formation. The more axles constituting the formation (tandem or tri-axle), the more common is the use of single wheels. The wide base single tires, is more commonly used in Europe.

However, although wide base single wheels might increase road damage through its smaller footprint and higher inflation pressure, it improves roll-over stability of the vehicle. This in turn has consequences for suspension design. As is discussed below, suspension stiffness is necessary for roll-over stability but increases road damage. It is therefore at least a theoretical possibility that the increased road damage induced by the change from dual wheels to super single wheels can be compensated for by reducing the spring stiffness. This improves the possibility to design an optimal suspension.

Another important aspect to take into account when comparing single and dual wheel assemblies is the concept of unequal load sharing of the dual wheels. When comparing dual and single wheel assemblies at equal wheel load, generally the assumption is made that the wheel load is shared equally between both wheels of the dual assembly.

However, in practice this might not be true. A number of reasons could cause an unequal load division (‘load imbalance’) between both wheels:

1. Differences in vertical stiffness between both wheels, because of
   - Differences in inflation pressure (mainly due to poor maintenance)
   - Different wheel structure (due to e.g. different brands)
2. Differences in vertical compression between both wheels, because of
   - Differences in diameter between both wheels
   - Bending of the vehicle axle
   - Transverse unevenness of the pavement surface

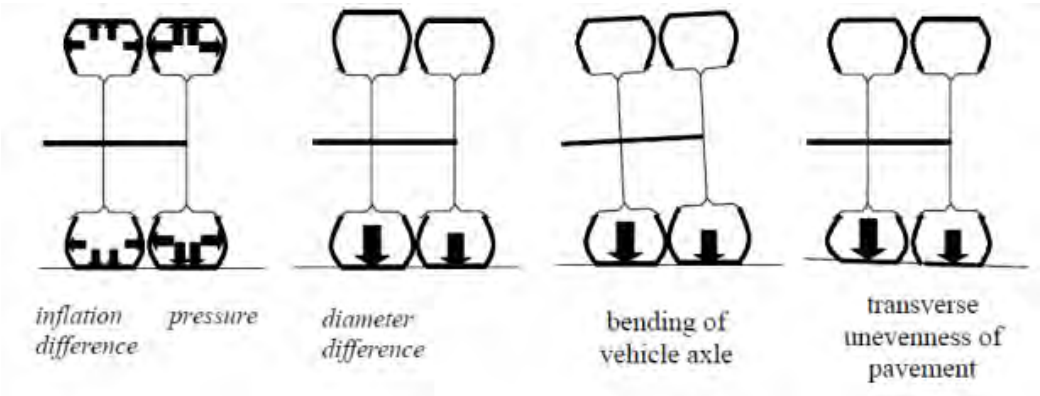

Fig. 97. Causes unequal load sharing between tyres in a dual tyre assembly (‘load imbalance’).

Axle- and wheel configuration also affect road damage in an indirect way, an effect that is denoted lateral wander.

In practice, not all wheels will pass at the same lateral position in a road section. Vehicles generally follow a slightly zigzagging course between the bounds of the traffic lane, which is called lateral

wander. Therefore, the wheel positions of consecutive vehicles will be transversely distributed over the pavement.

The probability distribution of the vehicle positions is a Laplace distribution, instead of the normal distribution that is often assumed. For a certain vehicle width and lateral wheel spacing, the probability distribution of the wheel (centre) positions is a Laplace distribution, too. However, the number of 'hits' by a wheel per cm pavement width is approximately normally distributed, due to the summation over various vehicle widths, wheel spacing, dual and single wheels, and various wheel widths.

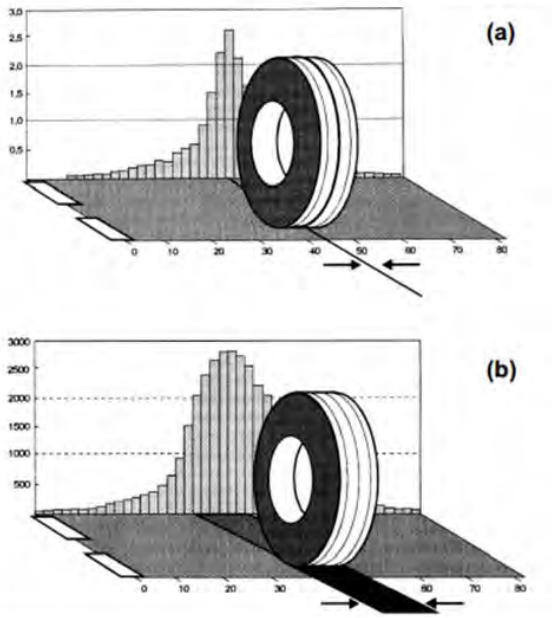

Fig. 98. Difference between probability distribution of the wheel positions (a), and the number of hits by a wheel per cm pavement width (b).

Lateral wander distributes pavement loading, and hence pavement wear, over a larger area of the pavement. This prolongs the pavement service life. The effects of lateral wander are different for the different distress modes. They also may differ between dual wheels and wide base singles.

Suspension effects

Vertical movements in the vehicle create a dynamic axle load that can be higher as well as lower than the static load. A road-friendly suspension decreases the magnitude of the vertical movements that are triggered by unevenness of the road, which in turn means a lower dynamic axle load, for a given static load. The dynamic axle load is affected by the type of suspension on the vehicle and its ability to reduce movements in various frequency ranges. In general, the dynamic load increases with spring stiffness. The dynamic load is also sensitive to the damping ratio, the speed of which the amplitude of movements is reduced. EU (directive 92/7/EEC) defines a road-friendly suspension as a one with a sprung mass frequency no greater than 2 Hz and a damping ratio above 20 percent of critical damping. It is also required that the Coulomb damping ratio does not exceed 50 percent of the viscous damping.

From a road wear perspective, the purpose of the suspension is to reduce motions to decrease the dynamic load. But the suspension characteristics have implications for road safety as well so there are certainly important tradeoffs. Reducing the stiffness in order to decrease the dynamic load also reduces the resistance to roll over.

The traditional truck suspension is constructed using spring leaves. The characteristics of this type of suspension vary considerably under different road and driving conditions. The friction between the leaves might result in a locked suspension in case the pavement is smooth and the speed moderate. This is caused by sliding friction between spring leaves and has been found to adversely affect

suspension performance. In the locked cases the suspension is stiff and the dampening abilities poor. Newer steel spring suspensions have been designed to remedy this problem by minimizing the contact area between individual leaves. With this construction stiffness is lower compared to the traditional design and a complete lock is not possible. The dampening effect is however reduced considerably why it is necessary to use hydraulic dampers.

In recent years, air suspension has been developed. These provide a low stiffness and a smooth deflection characteristic. Air suspensions are used in combination with hydraulic dampers.

Hydraulic dampers (shock absorbers) are common in modern trucks in combination both with leaf and air springs. Their force generating characteristics depend on the amplitude and frequency of the imposed motion. A semi-active damper is able to dissipate energy at a continuously, variable and controllable rate. It can be switched off when it is required to feed power into the suspension.

Dead loads

The dead load over a point consists of the total width of soil placed over this point. That is means that each layer will have to support the dead load of its upper layer.

Apart from the depth, the effects of this named dead load over the buried pipes will depend of the characteristics of the material. In a system with a rigid pipe the totality of the loads are resisted by the strength of the pipe material, while in the case of the flexible pipe, as said before, its deformation brings the development of lateral pressures which help to support the vertical load. As a result, the load supported by a flexible pipe for a given depth is less than for a rigid pipe.

“Marston” approach follows several considerations that makes it useful and accurate for the calculations of loads in the case of rigid tubes. For the particular case of a flexible pipe, a deviation of around a 30% of the load over the pipe occurs. Research data point that the effective load on a flexible conduit lies somewhere between the Marston predictions and the called “prism load”. The method followed for calculating the load over a flexible pipe will be, therefore, the prism (or embankment) load, since it considers the weight of the prism of soil placed over the pipe (figure 3). On a long term basis, the load may approach the prism load.

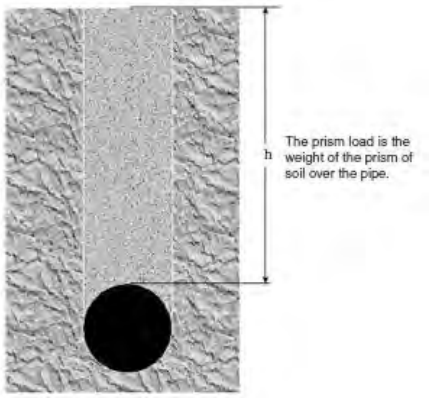

Fig. 99. Load over the buried pipe due to the weight of the soil.

The weight of soil over the pipe in the prism load method is calculated through the expression:

$$P_{dead} = \gamma * H$$

Where P_{dead} accounts for the weight of soil at depth H (kg/m^2)

H is the depth at which soil pressure is required

γ represents the unit weight of soil

Certain types of failures observed in pipes over the years suggest that only under ideal conditions is a pipeline truly subjected to only vertical earth loading. There are other forces that in some way produce

axial bending stresses in the pipe. These forces can be large, highly variable and localized, and may not lend themselves to a quantitative analysis with any degree of confidence. Some of these additional conditions are non-uniform bedding, differential settlement or ground movements. For convenience and simplicity these kinds of conditions won't be taken into account throughout this work.

Behaviour limits

As occurs with every constructive work, there are certain limitations which should not be exceeded in the design of the system road and buried pipes. For this reason, a quality design is endorsed by technical criteria which allow a long term service life of this system as a whole and of their single components. Here, It will be exposed several factors to take into account at the time to get a proper design of the system.

Pavement distress modes

Pavement wear or pavement distress is the degradation of pavement quality due to loading by traffic and/or climate. For flexible pavements, the following distress modes (visible distress together with the deterioration process causing it) will have to take into account:

1. Cracking
   - Fatigue cracking
   - Thermal cracking
   - Surface cracking
   - Reflective cracking

2. Rutting
   - Primary rutting
   - Secondary rutting
   - Abrasion rutting

3. Other distress modes
   - Raveling
   - Roughness
   - Potholes

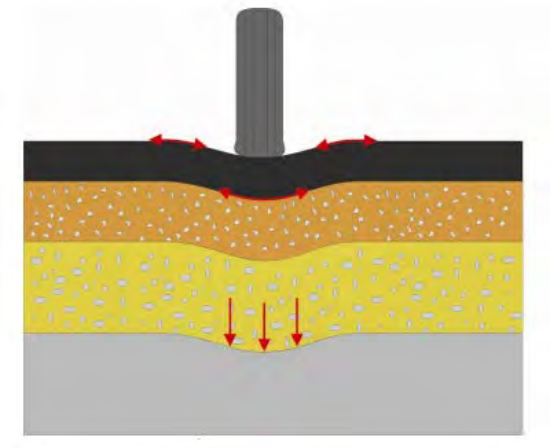

Fig. 100. Typical asphalt pavement construction.

It should be noticed that, after performing several studies about the effects over the road from each distress modes. The fatigue cracking was selected as the main distress mode to take into consideration in our study.

Here, it will be described all these named distress modes:

Cracking

There are four main types of cracking to take into account at the time to design the composition of a road (fatigue cracking, thermal cracking, surface cracking and reflective cracking). Due to the main purpose of this document, structural analysis of a buried pipe system, only the outcomes from the fatigue cracking analysis will be presented. This selected type of cracking will be highlighted and deeply explained after the brief explanation of the existing different types of cracking.

Here, a brief explanation of these types will be exposed.

Fatigue cracking: being cracking in the bituminous or cement bound material originating at the bottom of the respective layers, due to fatigue of the material by a great number of repetitions of bending due to wheel loads (Fatigue defined in this way is used as a parameter in pavement design. This does not include surface cracking and cracking due to thermal cycling, although these are also due to fatigue because of repeated stress cycles.)

Thermal cracking: being cracking in the bituminous material due to tensile stresses caused by temperature changes.

Surface cracking: being cracking in the bituminous material originating at the surface of the pavement, due to fatigue of the material by a great number of shear loadings of the pavement surface by the tire (Ageing of bituminous materials plays an important role here, too.)

Reflective cracking: being cracking of the (top) bituminous layers (often in a composite structure) as a result of cracks or joints in bound layers below.

Fatigue cracking:

The traffic load long term effect is the fatigue damage in the materials of the road's layers. The main characteristic of this kind of damage is its cracking behaviour, starting in the lower fiber of the asphalt layer, where the traction stress is bigger, spreading vertically until the top fiber of the material, held in the surface of the asphalt layer.

Fatigue damage means the exhaustion of the material due to the stress state induced over it, which will be far away from its braking value. The final consequence of this exhaustion state will be the cracking of the material.

Some laboratory experiments have showed that the existing relation between the material deformation, ε, and the fatigue life of that material was related by the expression:

$$N = k_1 \varepsilon^{k_2}$$

Where:

N represents the number of loads cycles until the material reached the deformation, ε, due to the fatigue effect.

K_1 and k_2 are constants which describe the fatigue behaviour of the material.

For describing the fatigue behaviour of the materials, a high number of studies have been performed to establish what kind of parameters would have more influence over the value of the constants, k1 and k2. Finally, the outcomes of these studies reflected that the parameters with more influence over the behaviour of the material would be the following:

- Elastic module
- Quantity of bitumen
- Viscosity of the bitumen
- Granulometry
- Nature of the aggregates
- Air content

- Temperature of the pavement

There are two types of fatigue damage, each one of them created by different stresses. One type regards the fatigue damage created by the tangential stress and the other type regards the vertical stress.

The outcome from the fatigue damage created by the tangential stress will be the useful life of the bitumen´s layer in millions of cycles. The outcomes from the fatigue damage created by the vertical stress will by the useful life of the square of land, in millions of cycles as well. These millions of cycles will be related to the years of the material´s useful life through the traffic intensity of the road.

On the one hand, it should be noticed that, to calculate the materials lifespan, it must be taken into account the meteorological seasons along the year. For this purpose the year will be divided in three meteorological seasons, each one of them with the following duration in percentage terms:

- Winter: 20%
- Spring – Autumn: 50%
- Summer: 30%

On the other hand, the most famous methodologies to establish the fatigue characteristics of the mix are: the SHELL method and the Asphalt institute method (AI). Although, the most common methodology used to obtain this number of cycles is the SHELL method.

Here, it will be exposed the simplified expressions of both methodologies to define a fatigue law of an asphalt mix:

- SHELL simplified expression:

$$N = \left((0.856 \cdot Vb + 1.08) \cdot \left(10^6 \cdot E\right)^{-0.36}\right)^5 \cdot \varepsilon^{-5}$$

Where:

Vb is the volume of bitumen in %.

E is the Elastic module of the material in MPa.

- AI simplified expression:

$$N = (0.0796 * C * (0.145 E^{-0.854}) * \varepsilon^{-3.291}$$

Where:

C is a correction factor expressed by:

$$C = 10^M$$

$$M = 4.84 * \left(\frac{V_b}{V_a + V_b} - 0.6875\right)$$

Where:

Va and Vb are the air volume and the bitumen volume respectively.

It should be noticed that, the volume of the bitumen used in the SHELL simplified expression was selected according with the Spanish road rules. The strain, Ɛ, used in this expression to obtain the millions of cycles that the road can withstand, will come from the outcomes of the program ALIZE.

Rutting

Rutting is the development of depressions in the pavement surface along the wheel paths, typically with a width of several decimeters and a length of tens to thousands of meters.

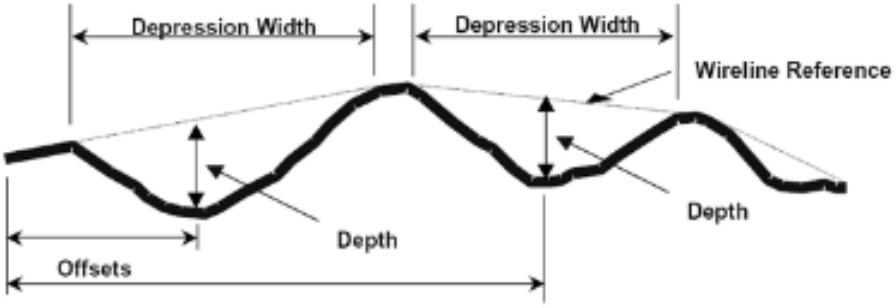

Fig. 101. Rutting measure with wireline reference.

The three main categories of routing are:

Primary rutting: rutting due to permanent deformation of bituminous layers, (Permanent deformation can be due to (post)compaction or (plastic and viscous) deformation caused by shearing stresses).

Secondary rutting: rutting due to permanent deformation in the subgrade or in granular layers below the asphalt layers.

Abrasion rutting: rutting due to abrasion of the pavement surface by studded tires.

Other distress modes

Raveling: being the loss of stones in the surface of the pavement as a result of failure of the bond between the aggregate and the binder by a great number of shear loadings in combination with ageing of the material. The primary case, is however insufficient quality of the pavement material.

Roughness: being (longitudinal) unevenness of the pavement, mostly due to several combined factors (rutting, cracking, potholes, uneven settlements, etc.).

Potholes: resulting either from local collapse due to structural defects, or from frost acting on water ingress (often through cracks). Potholes are not necessarily caused by loading but mainly due to insufficient quality of the pavement

Road Results

Stress and Strains

In this section it will be presented the resulting outcomes from the stress and strains analyses performed with ALIZE. These outcomes are classified according to the three different seasons considered, with the aim to show the influence of the exterior conditions on the materials properties, and consequently on the stress and displacement of the element.

The values reflected in the tables of this point correspond to the vertical and tangential stresses, as well as the vertical and tangential strains. The first value of each layer corresponds to the fiber located on the top of the layer while the second value corresponds to the fiber located at the bottom of the layer.

It should be noticed that the results come from the analyses performed considering the most unfavourable load hypothesis (loads combinations).

Winter

At this point, it will be presented the outcomes from the following configurations:

- Base case
- Base case plus buried pipes in wearing asphalt course (depth equal to 0.0375 m)
- Base case plus buried pipes in binding asphalt course (depth equal to 0.09 m)
- Base case plus buried pipes in asphalt base course (depth equal to 0.18 m)
- Base case plus buried pipes in the fourth layer (depth equal to 0.33 m)

Layers	Depth	Stress		Strain (1/1000)	
		Tangential (N/mm2)	Vertical (N/mm2)	Tangential	Vertical
Wearing asphalt course	0.00	1.052	0.649	0.033	0.007
	5.00	0.482	0.587	0.011	0.018
Binding asphalt course	5.00	0.475	0.587	0.011	0.019
	13.00	-0.085	0.275	-0.007	0.017
Asphalt base course	13.00	-0.078	0.275	-0.007	0.018
	23.00	-0.710	0.024	-0.030	0.021
Aggregate base	23.00	-0.007	0.024	-0.030	0.072
	43.00	-0.015	0.010	-0.034	0.048
Subgrade	43.00	-0.001	0.010	-0.034	0.103

Table 46. Stresses and Strains (Winter, Base case).

Layers	Depth	Stress		Strain (1/1000)	
		Tangential (N/mm2)	Vertical (N/mm2)	Tangential	Vertical
Wearing asphalt course	0.00	0.971	0.649	0.035	0.010
	5.00	0.481	0.592	0.013	0.022
Binding asphalt course	5.00	0.523	0.592	0.013	0.018
	13.00	-0.071	0.282	-0.007	0.017
Asphalt base course	13.00	-0.065	0.282	-0.007	0.018
	23.00	-0.728	0.025	-0.031	0.022
Aggregate base	23.00	-0.007	0.025	-0.031	0.074
	43.00	-0.010	0.010	-0.035	0.049
Subgrade	43.00	-0.001	0.010	-0.035	0.106

Table 47. Stresses and Strains (Winter, Wearing asphalt course).

Layers	Depth	Stress		Strain (1/1000)	
		Tangential (N/mm2)	Vertical (N/mm2)	Tangential	Vertical
Wearing asphalt course	0.00	1.070	0.649	0.034	0.006
	5.00	0.472	0.587	0.011	0.019
Binding asphalt course	5.00	0.440	0.587	0.011	0.022
	13.00	-0.058	0.279	-0.007	0.018
Asphalt base course	13.00	-0.067	0.279	-0.007	0.018
	23.00	-0.717	0.024	-0.031	0.022
Aggregate base	23.00	-0.007	0.024	-0.031	0.073
	43.00	-0.010	0.010	-0.034	0.048
Subgrade	43.00	-0.001	0.010	-0.034	0.104

Table 48. Stresses and Strains (Winter, Binding asphalt course).

Layers	Depth	Stress		Strain (1/1000)	
		Tangential (N/mm2)	Vertical (N/mm2)	Tangential	Vertical
Wearing asphalt course	0.00	1.067	0.649	0.034	0.006
	5.00	0.481	0.585	0.011	0.018
Binding asphalt course	5.00	0.474	0.585	0.011	0.019
	13.00	-0.112	0.270	-0.008	0.018
Asphalt base course	13.00	-0.090	0.270	-0.008	0.019
	23.00	-0.685	0.025	-0.032	0.022
Aggregate base	23.00	-0.007	0.025	-0.032	0.074
	43.00	-0.015	0.010	-0.035	0.049
Subgrade	43.00	-0.001	0.010	-0.035	0.105

Table 49. Stresses and Strains (Winter, Asphalt base course).

Layers	Depth	Stress		Strain (1/1000)	
		Tangential (N/mm2)	Vertical (N/mm2)	Tangential	Vertical
Wearing asphalt course	0.00	1.051	0.649	0.033	0.007
	5.00	0.481	0.587	0.011	0.018
Binding asphalt course	5.00	0.474	0.587	0.011	0.019
	13.00	-0.084	0.275	-0.007	0.017
Asphalt base course	13.00	-0.078	0.275	-0.007	0.018
	23.00	-0.709	0.024	-0.030	0.021
Aggregate base	23.00	-0.007	0.024	-0.030	0.071
	43.00	-0.015	0.010	-0.034	0.047
Subgrade	43.00	-0.001	0.010	-0.034	0.103

Table 50. Stresses and Strains (Winter, Aggregate base).

Spring - Autumn

At this point, it will be presented the outcomes from the following configurations:

- Base case
- Base case plus buried pipes in wearing asphalt course (depth equal to 0.0375 m)
- Base case plus buried pipes in binding asphalt course (depth equal to 0.09 m)
- Base case plus buried pipes in asphalt base course (depth equal to 0.18 m)
- Base case plus buried pipes in the fourth layer (depth equal to 0.33 m)

Layers	Depth	Stress		Strain (1/1000)	
		Tangential (N/mm2)	Vertical (N/mm2)	Tangential	Vertical
Wearing asphalt course	0.00	1.011	0.649	0.051	0.004
	5.00	0.464	0.589	0.016	0.031
Binding asphalt course	5.00	0.460	0.589	0.016	0.032
	13.00	-0.065	0.284	-0.013	0.033
Asphalt base course	13.00	-0.056	0.284	-0.013	0.034
	23.00	-0.621	0.037	-0.047	0.044
Aggregate base	23.00	-0.011	0.037	-0.047	0.111
	43.00	-0.022	0.013	-0.049	0.067
Subgrade	43.00	-0.001	0.013	-0.049	0.143

Table 51. Stresses and Strains (Spring - Autumn, Base case).

Layers	Depth	Stress		Strain (1/1000)	
		Tangential (N/mm2)	Vertical (N/mm2)	Tangential	Vertical
Wearing asphalt course	0.00	0.857	0.649	0.047	0.016
	5.00	0.426	0.594	0.014	0.039
Binding asphalt course	5.00	0.452	0.594	0.014	0.033
	13.00	-0.040	0.297	-0.012	0.032
Asphalt base course	13.00	-0.031	0.297	-0.012	0.034
	23.00	-0.543	0.049	-0.042	0.040
Aggregate base	23.00	-0.002	0.000	-0.042	0.129
	43.00	-0.009	0.005	-0.019	0.026
Subgrade	43.00	-0.001	0.005	-0.019	0.053

Table 52. Stresses and Strains (Spring - Autumn, Wearing asphalt course).

Layers	Depth	Stress		Strain (1/1000)	
		Tangential (N/mm2)	Vertical (N/mm2)	Tangential	Vertical
Wearing asphalt course	0.00	1.027	0.649	0.052	0.003
	5.00	0.452	0.590	0.016	0.032
Binding asphalt course	5.00	0.430	0.590	0.016	0.037
	13.00	-0.040	0.288	-0.013	0.035
Asphalt base course	13.00	-0.046	0.288	-0.013	0.034
	23.00	-0.626	0.038	-0.048	0.044
Aggregate base	23.00	-0.011	0.038	-0.048	0.112
	43.00	-0.022	0.013	-0.050	0.068
Subgrade	43.00	-0.001	0.013	-0.050	0.144

Table 53. Stresses and Strains (Spring - Autumn, Binding asphalt course).

Layers	Depth	Stress		Strain (1/1000)	
		Tangential (N/mm2)	Vertical (N/mm2)	Tangential	Vertical
Wearing asphalt course	0.00	1.024	0.649	0.052	0.003
	5.00	0.463	0.587	0.016	0.031
Binding asphalt course	5.00	0.459	0.587	0.016	0.031
	13.00	-0.091	0.279	-0.015	0.034
Asphalt base course	13.00	-0.066	0.279	-0.015	0.037
	23.00	-0.595	0.038	-0.049	0.045
Aggregate base	23.00	-0.011	0.038	-0.049	0.114
	43.00	-0.022	0.013	-0.050	0.069
Subgrade	43.00	-0.001	0.013	-0.050	0.145

Table 54. Stresses and Strains (Spring - Autumn, Asphalt base course).

Layers	Depth	Stress		Strain (1/1000)	
		Tangential (N/mm2)	Vertical (N/mm2)	Tangential	Vertical
Wearing asphalt course	0.00	1.010	0.649	0.051	0.004
	5.00	0.464	0.589	0.016	0.031
Binding asphalt course	5.00	0.460	0.589	0.016	0.032
	13.00	-0.065	0.284	-0.013	0.033
Asphalt base course	13.00	-0.056	0.284	-0.013	0.034
	23.00	-0.618	0.037	-0.047	0.043
Aggregate base	23.00	-0.011	0.037	-0.047	0.110
	43.00	-0.023	0.013	-0.049	0.067
Subgrade	43.00	-0.001	0.013	-0.049	0.143

Table 55. Stresses and Strains (Spring - Autumn, Aggregate base).

Summer

In this point, it will be presented the outcomes from the following configurations:

- Base case
- Base case plus buried pipes in wearing asphalt course (depth equal to 0.0375 m)
- Base case plus buried pipes in binding asphalt course (depth equal to 0.09 m)
- Base case plus buried pipes in asphalt base course (depth equal to 0.18 m)
- Base case plus buried pipes in the fourth layer (depth equal to 0.33 m)

Layers	Depth	Stress		Strain (1/1000)	
		Tangential (N/mm2)	Vertical (N/mm2)	Tangential	Vertical
Wearing asphalt course	0.00	0.872	0.649	0.096	-0.064
	5.00	0.435	0.599	0.023	0.091
Binding asphalt course	5.00	0.437	0.599	0.023	0.085
	13.00	0.010	0.321	-0.042	0.106
Asphalt base course	13.00	0.010	0.321	-0.004	0.106
	23.00	-0.421	0.078	-0.096	0.141
Aggregate base	23.00	-0.021	0.078	-0.096	0.230
	43.00	-0.040	0.022	-0.089	0.118
Subgrade	43.00	-0.003	0.022	-0.089	0.245

Table 56. Stresses and Strains (Summer, Base case).

Layers	Depth	Stress		Strain (1/1000)	
		Tangential (N/mm2)	Vertical (N/mm2)	Tangential	Vertical
Wearing asphalt course	0.00	0.703	0.649	0.067	0.036
	5.00	0.373	0.603	0.009	0.126
Binding asphalt course	5.00	0.367	0.603	0.009	0.105
	13.00	0.010	0.337	-0.044	0.112
Asphalt base course	13.00	0.010	0.337	-0.044	0.112
	23.00	-0.324	0.105	-0.080	0.124
Aggregate base	23.00	0.000	0.105	-0.080	0.268
	43.00	0.006	0.053	-0.015	0.112
Subgrade	43.00	0.001	0.053	-0.015	0.053

Table 57. Stresses and Strains (Summer, Wearing asphalt course).

Layers	Depth	Stress		Strain (1/1000)	
		Tangential (N/mm2)	Vertical (N/mm2)	Tangential	Vertical
Wearing asphalt course	0.00	0.892	0.649	0.100	-0.023
	5.00	0.419	0.598	0.023	0.096
Binding asphalt course	5.00	0.419	0.598	0.023	0.097
	13.00	0.009	0.321	-0.045	0.116
Asphalt base course	13.00	0.009	0.321	-0.045	0.116
	23.00	-0.399	0.081	-0.100	0.147
Aggregate base	23.00	-0.021	0.081	-0.100	0.239
	43.00	-0.041	0.023	-0.091	0.121
Subgrade	43.00	-0.003	0.023	-0.091	0.251

Table 58. Stresses and Strains (Summer, Binding asphalt course).

Layers	Depth	Stress		Strain (1/1000)	
		Tangential (N/mm2)	Vertical (N/mm2)	Tangential	Vertical
Wearing asphalt course	0.00	0.883	0.649	0.098	-0.065
	5.00	0.434	0.597	0.023	0.091
Binding asphalt course	5.00	0.437	0.597	0.023	0.084
	13.00	-0.016	0.316	-0.046	0.112
Asphalt base course	13.00	0.004	0.316	-0.046	0.116
	23.00	-0.396	0.079	-0.099	0.146
Aggregate base	23.00	-0.022	0.079	-0.099	0.236
	43.00	-0.041	0.023	-0.091	0.120
Subgrade	43.00	-0.003	0.023	-0.091	0.248

Table 59. Stresses and Strains (Summer, Asphalt base course).

Layers	Depth	Stress		Strain (1/1000)	
		Tangential (N/mm2)	Vertical (N/mm2)	Tangential	Vertical
Wearing asphalt course	0.00	0.870	0.649	0.096	-0.064
	5.00	0.434	0.599	0.023	0.092
Binding asphalt course	5.00	0.436	0.599	0.023	-0.046
	13.00	0.010	0.321	-0.042	0.106
Asphalt base course	13.00	0.010	0.321	-0.042	0.106
	23.00	-0.417	0.079	-0.096	0.140
Aggregate base	23.00	-0.021	0.079	-0.096	0.228
	43.00	-0.041	0.022	-0.089	0.117
Subgrade	43.00	-0.003	0.022	-0.089	0.244

Table 60. Stresses and Strains (Summer, Aggregate base).

Stress and Strain under simple axle and tandem axle

Here, it will be presented the resulting outcomes from the stress and strain analyses for a simple axle and tandem axle. These outcomes are classified according to the three different seasons considered, with the aim to show the influence of the exterior conditions on the materials properties, and consequently on the stress and displacement of the element.

The values reflected in the tables of this point correspond to the vertical and tangential stresses, as well as the vertical and tangential strains. The first value of each layer corresponds to the fiber located on the top of the layer while the second value corresponds to the fiber located at the bottom of the layer.

It should be noticed that the outcomes correspond to the analyses that consider special load hypothesis. In these special load hypothesis there will be one type of load that prevails over the rest of the combinations, for each case. For this reason, the values reflected in each fiber will correspond to the most unfavourable outcomes of these analyses. Here are the type of loads that prevail over the rest of the combinations:

- Load under simple axle
- Load under one of the twin wheels (Tandem)
- Load under the centre of the twin wheels (Tandem)

Winter

At this point, it will be presented the outcomes from the following configurations:

- Base case
- Base case plus buried pipes in wearing asphalt course (depth equal to 0.0375 m)
- Base case plus buried pipes in binding asphalt course (depth equal to 0.09 m)
- Base case plus buried pipes in asphalt base course (depth equal to 0.18 m)
- Base case plus buried pipes in the fourth layer (depth equal to 0.33 m)

It should be noticed that the letters A, B and C will have the following meanings:

- A: Load Under simple axle
- B: Load Under one of the twin wheels (Tandem)
- C: Load Under the centre of the twin wheels (Tandem)

Layers	Depth	Result output							
		Tangential Strain (1/1000)		Tangential stress (N/mm2)		Vertical strain (1/1000)		Vertical stress (N/mm2)	
Wearing asphalt course	0.00	0.049	B	1.394	B	-0.023	C	0.649	A
	5.00	0.022	C	0.674	B	-0.013	C	0.588	B
Binding asphalt course	5.00	0.022	C	0.661	B	-0.013	C	0.588	B
	13.00	-0.009	B	-0.132	C	0.018	B	0.280	B
Asphalt base course	13.00	-0.009	B	-0.127	C	0.019	B	0.280	B
	23.00	-0.047	C	-0.132	C	0.028	B	0.033	B
Aggregate base	23.00	-0.047	C	-0.011	C	0.097	B	0.033	B
	43.00	-0.062	C	-0.026	C	0.083	C	0.018	C
Subgrade	43.00	-0.062	C	-0.001	C	0.182	C	0.018	C

Table 61. Stresses and Strains Simple axle and Tandem (Winter, Base case).

Layers	Depth	Result output							
		Tangential Strain (1/1000)		Tangential stress (N/mm2)		Vertical strain (1/1000)		Vertical stress (N/mm2)	
Wearing asphalt course	0.00	0.052	B	1.281	B	-0.025	C	0.649	A
	5.00	0.025	C	0.660	B	-0.015	C	0.593	B
Binding asphalt course	5.00	0.025	C	0.729	B	-0.015	C	0.593	B
	13.00	-0.008	B	-0.112	C	0.018	B	0.287	B
Asphalt base course	13.00	-0.008	B	-0.106	C	0.018	B	0.287	B
	23.00	-0.048	C	-1.039	C	0.029	B	0.034	B
Aggregate base	23.00	-0.048	C	-0.011	C	0.099	B	0.034	B
	43.00	-0.064	C	-0.027	C	0.085	C	0.018	C
Subgrade	43.00	-0.064	C	-0.001	C	0.188	C	0.018	C

Table 62. Stresses and Strains simple axle and Tandem (Winter, Wearing asphalt course).

Layers	Depth	Result output							
		Tangential Strain (1/1000)		Tangential stress (N/mm2)		Vertical strain (1/1000)		Vertical stress (N/mm2)	
Wearing asphalt course	0.00	0.050	B	1.416	B	-0.024	C	0.649	A
	5.00	0.022	C	0.668	B	-0.014	C	0.588	B
Binding asphalt course	5.00	0.022	C	0.612	B	-0.013	C	0.588	B
	13.00	-0.009	B	-0.106	C	0.019	B	0.283	B
Asphalt base course	13.00	-0.009	B	-0.115	C	0.018	B	0.283	B
	23.00	-0.048	C	-1.024	B	0.028	B	0.033	B
Aggregate base	23.00	-0.048	C	-0.011	C	0.098	B	0.033	B
	43.00	-0.063	C	-0.026	C	0.083	C	0.018	C
Subgrade	43.00	-0.063	C	-0.001	C	0.184	C	0.018	C

Table 63. Stresses and Strains Simple axle and Tandem (Winter, Binding asphalt course).

Layers	Depth	Result output							
		Tangential Strain (1/1000)		Tangential stress (N/mm2)		Vertical strain (1/1000)		Vertical stress (N/mm2)	
Wearing asphalt course	0.00	0.050	B	1.411	B	-0.024	C	0.649	A
	5.00	0.022	C	0.672	B	-0.013	C	0.586	B
Binding asphalt course	5.00	0.022	C	0.660	B	-0.013	C	0.586	B
	13.00	-0.011	B	-0.162	C	0.019	B	0.275	B
Asphalt base course	13.00	-0.011	B	-0.141	C	0.020	B	0.275	B
	23.00	-0.050	C	-0.981	C	0.029	B	0.034	B
Aggregate base	23.00	-0.050	C	-0.011	C	0.099	B	0.034	B
	43.00	-0.064	C	-0.027	C	0.085	C	0.018	C
Subgrade	43.00	-0.064	C	-0.001	C	0.186	C	0.018	C

Table 64. Stresses and Strains Simple axle and Tandem (Winter, Asphalt base course).

Layers	Depth	Result output							
		Tangential Strain (1/1000)		Tangential stress (N/mm2)		Vertical strain (1/1000)		Vertical stress (N/mm2)	
Wearing asphalt course	0.00	0.049	B	1.392	B	-0.023	C	0.649	A
	5.00	0.022	C	0.673	B	-0.013	C	0.588	B
Binding asphalt course	5.00	0.022	C	0.661	B	-0.013	C	0.588	B
	13.00	-0.009	B	-0.132	C	0.018	B	0.280	B
Asphalt base course	13.00	-0.009	B	-0.126	C	0.019	B	0.280	B
	23.00	-0.047	C	-1.016	C	0.028	B	0.033	B
Aggregate base	23.00	-0.047	C	-0.011	C	0.098	B	0.033	B
	43.00	-0.063	C	-0.027	C	0.082	C	0.018	C
Subgrade	43.00	-0.063	C	-0.001	C	0.182	C	0.018	C

Table 65. Stresses and Strains Simple axle and Tandem (Winter, Aggregate base).

Spring - Autumn

At this point, it will be presented the outcomes from the following configurations:

- Base case
- Base case plus buried pipes in wearing asphalt course (depth equal to 0.0375 m)
- Base case plus buried pipes in binding asphalt course (depth equal to 0.09 m)
- Base case plus buried pipes in asphalt base course (depth equal to 0.18 m)
- Base case plus buried pipes in the fourth layer (depth equal to 0.33 m)

It should be noticed that the letters A, B and C will have the following meanings:

- A: Load Under simple axle
- B: Load Under one of the twin wheels (Tandem)
- C: Load Under the centre of the twin wheels (Tandem)

Layers	Depth	Result output							
		Tangential Strain (1/1000)		Tangential stress (N/mm2)		Vertical strain (1/1000)		Vertical stress (N/mm2)	
Wearing asphalt course	0.00	0.074	B	1.281	B	-0.044	C	0.649	A
	5.00	0.031	C	0.619	B	-0.027	C	0.590	B
Binding asphalt course	5.00	0.031	C	0.611	B	-0.027	C	0.590	B
	13.00	-0.016	B	-0.103	C	0.034	B	0.290	B
Asphalt base course	13.00	-0.016	B	-0.096	C	0.035	B	0.290	B
	23.00	-0.072	C	-0.850	B	0.055	B	0.048	B
Aggregate base	23.00	-0.072	C	-0.017	C	0.142	B	0.048	B
	43.00	-0.089	C	-0.038	C	0.114	C	0.023	C
Subgrade	43.00	-0.089	C	-0.002	C	0.246	C	0.023	C

Table 66. Stresses and Strains Simple axle and Tandem (Spring - Autumn, Base case).

Layers	Depth	Result output							
		Tangential Strain (1/1000)		Tangential stress (N/mm2)		Vertical strain (1/1000)		Vertical stress (N/mm2)	
Wearing asphalt course	0.00	0.066	B	10.597	B	-0.035	C	6.620	A
	5.00	0.029	C	5.452	B	-0.023	C	6.075	B
Binding asphalt course	5.00	0.029	C	5.880	B	-0.024	C	6.075	B
	13.00	-0.013	B	-0.594	C	0.033	B	3.115	B
Asphalt base course	13.00	-0.013	B	-0.544	C	0.034	B	3.115	B
	23.00	-0.061	C	-7.148	B	0.047	B	0.665	B
Aggregate base	23.00	-0.061	C	-0.025	A	0.166	B	0.665	B
	43.00	-0.038	C	-0.173	C	0.049	C	0.094	C
Subgrade	43.00	-0.038	C	-0.013	C	0.101	C	0.094	C

Table 67. Stresses and Strains Simple axle and Tandem (Spring - Autumn, Wearing asphalt course).

Layers	Depth	Result output							
		Tangential Strain (1/1000)		Tangential stress (N/mm2)		Vertical strain (1/1000)		Vertical stress (N/mm2)	
Wearing asphalt course	0.00	0.075	B	1.300	B	-0.044	C	0.649	A
	5.00	0.031	C	0.609	B	-0.027	C	0.591	B
Binding asphalt course	5.00	0.031	C	0.569	B	-0.027	C	0.591	B
	13.00	-0.015	B	-0.079	C	0.036	B	0.294	B
Asphalt base course	13.00	-0.015	B	-0.085	C	0.035	B	0.294	B
	23.00	-0.072	C	-0.855	B	0.055	B	0.049	B
Aggregate base	23.00	-0.072	C	-0.016	C	0.144	B	0.049	B
	43.00	-0.090	C	-0.038	C	0.115	C	0.024	C
Subgrade	43.00	-0.090	C	-0.002	C	0.248	C	0.024	C

Table 68. Stresses and Strains Simple axle and Tandem (Spring - Autumn, Binding asphalt course).

Layers	Depth	Result output							
		Tangential Strain (1/1000)		Tangential stress (N/mm2)		Vertical strain (1/1000)		Vertical stress (N/mm2)	
Wearing asphalt course	0.00	0.075	B	1.295	B	-0.045	C	0.649	A
	5.00	0.031	C	0.616	B	-0.026	C	0.588	B
Binding asphalt course	5.00	0.031	C	0.609	B	-0.026	C	0.588	B
	13.00	-0.018	B	-0.126	C	0.035	B	0.286	B
Asphalt base course	13.00	-0.018	B	-0.107	C	0.038	B	0.286	B
	23.00	-0.074	C	-0.815	B	0.057	B	0.049	B
Aggregate base	23.00	-0.074	C	-0.017	C	0.146	B	0.049	B
	43.00	-0.091	C	-0.039	C	0.116	C	0.024	C
Subgrade	43.00	-0.091	C	-0.002	C	0.251	C	0.024	C

Table 69. Stresses and Strains Simple axle and Tandem (Spring - Autumn, Asphalt base course).

Layers	Depth	Result output							
		Tangential Strain (1/1000)		Tangential stress (N/mm2)		Vertical strain (1/1000)		Vertical stress (N/mm2)	
Wearing asphalt course	0.00	0.074	B	1.279	B	-0.044	C	0.649	A
	5.00	0.031	C	0.618	B	-0.027	C	0.590	B
Binding asphalt course	5.00	0.031	C	0.611	B	-0.027	C	0.590	B
	13.00	-0.016	B	-0.101	C	0.034	B	0.290	B
Asphalt base course	13.00	-0.016	B	-0.095	C	0.035	B	0.290	B
	23.00	-0.072	C	-0.847	B	0.055	B	0.049	B
Aggregate base	23.00	-0.071	C	-0.017	C	0.143	B	0.049	B
	43.00	-0.089	C	-0.039	C	0.113	C	0.023	C
Subgrade	43.00	-0.089	C	-0.002	C	0.246	C	0.023	C

Table 70. Stresses and Strains Simple axle and Tandem (Spring - Autumn, Aggregate base).

Summer

At this point, it will be presented the outcomes from the following configurations:

- Base case
- Base case plus buried pipes in wearing asphalt course (depth equal to 0.0375 m)
- Base case plus buried pipes in binding asphalt course (depth equal to 0.09 m)
- Base case plus buried pipes in asphalt base course (depth equal to 0.18 m)
- Base case plus buried pipes in the fourth layer (depth equal to 0.33 m)

It should be noticed that the letters A, B and C will have the following meanings:

- A: Load Under simple axle
- B: Load Under one of the twin wheels (Tandem)
- C: Load Under the centre of the twin wheels (Tandem)

Layers	Depth	Result output							
		Tangential Strain (1/1000)		Tangential stress (N/mm2)		Vertical strain (1/1000)		Vertical stress (N/mm2)	
Wearing asphalt course	0.00	0.139	C	1.009	B	-0.128	C	0.649	A
	5.00	0.047	C	0.520	B	-0.092	C	0.600	B
Binding asphalt course	5.00	0.047	C	0.529	B	-0.092	C	0.600	B
	13.00	-0.045	B	-0.012	C	0.106	A	0.328	B
Asphalt base course	13.00	-0.045	B	-0.012	C	0.106	A	0.328	B
	23.00	-0.135	C	-0.523	B	0.161	B	0.092	B
Aggregate base	23.00	-0.135	C	-0.030	C	0.269	B	0.092	B
	43.00	-0.156	C	-0.067	C	0.188	C	0.037	C
Subgrade	43.00	-0.156	C	-0.005	C	0.397	C	0.037	C

Table 71. Stresses and Strains Simple axle and Tandem (Summer, Base case).

Layers	Depth	Result output							
		Tangential Strain (1/1000)		Tangential stress (N/mm2)		Vertical strain (1/1000)		Vertical stress (N/mm2)	
Wearing asphalt course	0.00	0.087	B	7.579	B	-0.066	C	6.620	A
	5.00	-0.007	C	0.399	B	-0.052	C	0.605	B
Binding asphalt course	5.00	-0.007	A	0.398	B	-0.053	C	0.605	B
	13.00	-0.048	B	-0.016	C	0.112	A	0.349	B
Asphalt base course	13.00	-0.048	B	-0.016	C	0.112	A	0.349	B
	23.00	-0.104	C	-0.358	B	0.130	B	0.128	B
Aggregate base	23.00	-0.104	C	0.004	C	0.312	B	0.128	B
	43.00	-0.024	C	0.022	C	0.171	C	0.082	C
Subgrade	43.00	-0.024	C	0.004	C	0.079	C	0.082	C

Table 72. Stresses and Strains Simple axle and Tandem (Summer, Wearing asphalt course).

Layers	Depth	Result output							
		Tangential Strain (1/1000)		Tangential stress (N/mm2)		Vertical strain (1/1000)		Vertical stress (N/mm2)	
Wearing asphalt course	0.00	0.142	B	1.030	B	-0.128	C	0.649	A
	5.00	0.044	C	0.505	B	-0.093	C	0.599	B
Binding asphalt course	5.00	0.044	C	0.503	B	-0.093	C	0.599	B
	13.00	-0.049	B	-0.014	C	0.116	A	0.329	B
Asphalt base course	13.00	-0.049	B	-0.014	C	0.116	A	0.329	B
	23.00	-0.140	C	-0.494	B	0.168	B	0.095	B
Aggregate base	23.00	-0.140	C	-0.031	C	0.277	B	0.095	B
	43.00	-0.160	C	-0.068	C	0.191	C	0.038	C
Subgrade	43.00	-0.160	C	-0.005	C	0.405	C	0.038	C

Table 73. Stresses and Strains Simple axle and Tandem (Summer, Binding asphalt course).

Layers	Depth	Result output							
		Tangential Strain (1/1000)		Tangential stress (N/mm2)		Vertical strain (1/1000)		Vertical stress (N/mm2)	
Wearing asphalt course	0.00	0.141	C	1.020	B	-0.129	C	0.649	A
	5.00	0.046	C	0.519	B	-0.091	C	0.598	B
Binding asphalt course	5.00	0.046	C	0.527	B	-0.091	C	0.598	B
	13.00	-0.050	B	-0.028	C	0.112	A	0.324	B
Asphalt base course	13.00	-0.050	B	-0.020	C	0.116	A	0.324	B
	23.00	-0.139	C	-0.491	B	0.167	B	0.094	B
Aggregate base	23.00	-0.139	C	-0.032	C	0.274	B	0.094	B
	43.00	-0.159	C	-0.068	C	0.190	C	0.037	C
Subgrade	43.00	-0.159	C	-0.005	C	0.402	C	0.037	C

Table 74. Stresses and Strains Simple axle and Tandem (Summer, Asphalt base course).

Layers	Depth	Result output							
		Tangential Strain (1/1000)		Tangential stress (N/mm2)		Vertical strain (1/1000)		Vertical stress (N/mm2)	
Wearing asphalt course	0.00	0.138	C	1.007	B	-0.128	C	0.649	A
	5.00	0.046	C	0.519	B	-0.091	C	0.600	B
Binding asphalt course	5.00	0.046	C	0.528	B	-0.092	C	0.600	B
	13.00	-0.044	B	-0.011	C	0.106	A	0.329	B
Asphalt base course	13.00	-0.044	B	-0.011	C	0.106	A	0.329	B
	23.00	-0.134	C	-0.518	B	0.160	B	0.093	B
Aggregate base	23.00	-0.134	C	-0.031	C	0.270	B	0.093	B
	43.00	-0.156	C	-0.069	C	0.186	C	0.037	C
Subgrade	43.00	-0.156	C	-0.005	C	0.396	C	0.037	C

Table 75. Stresses and Strains Simple axle and Tandem (Summer, Aggregate base).

Tests with resin

Stress and Strains.

In this section it will be presented the resulting outcomes from the stress and strains analyses performed with ALIZE. These outcomes are classified according to the three different seasons considered, with the aim to show the influence of the exterior conditions on the materials properties, and consequently on the stress and displacement of the element.

The values reflected in the tables of this point correspond to the vertical and tangential stresses, as well as the vertical and tangential strains. The first value of each layer corresponds to the fiber located on the top of the layer while the second value corresponds to the fiber located at the bottom of the layer.

It should be noticed that the results come from the analyses performed considering the most unfavourable load hypothesis (loads combinations).

Winter

At this point, it will be presented the outcomes from the following configurations:

- Base case plus Epoxy Resin plus buried pipes in binding asphalt course
- Base case plus Epoxy Resin plus buried pipes in asphalt base course
- Base case plus Epoxy Resin plus buried pipes in aggregate base

Layers	Depth (cm)	Stress		Strain (1/1000)	
		Tangential (N/mm2)	Vertical (N/mm2)	Tangential	Vertical
Epoxy resin layer	0.00	0.398	0.649	0.034	0.168
	0.1	0.396	0.650	0.034	0.168
Wearing asphalt course	0.1	1.065	0.650	0.034	0.006
	5.1	0.469	0.587	0.011	0.019
Binding asphalt course	5.1	0.437	0.587	0.011	0.022
	13.1	-0.058	0.278	-0.007	0.018
Asphalt base course	13.1	-0.068	0.278	-0.007	0.018
	23.1	-0.716	0.024	-0.031	0.022
Aggregate base	23.1	-0.007	0.024	-0.031	0.072
	43.1	-0.015	0.010	-0.034	0.048
Subgrade	43.1	-0.001	0.010	-0.034	0.104

Table 76. Stresses and Strains (Winter, Resin, Binding asphalt course).

Layers	Depth (cm)	Stress		Strain (1/1000)	
		Tangential (N/mm2)	Vertical (N/mm2)	Tangential	Vertical
Epoxy resin layer	0.00	0.397	0.649	0.034	0.168
	0.1	0.396	0.650	0.034	0.168
Wearing asphalt course	0.1	1.062	0.650	0.034	0.006
	5.1	0.478	0.584	0.011	0.018
Binding asphalt course	5.1	0.471	0.584	0.011	0.019
	13.1	-0.112	0.269	-0.008	0.018
Asphalt base course	13.1	-0.090	0.269	-0.008	0.019
	23.1	-0.683	0.025	-0.032	0.022
Aggregate base	23.1	-0.007	0.025	-0.032	0.074
	43.1	-0.015	0.010	-0.035	0.049
Subgrade	43.1	-0.001	0.010	-0.035	0.105

Table 77. Stresses and Strains (Winter, Resin, Asphalt base course).

Layers	Depth (cm)	Stress		Strain (1/1000)	
		Tangential (N/mm2)	Vertical (N/mm2)	Tangential	Vertical
Epoxy resin layer	0.00	0.395	0.649	0.033	0.168
	0.1	0.393	0.650	0.033	0.169
Wearing asphalt course	0.1	1.046	0.650	0.033	0.007
	5.1	0.478	0.586	0.011	0.018
Binding asphalt course	5.1	0.471	0.586	0.011	0.019
	13.1	-0.085	0.274	-0.007	0.017
Asphalt base course	13.1	-0.078	0.274	-0.007	0.018
	23.1	-0.707	0.024	-0.030	0.021
Aggregate base	23.1	-0.007	0.024	-0.030	0.071
	43.1	-0.015	0.010	-0.034	0.047
Subgrade	43.1	-0.001	0.010	-0.034	0.103

Table 78. Stresses and Strains (Winter, Resin, Aggregate base).

Spring - Autumn

At this point, it will be presented the outcomes from the following configurations:

- Base case plus Epoxy Resin plus buried pipes in binding asphalt course
- Base case plus Epoxy Resin plus buried pipes in asphalt base course
- Base case plus Epoxy Resin plus buried pipes in aggregate base

Layers	Depth (cm)	Stress		Strain (1/1000)	
		Tangential (N/mm2)	Vertical (N/mm2)	Tangential	Vertical
Epoxy resin layer	0.00	0.461	0.649	0.052	0.152
	0.1	0.459	0.650	0.051	0.153
Wearing asphalt course	0.1	1.021	0.650	0.051	0.004
	5.1	0.448	0.589	0.015	0.032
Binding asphalt course	5.1	0.426	0.589	0.015	0.037
	13.1	-0.040	0.287	-0.013	0.035
Asphalt base course	13.1	-0.047	0.287	-0.013	0.033
	23.1	-0.625	0.037	-0.048	0.044
Aggregate base	23.1	-0.011	0.037	-0.048	0.112
	43.1	-0.022	0.013	-0.050	0.068
Subgrade	43.1	-0.001	0.013	-0.050	0.144

Table 79. Stresses and Strains (Spring - Autumn, Resin, Binding asphalt course).

Layers	Depth (cm)	Stress		Strain (1/1000)	
		Tangential (N/mm2)	Vertical (N/mm2)	Tangential	Vertical
Epoxy resin layer	0.00	0.461	0.649	0.052	0.152
	0.1	0.458	0.650	0.051	0.153
Wearing asphalt course	0.1	1.018	0.650	0.051	0.004
	5.1	0.459	0.586	0.016	0.031
Binding asphalt course	5.1	0.455	0.586	0.016	0.032
	13.1	-0.092	0.278	-0.015	0.034
Asphalt base course	13.1	-0.066	0.278	-0.015	0.036
	23.1	-0.594	0.038	-0.049	0.045
Aggregate base	23.1	-0.011	0.038	-0.049	0.114
	43.1	-0.022	0.013	-0.050	0.069
Subgrade	43.1	-0.001	0.013	-0.050	0.145

Table 80. Stresses and Strains (Spring - Autumn, Resin, Asphalt base course).

Layers	Depth (cm)	Stress		Strain (1/1000)	
		Tangential (N/mm2)	Vertical (N/mm2)	Tangential	Vertical
Epoxy resin layer	0.00	0.457	0.649	0.051	0.153
	0.1	0.454	0.650	0.050	0.154
Wearing asphalt course	0.1	0.446	0.650	0.050	0.005
	5.1	0.460	0.588	0.016	0.031
Binding asphalt course	5.1	0.455	0.588	0.016	0.032
	13.1	-0.065	0.283	-0.013	0.033
Asphalt base course	13.1	-0.056	0.283	-0.013	0.034
	23.1	-0.616	0.037	-0.047	0.043
Aggregate base	23.1	-0.011	0.037	-0.047	0.109
	43.1	-0.022	0.013	-0.049	0.067
Subgrade	43.1	-0.001	0.013	-0.049	0.142

Table 81. Stresses and Strains (Spring - Autumn, Resin, Aggregate base).

Summer

At this point, it will be presented the outcomes from the following configurations:

- Base case plus Epoxy Resin plus buried pipes in binding asphalt course
- Base case plus Epoxy Resin plus buried pipes in asphalt base course
- Base case plus Epoxy Resin plus buried pipes in aggregate base

Layers	Depth (cm)	Stress		Strain (1/1000)	
		Tangential (N/mm2)	Vertical (N/mm2)	Tangential	Vertical
Epoxy resin layer	0.00	0.622	0.649	0.098	0.113
	0.1	0.614	0.650	0.096	0.115
Wearing asphalt course	0.1	0.872	0.650	0.096	-0.064
	5.1	0.414	0.599	0.023	0.098
Binding asphalt course	5.1	0.414	0.599	0.023	0.099
	13.1	0.031	0.324	-0.041	0.110
Asphalt base course	13.1	0.016	0.324	-0.041	0.106
	23.1	-0.423	0.079	-0.097	0.142
Aggregate base	23.1	-0.021	0.079	-0.097	0.232
	43.1	-0.041	0.022	-0.089	0.119
Subgrade	43.1	-0.003	0.022	-0.089	0.246

Table 82. Stresses and Strains (Summer, Resin, Binding asphalt course).

Layers	Depth (cm)	Stress		Strain (1/1000)	
		Tangential (N/mm2)	Vertical (N/mm2)	Tangential	Vertical
Epoxy resin layer	0.00	0.624	0.649	0.099	0.112
	0.1	0.616	0.650	0.096	0.114
Wearing asphalt course	0.1	0.875	0.650	0.096	-0.065
	5.1	0.428	0.595	0.023	0.092
Binding asphalt course	5.1	0.430	0.595	0.023	0.085
	13.1	0.003	0.314	-0.046	0.112
Asphalt base course	13.1	0.003	0.314	-0.046	0.116
	23.1	-0.394	0.079	-0.099	0.145
Aggregate base	23.1	-0.021	0.079	-0.099	0.234
	43.1	-0.041	0.022	-0.090	0.120
Subgrade	43.1	-0.003	0.022	-0.090	0.247

Table 83. Stresses and Strains (Summer, Resin, Asphalt base course).

Layers	Depth (cm)	Stress		Strain (1/1000)	
		Tangential (N/mm2)	Vertical (N/mm2)	Tangential	Vertical
Epoxy resin layer	0.00	0.613	0.649	0.096	0.115
	0.1	0.606	0.650	0.094	0.117
Wearing asphalt course	0.1	0.862	0.650	0.094	-0.064
	5.1	0.428	0.598	0.023	0.093
Binding asphalt course	5.1	0.430	0.598	0.023	0.086
	13.1	0.009	0.320	-0.042	0.106
Asphalt base course	13.1	0.009	0.320	-0.042	0.106
	23.1	-0.415	0.078	-0.095	0.139
Aggregate base	23.1	-0.021	0.078	-0.095	0.226
	43.1	-0.041	0.022	-0.088	0.117
Subgrade	43.1	-0.003	0.022	-0.088	0.243

Table 84. Stresses and Strains (Summer, Resin, Aggregate base).

Stress and Strain under simple axle and tandem axle

Here, it will be presented the resulting outcomes from the stress and strain analyses for a simple axle and tandem axle. These outcomes are classified according to the three different seasons considered, with the aim to show the influence of the exterior conditions on the materials properties, and consequently on the stress and displacement of the element.

The values reflected in the tables of this point correspond to the vertical and tangential stresses, as well as the vertical and tangential strains. The first value of each layer corresponds to the fiber located on the top of the layer while the second value corresponds to the fiber located at the bottom of the layer.

It should be noticed that the outcomes correspond to the analyses that consider special load hypothesis. In these special load hypothesis there will be one type of load that prevails over the rest of the combinations, for each case. For this reason, the values reflected in each fiber will correspond to the most unfavourable outcomes of these analyses. Here are the type of loads that prevail over the rest of the combinations:

- Load under simple axle
- Load under one of the twin wheels (Tandem)
- Load under the centre of the twin wheels (Tandem)

Winter

In this point will be presented the outcomes from the following configurations:

- Base case plus Epoxy Resin plus buried pipes in binding asphalt course
- Base case plus Epoxy Resin plus buried pipes in asphalt base course
- Base case plus Epoxy Resin plus buried pipes in aggregate base

It should be notice that the letters A, B and C will have the following meanings:

- A: Load Under simple axle
- B: Load Under one of the twin wheels (Tandem)
- C: Load Under the centre of the twin wheels (Tandem)

Layers	Depth (cm)	Result output							
		Tangential Strain (1/1000)		Tangential stress (N/mm2)		Vertical strain (1/1000)		Vertical stress (N/mm2)	
Epoxy resin layer	0.00	0.050	B	0.444	B	-0.035	C	0.649	A
	0.1	0.050	B	0.442	B	-0.034	C	-0.016	C
Wearing asphalt course	0.1	0.050	B	1.410	B	-0.024	C	-0.016	C
	5.1	0.022	C	0.664	B	-0.014	C	0.587	B
Binding asphalt course	5.1	0.022	C	0.608	B	-0.013	C	0.587	B
	13.1	-0.009	B	-0.107	C	0.019	B	0.282	B
Asphalt base course	13.1	-0.009	B	-0.115	C	0.018	B	0.282	B
	23.1	-0.048	C	-1.022	B	0.028	B	0.033	B
Aggregate base	23.1	-0.048	C	-0.011	C	0.097	B	0.033	B
	43.1	-0.063	C	-0.026	C	0.083	C	0.018	C
Subgrade	43.1	-0.063	C	-0.001	C	0.184	C	0.018	C

Table 85. Stresses and Strains Simple axle and Tandem (Winter, Resin, Binding asphalt course).

Layers	Depth (cm)	Result output							
		Tangential Strain (1/1000)		Tangential stress (N/mm2)		Vertical strain (1/1000)		Vertical stress (N/mm2)	
Epoxy resin layer	0.00	0.050	B	0.443	B	-0.035	C	0.649	A
	0.1	0.050	B	0.441	B	-0.035	C	-0.016	C
Wearing asphalt course	0.1	0.050	B	1.405	B	-0.024	C	-0.016	C
	5.1	0.022	C	0.668	B	-0.013	C	0.585	B
Binding asphalt course	5.1	0.022	C	0.656	B	-0.013	C	0.585	B
	13.1	-0.011	B	-0.162	C	0.019	B	0.274	B
Asphalt base course	13.1	-0.011	B	-0.142	C	0.020	B	0.274	B
	23.1	-0.049	C	-0.979	C	0.029	B	0.034	B
Aggregate base	23.1	-0.049	C	-0.011	C	0.099	B	0.034	B
	43.1	-0.064	C	-0.027	C	0.084	C	0.018	C
Subgrade	43.1	-0.064	C	-0.001	C	0.186	C	0.018	C

Table 86. Stresses and Strains Simple axle and Tandem (Winter, Resin, Asphalt base course).

Layers	Depth (cm)	Result output							
		Tangential Strain (1/1000)		Tangential stress (N/mm2)		Vertical strain (1/1000)		Vertical stress (N/mm2)	
Epoxy resin layer	0.00	0.049	B	0.440	B	-0.034	C	0.649	A
	0.1	0.049	B	0.438	B	-0.034	C	-0.016	C
Wearing asphalt course	0.1	0.049	B	1.387	B	-0.023	C	-0.016	C
	5.1	0.022	C	0.670	B	-0.013	C	0.587	B
Binding asphalt course	5.1	0.022	C	0.657	B	-0.013	C	0.587	B
	13.1	-0.009	B	-0.133	C	0.018	B	0.279	B
Asphalt base course	13.1	-0.009	B	-0.127	C	0.018	B	0.279	B
	23.1	-0.047	C	-1.014	C	0.028	B	0.033	B
Aggregate base	23.1	-0.047	C	-0.011	C	0.095	B	0.033	B
	43.1	-0.062	C	-0.027	C	0.082	C	0.018	C
Subgrade	43.1	-0.062	C	-0.001	C	0.182	C	0.018	C

Table 87. Stresses and Strains Simple axle and Tandem (Winter, Resin, Aggregate base).

Spring - Autumn

In this point will be presented the outcomes from the following configurations:

- Base case plus Epoxy Resin plus buried pipes in binding asphalt course
- Base case plus Epoxy Resin plus buried pipes in asphalt base course
- Base case plus Epoxy Resin plus buried pipes in aggregate base

It should be notice that the letters A, B and C will have the following meanings:

- A: Load Under simple axle
- B: Load Under one of the twin wheels (Tandem)
- C: Load Under the centre of the twin wheels (Tandem)

Layers	Depth (cm)	Result output							
		Tangential Strain (1/1000)		Tangential stress (N/mm2)		Vertical strain (1/1000)		Vertical stress (N/mm2)	
Epoxy resin layer	0.00	0.076	B	0.527	B	-0.048	C	0.649	A
	0.1	0.075	B	0.524	B	-0.048	C	-0.016	C
Wearing asphalt course	0.1	0.075	B	1.293	B	-0.044	C	-0.016	C
	5.1	0.031	C	0.604	B	-0.027	C	0.590	B
Binding asphalt course	5.1	0.031	C	0.565	B	-0.027	C	0.590	B
	13.1	-0.015	B	-0.080	C	0.036	B	0.293	B
Asphalt base course	13.1	-0.015	B	-0.085	C	0.034	B	0.293	B
	23.1	-0.072	C	-0.853	B	0.055	B	0.049	B
Aggregate base	23.1	-0.072	C	-0.016	C	0.143	B	0.049	B
	43.1	-0.090	C	-0.038	C	0.115	C	0.023	C
Subgrade	43.1	-0.090	C	-0.002	C	0.248	C	0.023	C

Table 88. Stresses and Strains Simple axle and Tandem (Spring - Autumn, Resin, Binding asphalt course).

Layers	Depth (cm)	Result output							
		Tangential Strain (1/1000)		Tangential stress (N/mm2)		Vertical strain (1/1000)		Vertical stress (N/mm2)	
Epoxy resin layer	0.00	0.076	B	0.526	B	-0.049	C	0.649	A
	0.1	0.074	B	0.522	B	-0.049	C	-0.016	C
Wearing asphalt course	0.1	0.074	B	1.288	B	-0.045	C	-0.016	C
	5.1	0.031	C	0.612	B	-0.026	C	0.587	B
Binding asphalt course	5.1	0.031	C	0.605	B	-0.026	C	0.587	B
	13.1	-0.018	B	-0.127	C	0.035	B	0.284	B
Asphalt base course	13.1	-0.018	B	-0.107	C	0.038	B	0.284	B
	23.1	-0.074	C	-0.813	B	0.057	B	0.049	B
Aggregate base	23.1	-0.074	C	-0.017	C	0.146	B	0.049	B
	43.1	-0.091	C	-0.039	C	0.116	C	0.024	C
Subgrade	43.1	-0.091	C	-0.002	C	0.250	C	0.024	C

Table 89. Table 28. Stresses and Strains Simple axle and Tandem (Spring - Autumn, Resin, Asphalt base course).

Layers	Depth (cm)	Result output							
		Tangential Strain (1/1000)		Tangential stress (N/mm2)		Vertical strain (1/1000)		Vertical stress (N/mm2)	
Epoxy resin layer	0.00	0.074	B	0.522	B	-0.048	C	0.649	A
	0.1	0.073	B	0.519	B	-0.048	C	-0.016	C
Wearing asphalt course	0.1	0.073	B	1.272	B	-0.044	C	-0.016	C
	5.1	0.031	C	0.613	B	-0.026	C	0.589	B
Binding asphalt course	5.1	0.031	C	0.606	B	-0.026	C	0.589	B
	13.1	-0.016	B	-0.102	C	0.034	B	0.289	B
Asphalt base course	13.1	-0.016	B	-0.095	C	0.035	B	0.289	B
	23.1	-0.071	C	-0.844	B	0.054	B	0.048	B
Aggregate base	23.1	-0.071	C	-0.017	C	0.140	B	0.048	B
	43.1	-0.089	C	-0.039	C	0.113	C	0.023	C
Subgrade	43.1	-0.089	C	-0.002	C	0.246	C	0.023	C

Table 90. Stresses and Strains Simple axle and Tandem (Spring - Autumn, Resin, Aggregate base).

Summer

In this point will be presented the outcomes from the following configurations:

- Base case plus Epoxy Resin plus buried pipes in binding asphalt course
- Base case plus Epoxy Resin plus buried pipes in asphalt base course
- Base case plus Epoxy Resin plus buried pipes in aggregate base

It should be notice that the letters A, B and C will have the following meanings:

- A: Load Under simple axle
- B: Load Under one of the twin wheels (Tandem)
- C: Load Under the centre of the twin wheels (Tandem)

Layers	Depth (cm)	Result output							
		Tangential Strain (1/1000)		Tangential stress (N/mm2)		Vertical strain (1/1000)		Vertical stress (N/mm2)	
Epoxy resin layer	0.00	0.140	C	0.735	B	-0.084	C	0.649	A
	0.1	0.138	C	0.727	B	-0.085	C	-0.016	C
Wearing asphalt course	0.1	0.138	C	1.009	B	-0.128	C	-0.016	C
	5.1	0.043	C	0.500	B	-0.092	C	0.600	B
Binding asphalt course	5.1	0.043	C	0.499	B	-0.092	C	0.600	B
	13.1	-0.043	B	0.000	C	0.110	A	0.331	B
Asphalt base course	13.1	-0.043	B	-0.006	C	0.106	A	0.331	B
	23.1	-0.135	C	-0.524	B	0.162	B	0.093	B
Aggregate base	23.1	-0.135	C	-0.030	C	0.270	B	0.093	B
	43.1	-0.157	C	-0.067	C	0.188	C	0.037	C
Subgrade	43.1	-0.157	C	-0.005	C	0.399	C	0.037	C

Table 91. Stresses and Strains Simple axle and Tandem (Summer, Resin, Binding asphalt course).

Layers	Depth (cm)	Result output							
		Tangential Strain (1/1000)		Tangential stress (N/mm2)		Vertical strain (1/1000)		Vertical stress (N/mm2)	
Epoxy resin layer	0.00	0.141	C	0.736	B	-0.086	C	0.649	A
	0.1	0.139	C	0.728	B	-0.087	C	-0.016	C
Wearing asphalt course	0.1	0.139	C	1.010	B	-0.130	C	-0.016	C
	5.1	0.045	C	0.512	B	-0.090	C	0.596	B
Binding asphalt course	5.1	0.045	C	0.520	B	-0.090	C	0.596	B
	13.1	-0.050	B	-0.030	C	0.112	A	0.322	B
Asphalt base course	13.1	-0.050	B	-0.022	C	0.116	A	0.322	B
	23.1	-0.139	C	-0.490	B	0.166	B	0.093	B
Aggregate base	23.1	-0.139	C	-0.032	C	0.273	B	0.093	B
	43.1	-0.158	C	-0.068	C	0.189	C	0.037	C
Subgrade	43.1	-0.158	C	-0.005	C	0.400	C	0.037	C

Table 92. Stresses and Strains Simple axle and Tandem (Summer, Resin, Asphalt base course).

Layers	Depth (cm)	Result output							
		Tangential Strain (1/1000)		Tangential stress (N/mm2)		Vertical strain (1/1000)		Vertical stress (N/mm2)	
Epoxy resin layer	0.00	0.138	C	0.726	B	-0.085	C	0.649	A
	0.1	0.136	C	0.718	B	-0.086	C	-0.016	C
Wearing asphalt course	0.1	0.136	C	0.997	B	-0.128	C	-0.016	C
	5.1	0.045	C	0.513	B	-0.090	C	0.599	B
Binding asphalt course	5.1	0.045	C	0.521	B	-0.091	C	0.599	B
	13.1	-0.045	B	-0.013	C	0.106	A	0.327	B
Asphalt base course	13.1	-0.045	B	-0.013	C	0.106	A	0.327	B
	23.1	-0.134	C	-0.516	B	0.159	B	0.092	B
Aggregate base	23.1	-0.134	C	-0.031	C	0.264	B	0.092	B
	43.1	-0.155	C	-0.068	C	0.185	C	0.037	C
Subgrade	43.1	-0.155	C	-0.005	C	0.395	C	0.037	C

Table 93. Stresses and Strains Simple axle and Tandem (Summer, Resin, Aggregate base).

Bibliography

Bernier M.: Ground-coupled heat pump system simulation. ASHRAE Transactions. 107, p.605-616, 2001

Bernier M. und Shirazi A. S.: Solar Heat Injection Into boreholes: A preliminary analysis, 2nd Canadian Solar Buildings Conference, Calgary, June 10-14, 2007

Carslaw H.S. und Jaeger J.C.: Conduction of Heat in Solids, Clarendon Press, Oxford University Press, 2nd Edition, 1947

Chiasson, A. - Advances in Modelling of Ground-Source Heat Pump Systems. Dissertation Oklahoma State University, 1999

Deng Z.: Modelling of standing column wells in ground source heat pumps, P.hD Thesis, Oklahoma State University, 2004

Diao N. et al.: Heat transfer in ground heat exchangers with groundwater advection, Int. Journal of Thermal Sciences, 43, 1203-1211, 2004

Eugster, W.J. und Laloui, L. - Workshop „Geothermische Response Tests“, Geothermische Vereinigung e.V. 49744 Geeste, 2002

Gustafson, A.-G. - Thermal Response Test - Numerical simulations and analyses, Lulea University of Technology, 2006

Gehlin S. - Thermal Response Test - In Situ Measurements of Thermal Properties in Hard Rock, Licentiate Thesis, Lulea 1998

Hanschke, Th. & Freund, R. Geothermal Response Tests mit geregeltem Wärmeeintrag - erste Betriebserfahrungen mit der neuen GRT-Messeinheit. 9. Geothermische Fachtagung Karlsruhe, October 2006

Hanschke, Th.; Kühl, J.-U.; Oldorf, B. & Uebigau M.: Energetischer Doppelnutzen; Energiepfähle und thermoaktive erdberührte Bauteile, Deutsches IngenieurBlatt, Ausgabe 07-08, 2010

Ingersoll L. R. et al.: Heat Conduction with Engineering, Geological and other applications, Madison, WI: The University of Wisconsin Press, 1954

Kastura T. et al.: Heat transfer experiments in the ground with groundwater advection, Proceedings of 10th Energy Conservation Thermal Energy Storage Conference Ecostock’2006, New Jersey

Kavanaugh S.P. et al.: Investigating Methods for Determining Soil and Rock Formation Thermal Properties From Short Term Field Tests, ASHRAE, Final Report September 1999 – September 2000

Koelbel T.: Grundwassereinfluss auf Erdwärmesonden: Geländeuntersuchungen und Modellrechnungen, Dissertation, Karlsruher Institut für Technologie, 2010

Sass, I. und Lehr, C.: Improvements on the Thermal Response Test Evaluation, Thirty-Sixth Workshop on Geothermal Reservoir Engineering Stanford University, 2011

Ministerio de Fomento – Gobierno de España: Código Técnico de la Edificación. Documento Básico de Seguridad Estructural – Cimientos (CTE DB SE-C), 2008

Comisión Permanente del Hormigón – Gobierno de España: Instrucción de Hormigón Estructural (EHE-08), 2008

European Committee for Standardization: Eurocode 2: Design of Concrete Structures

European Committee for Standardization: Eurocode 7: Geotechnical Design